Neurofibromatosis Type 1 Modeling in Swine: Targeting *NF1* mRNA Splicing

By

Dominic Thomas Schomberg

A dissertation submitted in partial fulfillment of
the requirements for the degree of

Doctor of Philosophy
(Animal Science)

at the

University of Wisconsin - Madison

2022

Date of final oral examination: June 15th, 2022

The dissertation is approved by the following members of the Final Oral Committee:

Dhanansayan Shanmuganayagam, PhD, Assistant Professor, Department of Animal and Dairy Sciences and Department of Surgery
Brian Kirkpatrick, PhD. Professor, Department of Animal and Dairy Sciences
Wei Guo, PhD, Assistant Professor, Department of Animal and Dairy Sciences
Bermans Iskandar, MD, Professor, Department of Neurological Surgery

DEDICATION

In loving memory of my late brother David William Schomberg, who passed away on June 9th, 2021 from an NF1 brain tumor.

Jesus said, “I am the resurrection and the life. Whoever believes in me, though he die, yet shall he live, and everyone who lives and believes in me shall never die.” - John 11:25-26

ACKNOWLEDGMENTS

I would like to thank staff and personnel within the University of Wisconsin—Madison Department of Animal and Dairy Sciences who have made special efforts to help my research succeed. To members of the Biomedical & Genomic Research Group lab Jennifer Meudt, Irshad Ali, and Taeyoung Shin, thank you for your devoted support and guidance with scientific experiments. To fellow graduate students Nathan Chesmore, Folagbayi Arowolo, Matthew Wielgat, and Hadjer Namous, thank you for your friendly comradery during this academic journey. And to my primary mentor Dhanansayan Shanmuganaygam, thank you for your expert training in the art of scientific investigation and for pushing me to realize my greatest academic potential.

I would also like to thank staff and facility managers from the University of Wisconsin—Madison Biotechnology Center and the Swine Research and Teaching Center who have contributed time and resources to advancing my research. To Dustin Rubenstein, Brent Lehman, and Jeremy Niece, thank you for your technical expertise and advice in all things molecular genetics. To Jamie Reichert, Ana Cecilia Escobar Lopez, Keri Graff, and Jennifer Frank, thank you for accommodating the many unique research requests within the swine facility.

I would like to specially thank Charles Konsitzke of the Biotechnology Center and Ryan Greier of NF North Central for their dedication to NF1 research abroad and for their personal words of encouragement in difficult times. Your support has been very important to me, as it has for many others with loved ones afflicted by this disease.

Finally, I would like to thank my wonderful family who have never ceased in their unconditional love and support. You demonstrate what it means to be a family and to have a place to call home. To my mother and father, I am grateful for the life you've given me and for the exemplary character you have shown through the years. To my siblings and in-laws, thank you all for being part of my life and believing in me, I love and care for every one of you. And to my beautiful wife, Jennifer, I love you beyond words and would not be where I am today without your steadfast support.

This work was supported by funding from the Biomedical & Genomic Research Group Discretionary Fund (University of Wisconsin-Madison), the Neurofibromatosis Network, and NF North Central. This work was also supported by the Office of the Assistant Secretary of Defense for Health Affairs and the Defense Health Agency J9, Research and Development Directorate, through the Neurofibromatosis Research Program (NFRP) under Award No. W81XWH-18-1- 0633. Opinions, interpretations, conclusions, and recommendations are those of the author and are not necessarily endorsed by the Department of Defense. Additional support for RRID:SCR_017759 was provided by the University of Wisconsin Carbone Cancer Center (NIH/NCI funding: 5P30CA014520-40).

TABLE OF CONTENTS

Page

LIST OF FIGURES

Page

LIST OF TABLES

Page

SUMMARY

Neurofibromatosis Type 1 (NF1) is a complex genetic disease that can display a variety of phenotypes including skin lesions, cardiovascular abnormalities, skeletal deformations, and nervous system tumors. Neurofibromas are the hallmark tumor associated with this disease and originate from transformed Schwann cells surrounding nerves. Malignant transformation of these tumors can occur and carries a very poor prognosis. Current medical treatments are almost exclusively symptomatic as very few NF1-specific therapies exist.

Thousands of unique mutations have been identified in *NF1* yet very few genotype-phenotype correlations have been identified. Splice site mutations are disproportionately found, however, and are frequently associated with tumor formation. Alternative splicing, a natural variation in splicing, also occurs with relatively high frequency in *NF1* but its functional role is not well known. Understanding variations in *NF1* splicing may help explain the phenotypic diversity and increased tumor incidence seen in patients. Relevant models that recapitulate the disease phenotype and genetic complexity are needed to study a complex disease like NF1. Recently developed NF1 swine models display NF1 phenotypes better than traditional animal models and may better model the genomic complexity of *NF1*, however, these studies have not been done.

To determine if swine effectively model *NF1* alternative splicing, several research aims were completed. 1) *NF1* alternatively spliced exons (ASEs) were identified in swine and their expression levels in a variety of tissues were quantified. 2) A cell culture platform for isolating, differentiating, and evaluating neuronal cell types was established for further *NF1* ASE studies. 3) Regulatory regions for several *NF1* ASEs were identified

and splice-switching oligonucleotides (SSOs) were used to confirm regulatory activity at these sites. 4) Downstream effects of *NF1* ASE modulation were evaluated in differentiating Schwann cells and shown to reduce tumorigenic effects associated with *NF1* function. The results of these aims show that swine effectively model *NF1* alternative splicing as seen in humans and can be used to evaluate *NF1* alternative splicing. They also demonstrate that modulation of *NF1* alternative splicing has functional downstream effects central to NF1 tumorigenesis and Schwann cell development. Overall, this work provides a relevant translational platform to study *NF1* alternative splicing and shows that SSOs can be used to modulate *NF1* ASE expression in a functionally significant way.

CHAPTER 1 – Neurofibromatosis Type 1 (NF1)

1.1. Clinical Presentation

Neurofibromatosis Type 1 (NF1) is a complex disease commonly characterized by various skin conditions that also affects multiple physiological systems. Individuals with NF1 have a decreased life expectancy of around 15 years compared to the general population [2]. In addition to multifaceted symptom presentation, patients have a significantly increased disposition for tumor formation. Tumors form with increased incidence on the dermis, in the brain, on cranial and peripheral nerves, and on the spinal cord. Current medical treatments are almost exclusively symptom based as very few NF1 specific therapies exist. NF1 has been challenging to diagnose with traditional clinical examination since many of its symptoms are not specific and may not manifest until later in life. Consequently, awareness of this disease within the medical community has lagged behind other rarer diseases that have more consistent, severe manifestations. While NF1 is classified as a rare disease by some leading medical organizations, typically defined as a condition affecting fewer than 1 in 2000 people, its true incidence may be higher in some populations [3, 4].

Formerly known as von Recklinghausen disease, NF1 was first given a formal, classical description in 1882 by Friedrich Daniel von Recklinghausen. This disease has been partially documented throughout history, however, he was the first to identify cutaneous, neurological, and visceral symptoms as being part of the same syndrome with origins in nervous tissue [5]. Prior to this, illustrations with close resemblance to NF1 have been found as early as the 15th century which depicted some classical manifestations of neurofibromas [6]. Recognition of some of the other hallmark characteristics, such as Lisch nodules and café-au-lait spots, of NF1 came later [7]. Medical science has made tremendous progress in

the last few decades, especially with the advent of genetic sequencing technology, and *NF1* was first mapped in humans in 1989 [8]. This served as a foundational moment for research into this disease as genetic analysis is now a core component of NF1 study and diagnosis. Further genetic studies have highlighted the increasingly diverse range of pathology associated with NF1, the involvement of *NF1* as a tumor suppressor in cancer more generally, and a puzzling lack of correlations between specific *NF1* mutations and symptoms.

1.1.1. Diagnosis

NF1 is one of the most commonly acquired monogenic inheritable genetic disorders [9]. It is autosomal dominant, demonstrates complete penetrance, and arises due to mutations within a single gene. Mutations within this gene can affect multiple distinct traits with varying degrees of severity making it a pleiotropic gene with variable expressivity. The presentation of specific clinical phenotypes is also highly variable between individuals with the same mutation which contributes to the overall complexity of understanding this gene and its associated disease [10]. The first consensus diagnostic criteria was established by the NIH in 1988 [11]. It stated a clinical assessment must find TWO or more of the following features:

- 6 or more café au lait macules (>0.5 cm in children or >1.5 cm in adults)
- 2 or more cutaneous/subcutaneous neurofibromas or one plexiform neurofibroma
- Axillary or inguinal freckling
- Optic pathway glioma
- 2 or more Lisch nodules (iris hamartomas seen on slit lamp examination)
- Bony dysplasia (sphenoid wing dysplasia, bowing of long bone ± pseudarthrosis)
- First degree relative with NF1

Other diseases may resemble NF1 on clinical presentation and have sometimes been referred to as NF1 subtypes. Some of the these syndromes include Legius syndrome with café-au-lait macules axillary freckling [12], Noonan syndrome with skeletal defects and cognitive deficits [13], Costello syndrome with hyperpigmentation and various tumors [14], Leopard syndrome with lentigines (dark freckling) [15], and Watson syndrome with Lisch nodules and cutaneous tumors [16]. More generally, NF1 and these other syndromes have been classified as RASopathies as they all involve mutations with Ras pathway genes [17]. Due to these other syndromes presenting similarly to NF1, clinical criteria alone can be insufficient for definitive diagnosis, particularly in young children [18].

Diagnosis was exclusively a clinical one prior to the advent of genetic testing and many cases were missed or attributed to other similar syndromes. Genetic testing has led to an increase in the known incidence of NF1 and most estimates currently state around 1 in 3,000 people throughout the world carry an *NF1* mutation [19]. Some studies now estimate true incidence to exceed 1 in 2,000 in certain populations [4, 20]. Formal clinical diagnostic criteria were updated in 2021 to reflect new genetic analysis capabilities [21]. This update introduced two new criteria to be considered in addition to the clinical criteria:

• A heterozygous pathogenic *NF1* variant with a variant allele fraction of 50% in apparently normal tissue such as white blood cells

• A child of a parent who meets the diagnostic criteria merits a diagnosis of NF1 if ONE or more of the other criteria are present

Routine genetic screening for *NF1* is not currently performed in any patient population, but newborn and prenatal screening is available and recommended for children of parents with NF1 [22, 23]. Current *NF1* screening methods have a detection rate approaching 100% but are overall less sensitive than many other genetic screens due to the exceptionally

large size of the gene [24]. With technological improvements in the future, it is conceivable that *NF1* genetic testing could become the primary means of diagnosis and could become part of standard newborn screening procedures.

1.1.2. Non-tumor Symptomatology

NF1 mortality is driven primarily by malignant transformation of neurofibromas but some symptoms such as cardiovascular disease contribute to overall mortality but to a lesser degree. Still other symptoms like some cutaneous manifestations, while not contributing to mortality, are cause for significant morbidity.

Skin conditions

The most common NF1 symptoms are those listed in the diagnostic criteria that involve the skin. These include café au lait skin macules (CALMs), dermal neurofibromas, freckling in the armpits or groin, and Lisch nodules (Figure 1). Most patients who exhibit 6 or more CALMs will be diagnosed with NF1, even if they have no other signs of the disorder. CALMs are frequently the first sign of NF1 found in infancy as other manifestations typically develop later. A single CALM is found in about 25% of otherwise healthy children but multiples, especially beyond six, are much more rare [25]. CALMs do not present any additional risk to health but can warrant further examination for NF1 or Legius syndrome. Likewise, Lisch nodules, melanocytic hamartomas of the iris, and inguinal freckling, due to melanin deposits in the skin, are also benign aside from cosmetic appearance [26]. Both typically present later in life and by puberty are found in a significant majority of NF1 patients.

Figure 1. Common cutaneous manifestations of NF1 - Café au lait macules (left), inguinal freckling (center), and Lisch nodules (right) [27, 28]

Non-CNS disorders

In addition to the common cutaneous sequelae, about 70% of NF1 patients also have more severe manifestations that may include learning difficulties, cardiovascular disorders, softening and curving of bones, and scoliosis [29]. Osteopenia is common and often suggests an underlying bone abnormality although one may not be observed in all patients [30]. This reduction in bone mineral content suggests dysfunction of osteoblastic or osteoclastic function. Indeed, osteoclast survival and osteoblastic differentiation has been shown to be Ras-dependent in NF1 mouse models [31]. Hypertension, vasculopathies of the renal and cerebral vessels, and congenital heart defects are all seen with greater frequency [32]. These cardiovascular pathologies are the second most significant cause of death for many NF1 patients, behind only tumors [33]. It is unclear if there is a common cell of origin or process that links these vascular etiologies together. Many different tissues have been suggested as causative such as nerves within the vessel wall, Schwann cell proliferation, mesodermal dysplasia, and fibromuscular hyperplasia [34, 35]. Endocrine disorders such as hyperthyroidism and precocious puberty are also seen in some NF1 patients [36].

Cognitive impairments

A majority of NF1 patients also experience some form of cognitive deficit, approaching up to 70% of patients by some estimates [37]. Some patients have no identifiable deficits while others may have only deficits in specific skills like visuospatial, visuomotor, language, or fine or gross motor skills [38, 39]. Others have observed more generalized deficits in learning, such as in reading or math, but severe generalized intellectual impairment is more rare [40]. Attention-deficit-hyperactivity disorder is also frequently diagnosed and may exacerbate these deficits [41]. Cellular and molecular mechanisms driving cognitive deficits are clearly complex, however, some specific neurobiological processes have been explored more closely. Learning deficits in *NF1* +/- mouse models have been attributed to hyperactivation of Ras signaling in GABAergic neurons. Further studies have shown hyperpolarization-activated cyclic nucleotide-gated current in interneurons also produced a deficit in mice that was rescued by the pharmaceutical lamotrigine [42]. Other NF1 mouse studies have found a reduction in cyclic AMP and concurrent loss of cortical thickness and shortened neural processes [43]. One behavioral study correlated a deficit in NF1 mouse spatial learning to dopamine levels in the hippocampus [44].

1.1.3. Tumorigenesis

NF1 predisposes individuals to a multitude of different tumor types, both benign and malignant. Overall incidence compared to the general population is between 5-15% greater, with most of the increased risk attributed to tumors associated with nerves and connective tissues. The majority NF1 tumors are benign but plexiform neurofibromas have about a 15%

chance of developing into malignant tumors compared to the general public [2]. NF1 patients also have a lower overall survival rate once diagnosis with malignancy is confirmed compared to patients with sporadic cancers [45].

Figure 2. Common tumors observed in NF1 [46]

Cutaneous

Lipomas and cutaneous neurofibromas (Figure 2) are the two skin lesions commonly observed in NF1 patients and, while not known to have malignant potential, are associated with significant morbidity due to the disfigurement associated with them [47]. Some will occasionally cause physiological problems due to the compression of surrounding tissues but usually resolve upon surgical removal. These neurofibromas are localized but are not encapsulated and do not show a clear association with myelinated nerves, like other more serious neurofibromas, but may be associated with nerve endings and perineurial cells [48] [49]. Similar to Lisch nodules and inguinal freckles, these lesions usually become clinically

evident after puberty. Pruritus is commonly associated with these lesions likely due to increased activation of mast cells [50]. Neurofibromas are composed of mast cells, a variety of fibroblasts, neoplastic Schwann cells, and occasionally adipocytes [51]. Recent evidence also suggests that the cell of origin for cutaneous neurofibromas reside in the hair roots of the dermis, sometimes referred to as skin-derived progenitor cells [52]. These cells share a common ectodermal lineage with other NF1 relevant cells of the skin, nerves, and myelinating tissue.

Central Nervous System

Tumors of the nervous system are much more debilitating than cutaneous tumors and are the most significant cause of mortality among the NF1 population [53]. The major classifications include spinal neurofibromas, optic pathway gliomas, brain gliomas, plexiform neurofibromas, and malignant peripheral nerve sheath tumors (MPNSTs) (Figure 2). These types of tumors frequently originate in the myelinating tissues of the nervous system and signify a poorer prognosis than tumors that do not involve nerve bundles [54]. Spinal neurofibromas are found in up to 40% of patients and have exhibited a familial pattern. While most other neurofibromas exhibit loss-of-heterozygosity in the *NF1* gene, only one-third of spinal tumors have this characteristic [55]. Fortunately, these tumors are generally benign and are often only found when the masses symptomatically compress nearby tissues.

Low-grade astrocytomas are present in about 15% of the NF1 pediatric population [56]. These tend to be benign but often involve the optic pathways and can become symptomatic. Females with optic gliomas appear to have greater incidence and referral for

treatment than male patients [57, 58]. Young females appear to have an increase incidence of NF1 malignancies overall, even when excluding optic gliomas [59]. While this difference could be due to a hormonal influence yet to be revealed, a sex-based dimorphism in cAMP signaling is known to be associated with low-grade glioma development in females as well as in mouse models of NF1 [60].

Plexiform neurofibromas arise from the myelinating cells of large nerve plexuses. While the tumor composition is overall similar to dermal neurofibromas, a far higher percentage display loss-of-heterozygosity and also have significantly increased incidence of developing into a malignant tumor [61]. The tumors are thought to originate from non-myelinating Schwann cells and thus may have an embryonic or adolescent origin [62]. The tumor microenvironment also has increased significance in plexiform neurofibromas. Interaction of NF1 haploinsufficient mast cells and fibroblasts with the *NF1*-/- Schwann cells appear to be involved with a key interaction in the initiation of plexiform neurofibroma [63]. Approximately 15% of plexiform neurofibromas will transform into a malignant tumor termed an MPNST [29]. NF1 patients have about a 10% lifetime risk of developing MPNSTs. While not exclusive to patients with NF1, they account for about 25% of cases and have worse treatment outcomes than non-NF1 patients [64]. Treatment can be difficult with as many as 50% of tumors reported as being unresectable, which further impedes the efficacy of adjuvant treatments like chemotherapy or radiotherapy. MPNST, as with many malignant tumors, have significant mutational heterogeneity associated with them which can make research into their origins challenging. One of the more consistent mutations found across MPNST tumors, however, is loss-of-heterozygosity in *TP53*, a cell cycle regulator and also a tumor suppressor [65].

Other Tumors

Several other tumors that do not have a clear origin in the skin or central nervous tissue, while generally more uncommon, are also seen with increased incidence in NF1 patients. Gastrointestinal stromal tumors (GISTs) are smooth muscle neoplasms found in 25% of patients at autopsy. Significantly, GISTs within the context of NF1 do not harbor the typical KIT or PDFG mutations, suggesting a different pathogenic mechanism [66]. Gastric carcinoid tumors with a loss-of-heterozygosity have also been found in NF1 patients in the absence of other predisposing factors [67]. Incidentally, studies have shown miR-107 is upregulated in gastric cancer and its inhibition increases NF1 protein levels, suggesting *NF1* is one of its targets in these cancers [68]. Juvenile myelomonocytic leukemia (JMML) incidence is 200-fold higher in the NF1 population [69]. Additionally, NF1 is one of the 20 most mutated genes in myeloid leukemias, suggesting an important role for NF1 as a tumor suppressor in immature myeloid cells [70]. Neuroblastomas and pheochromocytomas, both tumors of the adrenal gland, present infrequently but do have loss-of-heterozygosity [71]. Glomus tumors and rhabdomyosarcoma are two other rare but significant tumors that are found within the NF1 spectrum of disease [32, 72]. More recently, breast cancer has been recognized as occurring more frequently in NF1 patients and the gene has been strongly implicated in the general mutational profile [73]. In fact, its presence also contributes to endocrine therapy resistance [74]. *NF1* alternative splicing, particularly the absence of one particular neurofibromin isoform, is identified as part of breast cancer progression [75, 76].

1.2. Molecular and Functional Characteristics

NF1 is located at chromosome 17q11.2 in humans and contains 61 exons (Figure 3). The gene spans 350kB of DNA, is transcribed into a 12 kB mRNA, and then translated into a 250-280 kDa protein product, neurofibromin, which forms a high-affinity dimer [77]. The promoter region is 484 bp upstream of the initiation codon and contains a 5' untranslated

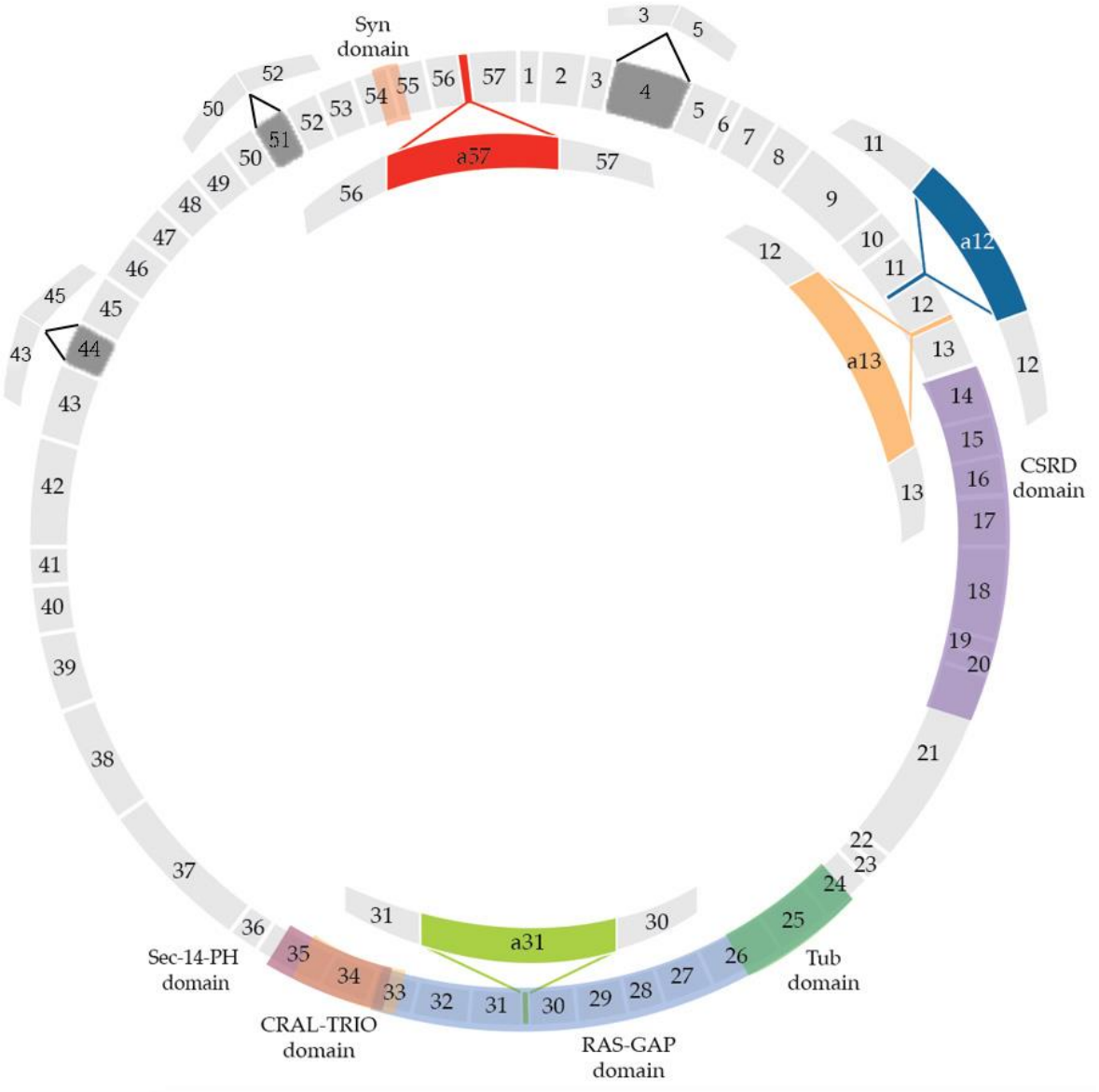

Figure 3. *NF1* Genomic Exons – A circularized representation of the *NF1* exons and functional domains rendered to scale.

region but no TATA or CCAAT boxes [78]. The 3' untranslated region, important for polyadenylation of pre-mRNA, is 3.2kb in length and has specific sites for proteins but their roles that have not yet been clearly elucidated [79]. Three other genes also lie within intron 35, EVI2A, EVI2B, and OMPG, however, these genes have not been associated with the *NF1* mutational profile or NF1 symptoms [80-82].

NF1 has several functional domains and downstream interactions within the cell (Figure 3). It regulates cell signaling for cell proliferation and differentiation and acts as a tumor suppressor. It also has many identified functional domains and communicates through several different signaling pathways, most notably the Ras/MAPK, PI3/Atk, and cAMP/PKA pathways. Neurofibromin is expressed in all cells of the body, but its activity appears to be much more important in certain cell types owning to its overall complexity. Regulation with respect to post-translational modification, epigenetics, or alternative splicing may be necessary to explain some of its functional difference [83].

1.2.1. Alternative Splicing

NF1 contains several alternatively spliced exons (ASEs) that are differentially expressed in various tissues which are translated into different neurofibromin isoforms (Figure 3). The average human gene produces 3 different isoforms, based on the published annotation data from Ensembl. RNA-seq data annotation, however, estimates this average could be as high as 7 different isoforms per gene [84]. Given the large number of exons in *NF1* (the average is 33 exons), a conservative estimate would give *NF1* 6 different isoforms. Currently, there are at least seven identified ASEs in the human *NF1* transcriptome, four of which are traditionally considered alternatively spliced [85]. If these four common ASEs are

spliced in every combination, there could be over 16 (2^4=16) different *NF1* isoforms. However, whole transcriptome analysis on *NF1* has not been performed as long-read sequencing has traditionally been technically challenging for large mRNA products.

Nomenclature

NF1 nomenclature has changed recently to better reflect upon the exon's constitutive or alternatively expressed nature. The four currently identified ASEs are denoted 11alt12, 12alt13, 30alt31, and 56alt57 [86]. For brevity or clarity, they can also be referred to as a12 or ASE 12 instead of 11alt12, etc.… Of the other 57 constitutively expressed exons, 3 of them have been found to be excluded from mature, polyadenylated mRNA transcripts: exon 4, 44, and 51 [85]. Other exons have been found to be excluded, but not in mature transcripts. For clarity, the nomenclature used in this work distinguishes the whole body of *NF1* ASEs into two subcategories: alternatively included exons (AIEs) and alternatively excluded exons (AEEs). In the conventional *NF1* nomenclature, AIEs are given a suffix or prefix to distinguish them from the other, more constitutively expressed exons, which are simply referred to by number. The AEEs are numbered regularly amongst the rest of the constitutively expressed exons and when referred to in the context of alternative splicing are prefaced with the phrase AEE indicating they are among the normally numbered exons but are being discussed in the context of its alternatively spliced nature.

Splicing Mechanisms

RNA-splicing reactions are carried out by a large ribonucleoprotein called a spliceosome. Specific regulatory exonic and intronic sequences interact with RNA-binding

proteins and act as a splice silencer or splice enhancer (Figure 4). Precisely defining enhancer and silencer proteins and mechanisms can be complex and is an intense area of research. Some RNA-binding proteins can function as either enhancers or silencers depending on the location along the pre-mRNA the sequence is located [87]. The most frequently studied *NF1* ASE, AIE 31, has multiple identified regulatory proteins which indicate it is under tight, complex control. Generally, two main classes of proteins, CUG-binding protein and embryonic lethal abnormal vision like family (CELF) and Muscleblind-like protein (MBNL), act in an antagonistic dose dependent manner [88]. CELF and Hu proteins promote AIE 31 skipping, while the MBNL and TIA-1/TIAR proteins promote its inclusion [88].

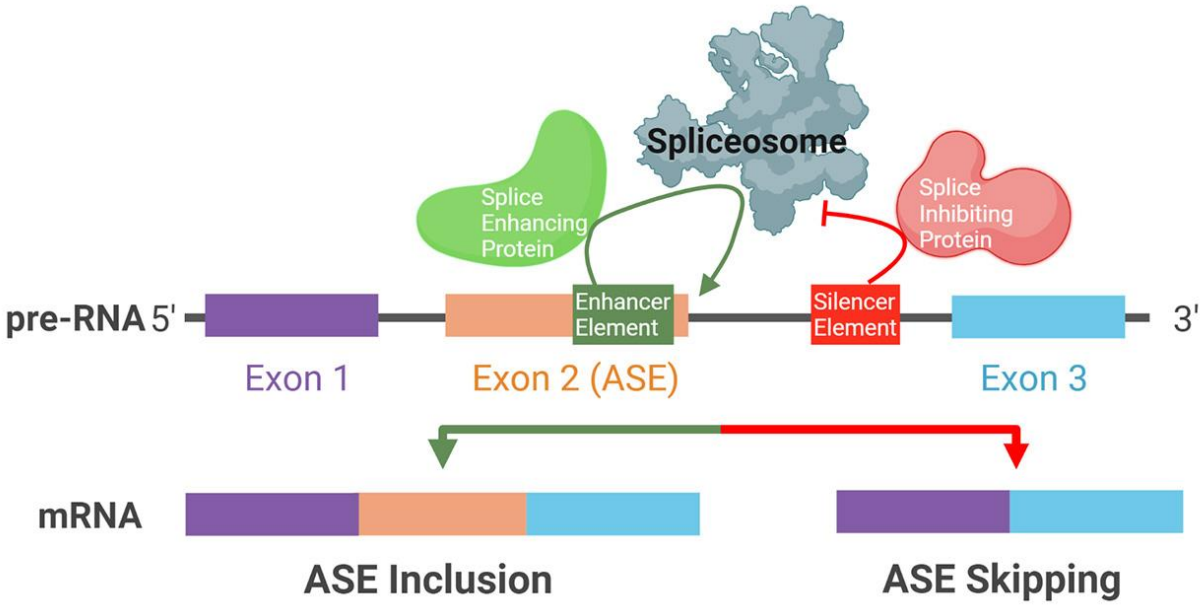

Figure 4. Splicing Mechanism - General schematic highlighting the role of RNA splicing elements that dictate ASE inclusion or skipping.

1.2.2. Neurofibromin

Neurofibromin is an established tumor suppressor, interacts with Ras-GTPases, and is part of the NMDA receptor complex neuronal synapses [89, 90]. Other functions have also been implied, like involvement in cellular orientation [91]. Given the genomic and

phenotypic complexity of NF1 and its associated disease, other functions are likely but have yet to be definitively elucidated, however, some important mechanistic features have been characterized.

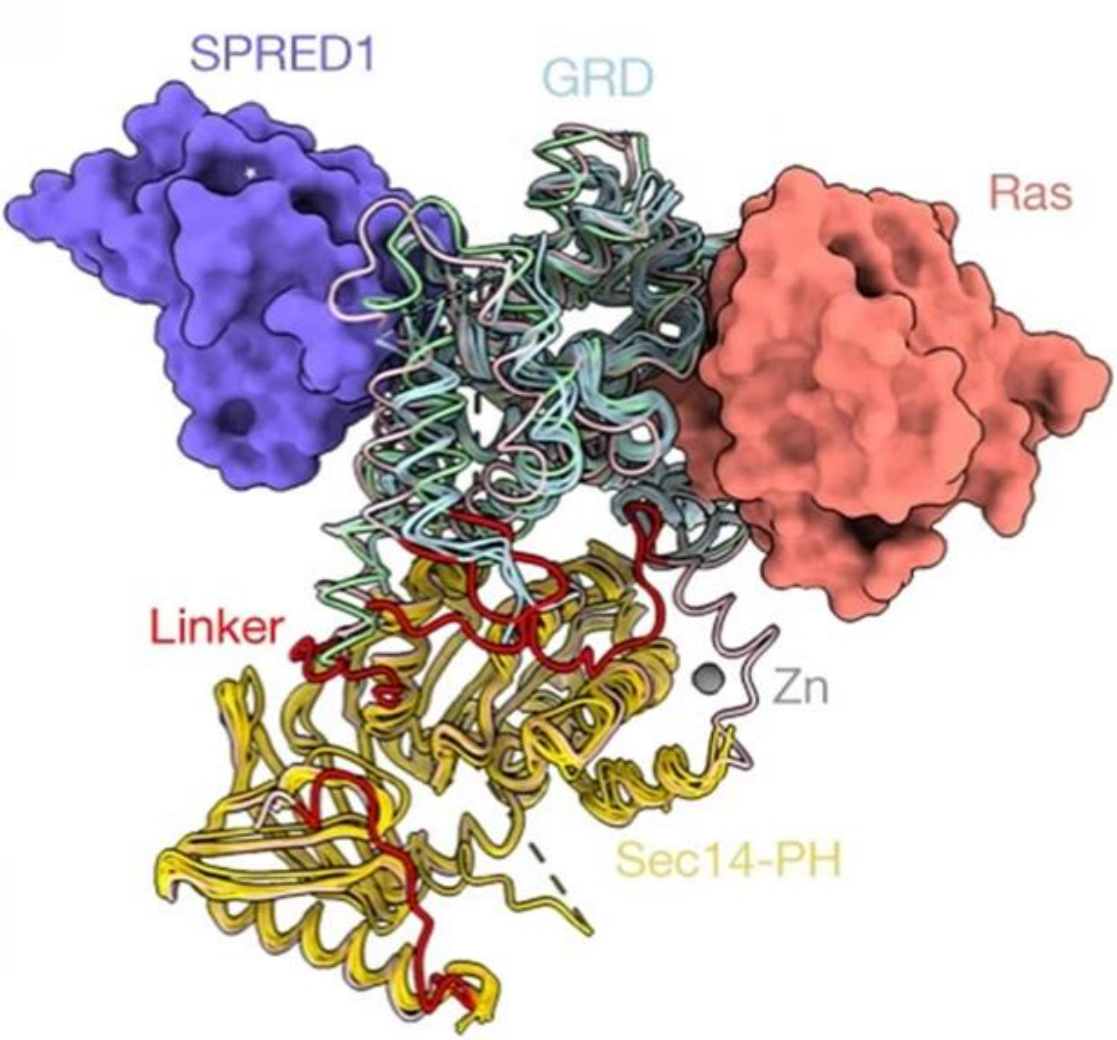

Figure 5. NF1 Protein Interaction – Neurofibromin backbone structure revealed by X-ray models. GRD (light blue) and Sec14-PH (yellow) domains interact with SPRED-1 (purple) and Ras (red) proteins stabilized by Zinc (gray) and interdomain linker (red) [92].

Functional Domains

The most well-known and well-studied domain in the neurofibromin protein is its GAP (GTPase activating protein)-related domain (GRD). Its function is to hydrolyze active, phosphorylated GTP-bound Ras into inactive GDP-bound Ras (Figure 3, 5). The GRD region also interacts with SPRED-1 and is required for optimal Ras inhibition [93]. Many other Ras regulating genes also undergo alternative splicing to regulate its activity [94]. GAP domains frequently undergo alternative splicing as well [95]. Within the *NF1* gene, AIE 31 directly modulates this GAP activity. According to most studies, inclusion of this ASE decreases GAP activity but also binds its target with higher affinity [96]. The tubulin-binding domain (TBD) is found directly upstream of the GRD domain. It interacts with various cytoskeleton elements and helps mediate neurofibromin dimerization which also decreases GAP activity [90]. The C-terminal domain (CTD) is also a tubulin binding domain involved with cell cycle progression and is located at a far downstream region within the gene. It also has a nuclear localization signal within it which decreased GAP activity [97]. Similarly, the cysteine-serine-rich domain (CSRD), located upstream of the GRD domain, interacts with the cytoskeleton and has a region that can be phosphorylated in a protein kinase C dependent manner thereby increasing GAP activity [98]. The Sec14 homologous-pleckstrin homologous domain (SecPH) is the other identified functional domain and located just downstream from the GRD domain. It functions as a lipid binding domain that can target both lipid membranes and non-membrane glycerophospholipid ligands [99].

Post-translational Modifications

Neurofibromin function can be regulated through post-translational modifications. It can be phosphorylated at its C-tail terminus consistent with its transport into the cytosol. Dephosphorylation, the basal state, directs neurofibromin to the nucleus. An active RasMAPK pathway enhances C-tail phosphorylation and is a feature found in other tumor suppressor genes [100]. Phosphorylation of the CTD domain inhibits its overall GAP activity [97], and phosphorylation of the CSRD domain promotes association with cytoskeletal elements [101]. Like most proteins, neurofibromin can be ubiquitinated as well and leads to proteasome degradation. This process is dynamically regulated and most active in cell states where increased Ras activity is needed to induce proliferation and differentiation [102]. Recently, neurofibromin via its SecPH domain was confirmed to undergo SUMOylation. It was suspected previously due to 15 SUMOylation motifs being found throughout the gene. This process localizes the protein to PML nuclear bodies and has the effect of stimulating Ras-GAP activity [103].

Signaling Pathways

Neurofibromin signals through several pathways. It regulates cAMP in two major ways. One requires interaction with the GRD domain and its downstream activity [104], and the other is neurotransmitter stimulated and involves the CTD domain [105]. These pathways are thought to be involved in memory formation, both short term and long term, respectively. Ras mediated signaling is transduced through several different pathways. Both the MAPK and PI-3K pathways enhance mitogenic activity and have been found to be increased in NF1 tumors [106]. The MAPK pathway, a highly conserved cascade of protein kinases, regulates

cell cycle progression and transcription while PI3K, via AKT and PDK1, is more involved with survival, protein translation, and cytoskeletal signaling [107]. On the other hand, the inactivation of the Ras-PI3K pathway, or in the absence of neurofibromin, enhances the mTOR pathway, promoting cell proliferation and survival and is increased in NF1 tumors [108]. The PI3K pathway is normally downregulated by phosphatase and tensin homologue deleted on chromosome ten (PTEN), a tumor suppressor that is often mutated in malignant NF1 tumors [109].

1.2.3. Tissue Distribution

The consensus dataset in the Human Protein Atlas indicates neurofibromin is expressed in relatively consistent overall levels in different tissues with higher levels in the retina, thyroid, and most nervous tissues [110]. Despite these modest differences, its activity in certain cell types appears to be much more important than in others so more nuanced mechanisms are likely involved.

NF1 ASEs are differentially expressed in different tissues to a much greater degree than the overall level of *NF1*. Tissue distribution patterns have been generalized, but not yet fully elucidated. AIE 12 is neuron-specific and contains complex splicing regulatory elements, AIE13 has been found to direct targeting to the intracellular membrane, AIE 31 is within the well-defined RAS-GAP domain of the NF1 protein and highly expressed in myelinating tissue, and AIE 57 is included in a muscle-specific isoform that may also have important roles during embryonic development. Of the *NF1* AEEs, 4 is excluded most often in blood, 44 is excluded most often in liver, and 51 is most often lost in liver, kidney, and skeletal muscle. In most other tissues, these AEEs are lost in fewer than 1% of mRNA

transcripts [85]. AIE 31 is the most well studied. Neurons show low levels of AIE 31 while glial cells have high levels [111]. Further, some nervous tissues show an increase in AIE 31 during embryonic development [112].

1.3. Mutational Landscape

Neurofibromin is involved in cell functions directly tied to tumorigenicity and mutations are strongly linked to the development and progression of multiple cancer types. Within the NF1 population, over 2,800 unique *NF1* germline mutations have been identified [113]. This number is likely much higher as many patients, particularly ones with less severe symptoms, do not pursue genetic analysis.

Transmission and Frequency

NF1 appears to mutate much more frequently than other genes, at a rate about 10-fold higher that most other inherited disease genes [61]. This may be partly explained by its relatively large size. However, it mutates at about the same rate as the dystrophin gene (DMD) which is 2.5 Mb, considerably larger than *NF1*. Mutations in the gene are generally distributed evenly across the entire gene, apart from a couple notable clusters in two exons, and a decreased incidence in a few others. About half of all point mutations or single nucleotide indels result in premature stop codons, and thus a truncated or quickly degraded neurofibromin protein [114]. The frequency of mutations that influence splicing is also significant in *NF1*, and seemingly more so than in other disease genes [115]. Approximately 50% of the *NF1* mutations are familial, inherited directly from a parent, while the other half arise from de novo mutations [28]. Some de novo mutations, estimated around 1 in 40,000,

are mosaic, meaning the mutation occurred during development and not all cells in the body harbor the mutation [116]. However, if the gonadal cells carry the mutation, any offspring will have full, generalized disease.

Genotype-phenotype associations

One of the more unique aspects about the mutational landscape of *NF1* is the lack of clear genotype-phenotype correlations. This has led to a broader search for other associations that may be helpful in developing targeted interventions or understanding the mechanisms driving clinical pathology. The few mutations that have a slightly increased incidence also appear to have some degree of predictive outcome. A 3 bp, in-frame deletion in exon 22 tends to produce a mild phenotype that lacks cutaneous neurofibromas and a missense mutation in exon 9 produces a phenotype with developmental delay but no neurofibromas [117]. A large microdeletion, that is a mutation that deletes the entire *NF1* gene plus surrounding genes, also produces a similarly severe phenotype that has high malignant tumor potential. More recently, mutations affecting a series of codons in exon 21 were identified which leads to plexiform and spinal neurofibromas in 75% of patients [113]. The variable expressivity could also be influenced by modifier genes, allelic variations, or environmental factors and not be directly associated with the gene itself [10].

Heterogeneity

NF1 is considered a tumor suppressor. Classically that means both alleles must be inactivated for the tumorigenic process to be initiated. Since biallelic inactivation of *NF1* is lethal *in utero*, patients are usually born with a heterozygous genotype (NF+/-). Exceptions

would be those with segmental NF1 or NF1 mosaicism. It is also possible a small subset of tissues develops a second allelic mutation *in utero*, thus initiating tumor development, but this has not yet been proven to occur. *NF1* heterogeneity has been shown to influence cells directly and indirectly as it modifies the cellular microenvironment. Fibroblasts' ability to orient themselves in their environment is impaired [91]. Astrocytes proliferate at a greater rate and have a synergistic effect with other tumor mutations of p53 and Rb [118]. Optic nerve glioma formation in a mouse model seems to depend on this heterogeneity [119]. Other cells, such as microglia or mast cells, could also be responsible for the seemingly heterogenetic effects seen with glia proliferation and tumor growth [120]. Interestingly, malignant transformation of some types of tumors are inhibited by *NF1* heterogeneity despite it increasing benign *de novo* tumorigenesis [121].

Splicing Abnormalities

Most human genes undergo natural exon skipping and a relatively high number of alternatively spliced genes are expressed in the central nervous system [122]. Consequently, splicing misregulation is increasingly being implicated in multiple neurological disorders, including NF1. Overall, it is estimated that 30% of *NF1* mutations negatively influence splicing [123]. Alternative splicing dysfunction is also known to be involved with tumorigenesis. Generally, most of these splice site mutations disrupt the normal splice sequences but some can influence splicing regulatory elements or even create new splice sites [124]. The latter of which can cause cryptic exon inclusion [125]. These splicing mutations could be a mechanism driving genotype-phenotype correlations in NF1patients [126]. Recently, an association has emerged showing a clear relationship between splice-site

mutations and the incidence of brain gliomas, including MPNSTs [127]. Interestingly, exon 9, which has a higher incidence of mutation, has been shown to have an especially high number of splice regulatory motifs that could influence mRNA splicing more generally [128].

1.4. Splice-switching Oligonucleotides

It is well established that many *NF1* mutations result in splicing abnormalities. Therapeutics that correct this splicing, therefore, could be used as therapy to treat NF1 symptoms or even as a preventive measure. No such therapeutics exist for NF1 at this time; however, one possible approach could involve the use of antisense oligonucleotides to modulate endogenous splicing.

Function and Design

Splice-switching oligonucleotides (SSOs), also generally referred to as antisense oligonucleotides, are short sequences of nucleotides, typically 15–30 base pairs long, designed to block the binding of splicing factors to pre-mRNA and can have inhibitory or enhancing effects depending on the target region's function (Figure 6). Inhibition can be achieved by targeting a known splice site to interfere with splicing protein interactions, block cryptic splice sites, or modulate alternative isoform expression [129]. SSOs can also be used to enhance splicing or restore exon inclusion, through targeting splicing silencer sequences (exonic or intronic), disrupting secondary RNA structures, or recruiting acting splice factors [130].

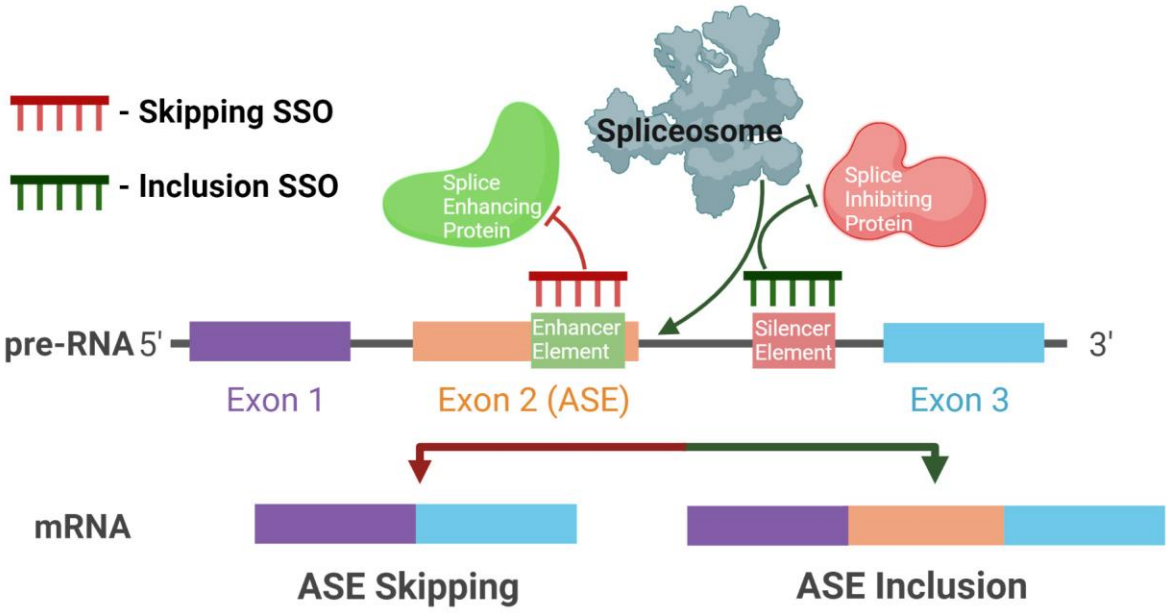

Figure 6. SSO Function – Schematic diagrams representing the mechanism of skipping SSOs (dark red) and inclusion SSOs (dark green).

When used in physiological systems, SSOs must be modified in particular ways, otherwise endogenous endonucleases and exonucleases will quickly degrade the products. The modifications generally involve changes to the phosphate backbone and/or sugar moiety of the nucleotide structure [131]. A common, efficacious set of modifications involves the addition of 2′–O–Me RNA nucleotides on the ends of SSOs to inhibit ribonuclease and DNase digestion and the substitution of a phosphorothioate on the ribose backbone to inhibit exonuclease and endonuclease digestion. Lock nucleic acids (LNAs) contain a 2'-O,4'-C-methylene nucleotide modification and confer similar resistance to other sugar modifications while also conferring higher binding affinity to the RNA target [132]. Phosphorodiamidate morpholinos (PMOs), are yet another novel modification that replaces the furanose ring with a morpholine ring and the phosphodiester backbone with a phosphorodiamidate backbone. PMOs have reduced binding affinity for plasma proteins due to their neutral charge which decreases accumulation within tissues *in vivo* that is seen with other SSOs [133]. The process of designing SSOs, which is to say identifying RNA target sequences, involves using a series

of predictive algorithms to locate the target region and then calculation of binding energies to maximize binding efficacy. RNA folding programs predict the most common secondary folding structure, then splice site evaluation programs predict the most likely regulatory regions. Combining these data allows for SSO targets to be identified that are partially open and thus accessible to free-floating SSOs but also partially closed so that their binding will disrupt the secondary structure. Finally, binding energies of SSOs with respect to self-complementarity, dimer and multiplex formation, target binding affinity, and off-target potential are taken into account to maximize efficacy in physiological conditions [134]. SSO modification also influences binding energies and must be considered. *In vitro* validation of SSOs efficacy is commonly performed using RT-qPCR to measure mRNA isoforms. This assay can be enhanced by introducing plasmids containing the targeted mRNA transcript into the cell which is especially helpful if the target is only weakly expressed in the given culture system [135].

Therapeutic Strategy

SSOs can be used as a research tool to modulate alternative splicing and study basic science mechanisms but also has potential as therapeutic to correct splicing defects [136]. They can also be used to modulate endogenously occurring alternative splicing for therapeutic ends [137]. An advantage of SSO therapy is that mRNA can potentially be restored to its natural state without modifying the DNA or introducing transgenes that permanently alter the patient's genome [138]. Dosing can also be dynamically adjusted and SSOs can be personalized to any mutation or target. SSOs gain access to many cell types within the body following parenteral administration but other tissues, such as the brain and

heart, require additional packaging or delivery modalities [139]. SSO can be taken up into cells quickly, usually between 24-72 hours for maximum efficacy to be reached, and can remain pharmacologically active for a week, as in the liver, or up to months, as in muscle tissue [140]. The first antisense oligonucleotide approved for humans was Fomivirsen and was used to treat cytomegalovirus caused retinitis. This paved the way for future therapies that used the same modality to correct splicing defects. The first SSO approved by the FDA was Eteplirson and was for the treatment of Duchenne muscular dystrophy. Patients with mutations that cause skipping of exon 51 (about 13% of patients) saw significant increases in dystrophin levels after 48 weeks of treatment [141]. It worked by inducing exon skipping of the frame-shifted exon thus producing a slightly shorter, but still functional protein. Nusinerson was approved shortly thereafter and aimed at treating spinal muscular atrophy by blocking a splice silencer mutation downstream of a splice enhancing site [142].

NF1 SSOs

Developing therapies that could modulate or restore normal *NF1* mRNA splicing would have a great impact for many NF1 patients. The ability to customize SSO sequences would be especially helpful for NF1 due to the large variety of mutations that influence splicing. However, very few studies have attempted to use SSO to target *NF1* splicing, and no published studies have explored their effects *in vivo.* One study, the first to use SSOs on the *NF1* gene, was able to restore splicing in primary human fibroblasts that contained deep intronic mutations which created a cryptic exon that was spliced into the pre-mRNA [123]. Another notable study was able to modulate AIE 31 in immortalized rat PC12 lines from a

pheochromocytoma [143]. *In vitro* work establishing efficacy of SSOs for *NF1* is important before *in vivo* experiments can be performed.

1.5. Research Models

Animal models have been critical in studying the basic mechanisms behind many diseases and NF1 is no exception. Drosophila, the common fruit fly, was one of the earliest models adopted to study the *NF1* gene. It retains about 60% homology with humans and has proven useful to study the roles of the GRD domain, cAMP signaling, and cognitive impairments [144]. Its *NF1* mediated adenylyl cyclase activity and the MAPK pathway share similarities to humans as well [105].

Mouse Models

Mouse models have also contributed greatly to a better understanding of basic mechanisms in NF1. With 90% percent homology to humans, genetic analysis lends to even better comparison and translatability to human disease. *NF1* +/- mice exposed to radiation develop tumors similar to humans, suggesting a congruent tumor suppressor function [145]. Pheochromocytomas and myeloid leukemias were also shown in mice following loss-of-heterozygosity [146]. Other models developed optic nerve gliomas dependent on *NF1* heterogeneity in the tumor microenvironment [119]. Heart defects and homozygous embryonic lethality is observed in NF1 mice [147]. Cre-recombinase conditional knock-out NF1 mice crossed with mice expressing the Cre protein in Schwann cells removed lethality from the otherwise lethal homozygous *NF1* embryonic genotype. Further, using these same mouse models to produce mice with *NF1*-/- Schwann cells in an *NF1*+/- microenvironment

led to the development of tumors closely resembling neurofibromas. Without this *NF1*+/- microenvironment, however, tumors did not form [148]. Further mouse studies have implicated *NF1* +/- mast cells in this process [149]. While many neurofibroma-like mouse tumor models have been developed, drugs showing efficacy in these models have not translated into successful trials in humans, nor have these mice reproduced many of the classical cutaneous lesions commonly seen in patients.

Swine Models

Medical swine models are emerging as promising alternatives to more accurately model human health and disease for scientific research [150]. They recapitulate complex disorders better than the more commonly used rodent animal models and serve as a more relevant translatable intermediary for developing efficacious therapies [151]. The genetic proximity of the swine to humans and the overwhelming anatomical, physiological and pathophysiological similarities make swine an ideal model to study the complexities of disease genetics and pathophysiology (Figure 7) [150]. Further, the higher sequence homology of swine with humans, about 98%, is believed to allow more accurate prediction of pharmacodynamic and pharmacokinetic properties of drugs compared with mice, leading to results which can be more directly translated to humans [152]. Translatability with respect to surgical procedures or nervous system anatomy are also much more favorable in swine [153]. Genetically engineered swine models are quickly changing the research landscape in many ways as well. Inducible cancer models allow for tumors to be selectively induced in any location using a KRAS/p53 GE swine model [154]. Xerographic organ transplants are also

being made possible by editing out immunogenic antigens and editing in key human transgenes [155].

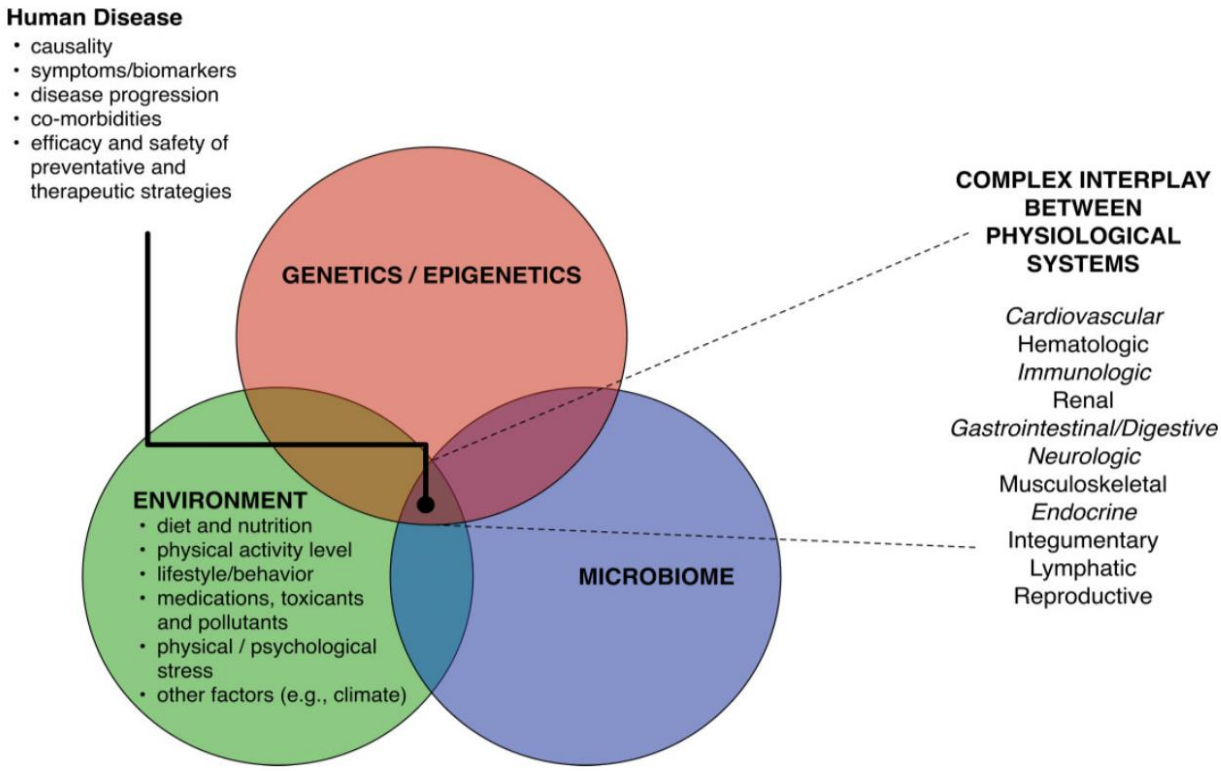

Figure 7. Swine Modeling - Intrinsic and extrinsic factors influence complex interplay of physiological systems in human disease. The complex interaction between genetics/epigenetics, environment and microbiome influences the (1) causality of human disease, (2) presentation of symptoms, (3) disease progression, (4) comorbidities, and (5) efficacy and safety of preventative and therapeutic strategies. The influence of the 3 factors is mechanistically mediated by the modulation of the interplay between multiple physiological systems [151].

Current NF1 Swine Models

The complexities of NF1 have necessitated the development of a more translatable animal model to accurately study the disease. Many physiological systems are affected by NF1, and the diverse presentation of clinical sequelae is likely driven by the interactions of the environment and the microbiome, which also need to be considered [151]. More closely modeling these influences will likely produce a better model for NF1. Genetically engineered

NF1 swine have only recently been created and are being validated at multiple research institutions, including the University of Wisconsin - Madison [1]. The validation of these NF1 swine models is an essential component to advancing the research goals of the NF1 community and has the potential to improve on many of the shortcomings that rodent models have. While NF1 mice model some aspects of NF1, none comprehensively models the disease nor its genetic underpinnings. NF1 swine models that have been recently developed reveal that they retain basic NF1 characteristics such as pigmentation abnormalities and tumor development, and most critically, neurofibromas [156]. They also present behavioral abnormalities and are amenable to advanced imaging technology like MRI [157]. NF1 swine models with multiple different mutations and species background as well as generational differences are making the swine even more comparable to human given the diversity of factors that influences NF1 disease in patients [158]. Along with the models, additional assessment will need to be developed in swine, particularly cognitive related aspects like nociception [159]. Nutritional and dietary considerations will also need to be evaluated [160].

NF1 Alternative Splicing in Swine

The difficulty of studying this complex gene and associated disease is further amplified by the genetic differences current animal models, namely rodents, have with humans [161]. Genetic studies in mouse models have helped reveal the role of splicing in neurological disease, but comparative analysis has revealed that pre-mRNA splicing of genes does not occur as frequently as it does in humans. Alternative splicing occurs in nearly all human genes but in as few as 63% of mouse genes [87]. With respect to NF1, mouse models differ in many key aspects, including in the number of *NF1* ASEs and expression of NF1

symptoms [85]. Conversely, the frequency of alternative splicing in swine suggests it is very close to humans [162]. Differences in alternative splicing between mice and humans may be why NF1 mouse models often display divergent phenotypes compared to humans [163]. Indeed, this may be a large part of why humans, despite having the same size genome and roughly the same amount of genes as mouse, display much more complex phenotypes [87]. Identification and characterization of swine *NF1* ASEs will be important in further validating swine as a relevant translatable model for NF1 research.

CHAPTER 2 -- Neuronal Differentiation of Swine Neurospheres and Adipose-derived Mesenchymal Stem Cells

2.1. Abstract

Swine models provide a premier research platform to facilitate translational biomedical research. Surgical techniques, pharmaceutical evaluation, studies of physiological disease, and the generation of human-compatible organs have benefited greatly from the increased utilization of biomedical swine models. Tissue culture methods for repairing, replacing, or regenerating tissues are also frequently developed using swine *in vitro* platforms. Mesenchymal stem cells (MSCs) derived from adipose tissue are an easily accessible cell source for generating a variety of therapeutically useful tissues and for cell-based mechanistic studies that retain high translatability to humans. Neurofibromatosis Type 1 is one such disease that is being increasingly modeled in swine, however, some cell culture systems have not been well validated. Optimization and validation of these *in vitro* methods is necessary to establish their viability as a relevant biomedical platform. In this study, MSCs were isolated from the backfat of swine and induced into non-adherent clusters of neural progenitors called neurospheres. These cells were also differentiated into Schwann cells and neurons to validate their use as a neuronal precursor cell source. Neurospheres were validated using morphometry analysis for diameter and sphere number, RT-qPCR to quantify expression levels of key neural progenitor markers (Nestin, Sox2, Oct4), and immunofluorescence to evaluate spatial distribution of neural progenitor proteins (Sox2, Oct4). Similarly, Schwann cells and dopaminergic neurons were evaluated for phenotypic changes in morphology, gene expression, and protein expression. Many neurosphere

induction protocols were systematically evaluated with variations in the culture surface, base media formulation, supplementations, growth factor concentrations (bFGF and EGF), and length of induction. One protocol was determined to be optimal for neurosphere induction with respect to gene expression, neurosphere size, and protein localization. These neurospheres were then compared to uninduced MSCs for use in neural differentiation. Compared to MSCs, neurons differentiated significantly better with respect to both morphology and gene expression of neuron markers MAP2 and TH. Schwann cells differentiated from neurospheres, however, they did not show enhancements in gene expression but did show increased expression of p75 and s100b compared to untreated MSC controls. *NF1* expression of alternatively spliced exon 12 increased significantly in these tissues and alternatively spliced exon 31 increased significantly in Schwann cells. These differentiation trends agree with those published using human tissues. Overall, these results establish an optimized protocol for inducing neurospheres and validate MSCs as a source for differentiating both Schwann cells and neurons *in vitro* from swine adipose tissue.

2.2. Introduction

Animal models are paramount to biomedical research. Many of the advancements made, from the molecular to the organismal level, have been made possible by using animal models. The Nobel Prize in Physiology and Medicine has been awarded to experimental studies dependent on animal research about 90% of the time [164]. Some of the most common animal models include Drosophila (fruit fly), Caenorhabditis elegans (nematodes), Danio rerio (zebrafish), Xenopus (frog), Mus musculus (mouse), Rattus norvegicus (rat), Canis familiaris (dog), Sus scrofa (swine), and Macaca mulatta (rhesus monkeys). The

ancient Greeks were among the first to use animals to study comparative anatomy and physiology [165], and their use as models for studying human physiology and disease increased dramatically beginning in the early 1900's [166, 167]. While many animal species could be used to better understand certain aspects of biology or disease pathology, an optimal choice can often be made depending on the scientific question, logistical constraints, and translatability of results [168].

Swine model use has increased markedly in the last 15 years according to the prevalence of published biomedical research articles [167]. The more nuanced and complex scientific biomedical inquiries become, the more important it is to use a model more concordant with human biology. Swine models can account for many of the physiological complexities found in humans due to their strong genetic, anatomical, physiological, and pathophysiological similarities and are free from many of the ethical issues associated with human tissues and non-human primates [151]. The lifespan, body composition, and phylogeny of swine are much more like human than other smaller animal models such as rodents. Swine are well suited for the preclinical evaluation of pharmaceutical and surgical interventions [169] and can be used to evaluate cell-based therapies with swine spinal cord injury models [170]. Complex non-communicable diseases like atherosclerosis and diabetes are also well modeled in swine [171]. Obesity, a physiologically complex manifestation of metabolic syndrome, is well modeled in swine and *in vitro* cell culture has provided insights into adipose development relevant to human [172].

Genetically engineered (GE) swine for agricultural use were first generated in the 1980's and recent improvements in embryo micromanipulation and genomic editing have facilitated the creation of GE biomedical swine for modeling cancer, atherosclerosis, cystic

fibrosis, and neurofibromatosis type 1 (NF1) [150, 173]. These GE swine models further broaden the biomedical utility of swine, especially with respect to genetic disorders that display complex phenotypes. NF1 is one such complex monogenic disorder for which swine models have become particularly useful [1, 157]. With such a variety of clinically identified mutations, *in vivo* and *in vitro* studies could greatly enhance basic understanding of the NF1 disease mechanism.

GE swine models also provide an opportunity to easily study the genetic and molecular characteristics of these genotypes using primary cell culture as opposed to immortalized or *in vitro* edited cell lines. However, primary culture of many cell types such as neurons is often not practical, therefore, developing a cell culture platform that uses easily obtainable stem cells and differentiates them into tissues of interest is desired. Establishing i*n vitro* cell culture methodology would complement *in vivo* and *ex vivo* studies being done using GE swine. Mesenchymal stem cells (MSCs) in many species are easily isolated from adipose tissue, offer an abundant source of stem cells with wide-ranging differentiation potential, and have been studied for use in several medical applications [174]. MSCs are frequently cultured *in vitro* and differentiated down a mesenchymal lineage to repair bone and cartilage defects or promote wound healing [175]. Other studies have used MSCs and transdifferentiated them to repair damaged nerves or heart tissues. Preclinical studies of safety and efficacy provide important information prior to conducting early phase clinical trials [176]. Successfully translating new potential therapies through the current regulatory framework and into a clinical setting is greatly enhanced by using relevant animal models [177]. The genetic, anatomical, and pathophysiological similarities of swine to human make them an optimal choice for validating these studies in both basic research and in a preclinical

setting. Most published studies use human-derived MSCs *in vitro* but swine-derived MSCs differentiation and induction protocols have not been as well developed despite their great potential as a preclinical model [178]. Validating methods for isolating, culturing, and differentiating MSCs into neural tissues in swine are useful to evaluate for safety and efficacy before using human MSCs in clinical practice.

Neurosphere culture is an *in vitro* cell culture strategy used to propagate neural stem cells and allows for more accurate modeling of cellular physiology *in vitro* [179]. A neurosphere culture system can be used to study neurological disorders and cancers that are otherwise too invasive and costly to study *in vivo* [180-182]. They are often used to evaluate the effect of various compounds in a controlled manner [183] and facilitate the large-scale production of neural stem cells used in cell replacement therapies [184]. Induction of neurospheres from cells like MSCs increases their multipotency, regenerative capacity, and trans-differentiation potential, particularly down neural lineages [185]. Cell culture protocols for adipose-derived MSCs are well established, however, there is less agreement between neurosphere induction, evaluation, and differentiation protocols. Among the published neurosphere inducing protocols in human, varied and even conflicting methods have been reported. Further, while some have been developed using human cells, few exist for swine. Research into cancer, neural development, and regenerative medicine would all benefit from an optimized neurosphere induction and validation protocol in swine.

Small alterations in the induction media leads to significant differences in their formation and multipotency, as evidenced by the current study. A literature analysis of neurosphere induction studies was conducted to provide a spectrum of media compositions and protocols commonly used [186-198]. These were organized according to certain

parameters (stem cell source, plating density, media composition, growth factor concentrations, and maintenance/passaging technique) and served as the basis for the neurosphere study. Adipose-derived MSCs were isolated from multiple swine and induced into neurospheres in a systematic manner under various conditions. Parameters used to validate neurospheres included measuring diameter, total number per well, and expression of neural progenitor markers [179, 199]. Finally, neurospheres were differentiated into neuronal cell types (dopaminergic neurons and Schwann cells) and evaluated for expression of neural markers. This work establishes standardized methodology for producing and validating neurospheres within a comprehensive *in vitro* platform for isolating, culturing, differentiating, and evaluating MSCs in swine.

2.3. Methods

Adipose-derived MSC Harvest

Experiments involving animals were conducted under protocols approved by the University of Wisconsin-Madison Institutional Animal Care and Use Committee in accordance with published National Institutes of Health and United States Department of Agriculture guidelines. Purebred conventional swine (Duroc x Landrace crosses) from the Swine Research and Teaching Center (UW-Madison, Wisconsin) were used to isolate MSCs from adipose tissues as recently described [200]. Immediately following euthanasia, adipose tissue (~30g) was excised from the neck backfat of swine and transported in DMEM with 2% Pen/Strep on ice to a sterile tissue culture hood. Each adipose sample was minced mechanically with a razor blade into $<3mm^3$ pieces and digested with 600 U/mL collagenase II (Sigma) in DMEM at 37^{o}C for 90 minutes on a 100 rpm shaker. The digested adipose was

centrifuged for 5 min at 500g after which the suspended lipids and supernatant were discarded. The remaining pellet was washed with DMEM, washed with RBC lysis buffer (Sigma), and then filtered through a 40 µM cell strainer. The cells were suspended in 10 mL of media consisting of DMEM/F12, 10% FBS, and 1% Pen/Strep and moved to a 10 cm tissue-treated culture dish in a 37ºC incubator with 5% CO2. The MSCs were passaged at least twice but fewer than ten times before being used for neurosphere induction or differentiation studies.

Neurosphere Induction

All neurosphere studies were performed in tissue-culture treated 24-well plates at 37ºC in a sterile incubator with 5% CO2. In most of the experiments, the culture surface was coated with a thin layer of sterile 1% agarose gelatin in DPBS. Premade 1% agarose gel was heated to boiling, quickly pipetted into each well to coat the entire surface, and immediately removed, after which the plate was allowed to completely solidify for at least 30 minutes. Neurosphere inductions were initiated with MSCs at 80-95% confluency. The MSCs in the culture vessel were rinsed with DPBS without ions, detached with 0.25% Trypsin on a 37ºC hotplate for 3 minutes, centrifuged into a pellet at 300 g, resuspended in 1 mL DPBS, and transferred into prepared 24-well plates at a density of 50,000 cells per well in 500 µL of neurosphere induction media. Cells were observed daily, and growth factors were replenished at full concentration on days 3, 6, and 10. 500 µL of additional media was added on day 3 and on day 8 if the neurospheres were not harvested.

Neurosphere Media Compositions and Conditions

The initial media composition and condition consisted of Neurobasal medium (ThermoFisher), 1% B27 supplement (ThermoFisher), 10 ng/mL epidermal growth factor (EGF, Sigma, E9644), 10 ng/mL basic fibroblast growth factor (bFGF, Sigma, F0291), and 1% Pen/Strep. MSCs in this culture media were induced for 8 days in agarose coated 24-wells. These average baseline conditions were determined from a literature search and pilot study [189]. To find an optimal induction protocol, several other media compositions and conditions were systematically evaluated in three sequential experimental groups. Group 1 varied the base media, supplements, or culture surface: DMEM/F12 replaced Neurobasal medium, 1% N2 supplement was added (ThermoFisher), B27 was replaced with 10% FBS, and wells were not coated with 1% agarose. After analysis of Group 1 data, the identified optimal condition was further modified in Group 2 experiments using various growth factor concentrations of EGF and/or bFGF: no growth factors, no EGF, no bFGF, 1 ng/mL of each, 20 ng/mL of each, 40 ng/mL each, 10 ng/mL EGF with 40 ng/mL bFGF, and 10ng/mL bFGF with 40 ng/mL EGF. Following analysis from Group 2, the new optimal condition was then used in Group 3 experiments that varied the total time of neurosphere induction: 3 days, 6 days, 10 days, and 12 days. Each experimental media group was performed in six replicate wells and each 24-well plate contained six replicate control wells.

Neuron Differentiation

Dopaminergic neuron differentiation was initiated with either MSCs or optimally induced neurospheres dissociated into single cells and performed in triplicate for each condition (Figure 8) [201]. On day 0, cells were plated in 24-well plates coated with poly-d-

lysine at a density of 25,000 cells per well and acclimated in neuron differentiation media with 1% FBS to facilitate attachment to the plate. Neuron differentiation media consisted of Neurobasal media with 1% B27 and 1% N2 supplement plus 10 ng/mL EGF, 10 ng/mL bFGF, 50 ng/mL BDNF, and GDNF. A half media change was performed every other day using complete differentiation media without FBS. Images were taken every four days and the experiment was ended after 14 days when the cells were harvested or submitted for immunofluorescence staining.

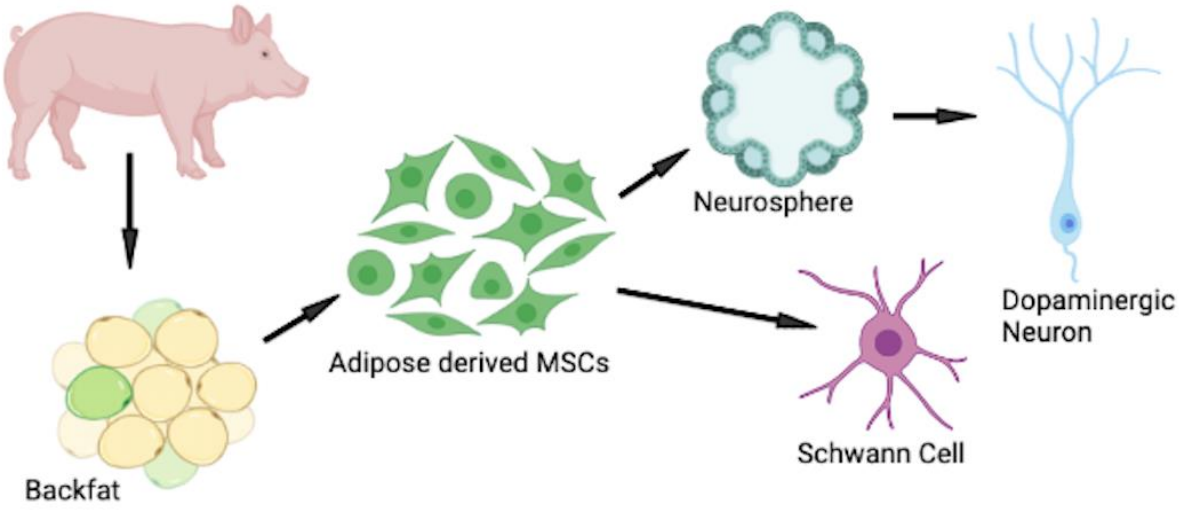

Figure 8. Neuronal Differentiation - Cell culture workflow for differentiation of Dopaminergic neurons and Schwann cells.

Schwann Cell Differentiation

Schwann cell differentiation was initiated with either MSCs or optimally induced neurospheres dissociated into single cells (Figure 8). A series of induction and differentiation medias were used as recently described [202]. On Day 0, cells were plated in tissue-culture treated 6-well plates at a density of 100,000 cells per well and acclimated in normal MSC media to facilitate attachment to the plate. On day 1, cell media was changed to DMEM plus 1 mM B-ME. On day 2 cell media was changed to DMEM with 10% FBS plus 3.5 ng/mL of

retinoic acid. Retinoic acid was added again on day 3 and 4. On day 5, cell media was changed to Schwann differentiation media consisting of DMEM with 10% FBS plus growth factors: 5 uM forskolin, 5 ng/mL PDGF, 10 ng/mL b-FGF, and 200 ng/uL heregulin-b1. Every four days a passage and full media change was performed and every other day a half media change was performed. Images were taken every four days and was continued to day 14 when the cells were harvested or submitted for immunofluorescence staining.

Morphometric analysis

Morphometric analysis was performed using Gen5 software on the Cytation 5 cell imaging multi-mode reader (BioTek). Prior to imaging, 500 µL of glycerol was gently layered on top of the media to stabilize neurosphere movement and allow for precise composite stitching of multiple images. 100 brightfield images were taken at a 4x magnification for each well and stitched together to create a single composite image. Programmed settings allowed the cellular analysis software module to automatically calculate average size (diameter) and number of neurospheres per well from the composite image. The software occasionally overestimated the number of neurospheres due to non-spherical formations and a manual adjustment was made with visual verification and count before final calculations and statistical analysis.

RT-qPCR

Immediately following imaging for neurospheres, Schwann cells, and neurons, mRNA was extracted for RT-qPCR analysis. Neurospheres from two replicate wells, neurons from two replicate wells, or Schwann cells from a single 6-well were transferred to a

centrifuge tube, washed with 1mL DPBS, centrifuged for 5 minutes at 500g into a pellet, and resuspended in 500 µL of Triazol. After 5 minutes of digestion, the medium was passed through a 25-gauge needle ten times. Total mRNA was extracted using the miRNeasy Mini Kit (Qiagen) and a total of 3 samples per experimental group were isolated. mRNA extraction was also performed on MSCs taken directly from monolayer culture as a baseline control. cDNA libraries were made using iScript cDNA Synthesis Kit (BioRad), prepared with iTaq Universal SYBR Green master mix (BioRad), and submitted for RT-qPCR in the CFXconnect Real-Time PCR Detection System (BioRad). Primers for control genes (RPL4, TBP, PPIA and/or b-actin) were used for each sample and performed in triplicate. Neurosphere specific primers targeted Nestin, Oct4 (encoded by POU5F1), and Sox2 (encoded by SRY-box transcription factor 2). Neuron specific primers targeted MAP2, NeuN, and TH. Schwann specific primers targeted p75, S100, Pitx3, and Ngn2. Primers targeting *NF1* and associated splice transcripts were also used in some experiments and are detailed in Chapter 3.

Immunocytochemistry

The optimal neurosphere induction was repeated and performed along with two variations. Condition 1 (MSC media) included DMEM/F12 with 10% FBS; Condition 2 (NB media) included Neurobasal medium and 1% B27 supplement; and Condition 3 (Optimal Media) included Neurobasal medium, 1% B27 supplement, 1% N2 supplement, 20 ng/mL EGF and 20 ng/mL bFGF. All neurospheres were induced in 1% agarose coated 24-well plates for 8 days. At the end of the induction period, these neurospheres were frozen in OCT compound (Tissue-Tek®) in a single layer, sectioned into 15 µM slices using a cryostat

(Leica CM3050S), and mounted on imaging slides [203]. Rabbit anti-Oct4 (1:100, Abcam, ab18976) and mouse anti-Sox2 (1:200, Abcam, ab79351) antibodies were used in conjunction with Alexa Fluor 430 goat anti-mouse (ThermoFisher) and Alexa Fluor 594 goat anti-rabbit (ThermoFisher) following Abcam guidelines. Blue Hoechst (1:1000, ThermoFisher) was applied for nuclear staining. Representative images capturing the spectrum of protein expression and localization were taken with the BioTek Cytation 5 cell imaging multi-mode reader using GFP, RFP, and DAPI filter cubes. Colocalization analysis was performed for the sectioned and fluorescently stained neurospheres. The Coloc2 plugin for ImageJ was used to generate a Pearson correlation coefficient for each pair of colors (Green/Oct4 vs Red/Sox2, Green/Oct4 vs Blue/Hoechst, Red/Sox2 vs Blue Hoechst). For each media condition 6 to 9 images were taken, and statistical analysis was performed using ANOVA and Tukey's post-hoc analysis to determine significance.

Schwann cell and neurospheres were washed with DPBS and fixed in their respective tissue culture wells following Abcam guidelines. Primary antibodies used for neurons included rabbit anti-TH and mouse anti-MAP2 (Abcam). Primary antibodies used for Schwann cells included rabbit anti-p75 and mouse anti-S100 (Abcam). The same secondary antibodies and imaging systems were used for all immunofluorescence experiments.

2.4. Results

Neurosphere Morphometry

Three sequential neurosphere experiments were conducted. All induction protocols began with 50,000 cells in 24-wells. In group 1, the N2 condition was statistically different with both a larger average diameter and fewer neurospheres than the condition without

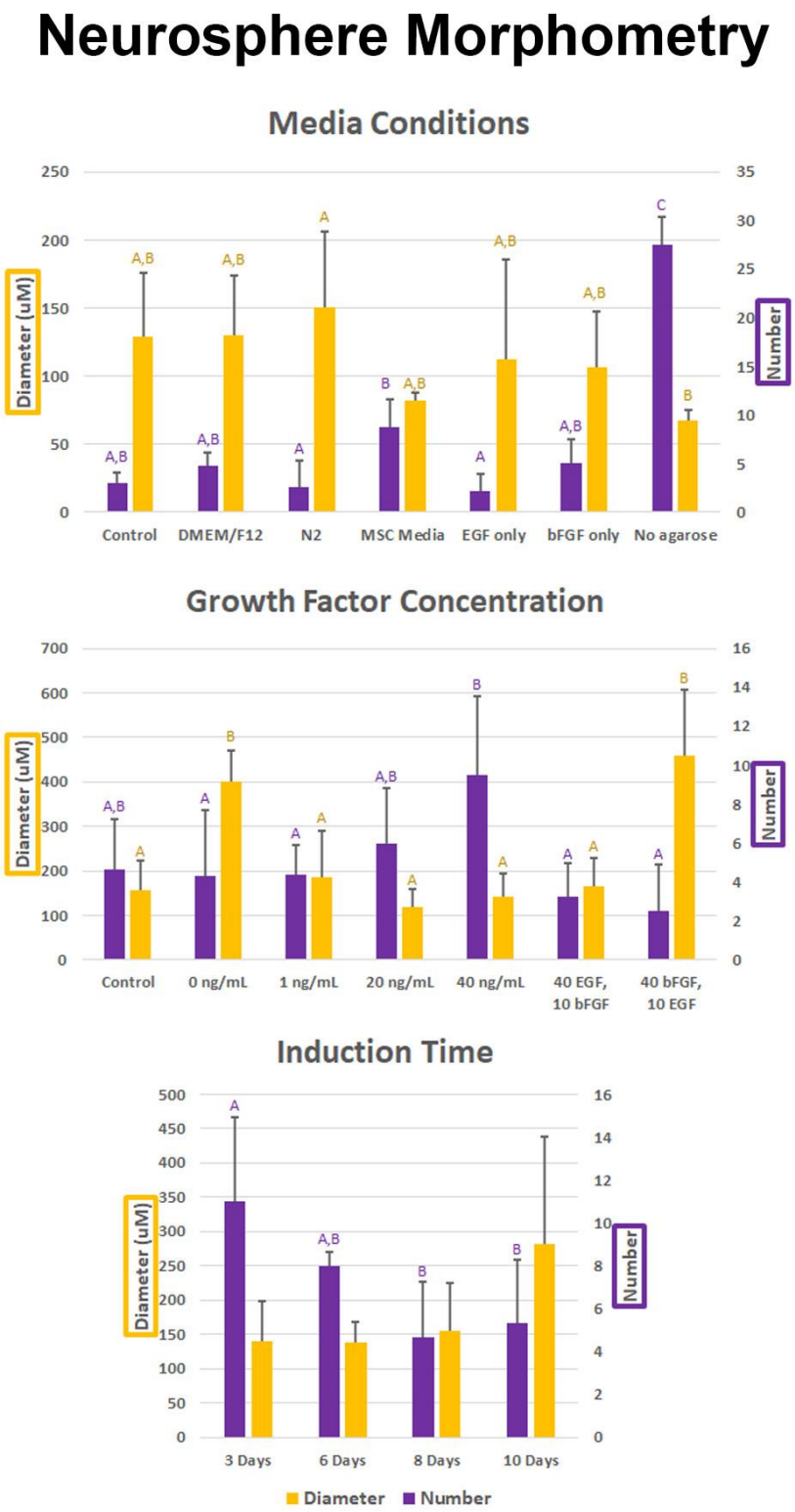

Figure 9. Morphometry - Average neurosphere diameter and total neurospheres induced per media condition (n=6 per condition). Significant differences ($p<0.05$) between conditions within the same experimental group are denoted with a pairwise lettering scheme.

agarose (Figure 9). The N2 condition also produced fewer neurospheres than the MSC media. In group 2, conditions with no growth factors and high bFGF with low EGF produced neurospheres with diameters greater than 250 uM (Figure 9). In group 3, a general trend was observed as induction time increased; fewer diameter neurospheres were observed, suggesting a gradual merging of spheres over time (Figure 9). No other conditions produced statistically significant differences in terms of neurosphere diameter or number. Overall, the average neurosphere induction condition produced 5 neurospheres with a diameter of 200 µM.

Neurosphere Gene Expression

The neurospheres from the same three sequential neurosphere experiments were also evaluated for gene expression of Nestin, Sox2, and Oct4. Group 1 conditions were all normalized to the control group. Results indicated N2 supplement condition, as a whole, increased all neural progenitor markers most significantly (Figure 10). Induction with DMEM/F12 was the second-best condition and increased all markers but not as significantly. Induction with MSC culture media and only bFGF increased Oct4 and Sox2 but not Nestin. Conditions with no agar coating and only EFG showed modest increases in gene expression. Group 2 experiments were normalized to the same control group conditions but now containing N2 supplement. The condition with 20 ng/mL of each growth factor showed the greatest increased Oct4 and Sox2 expression followed by the condition without any growth factors. The other conditions showed very little increase in Oct4 and Sox 2 but did show a small but significant increase in Nestin (Figure 10). Group 3 experiments

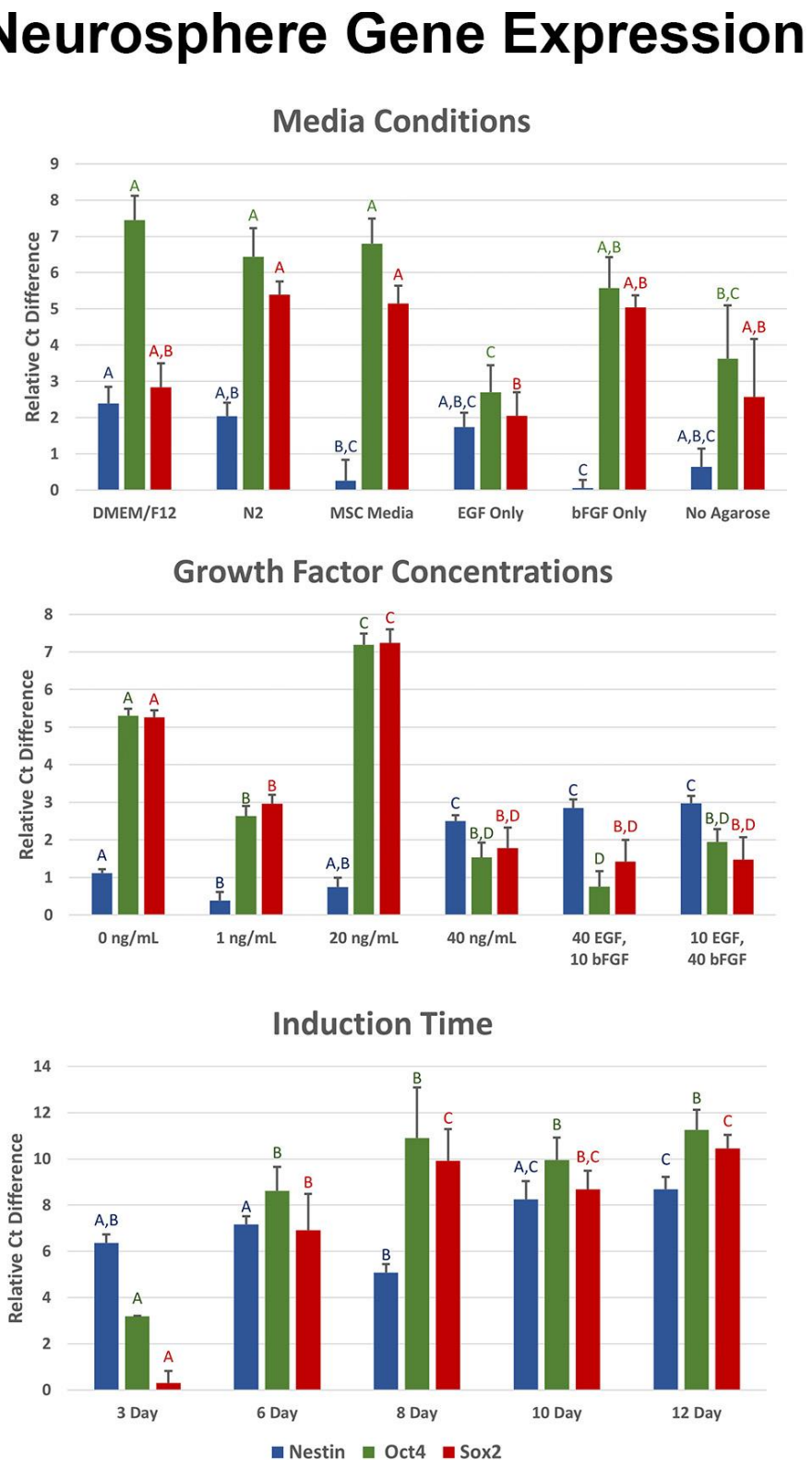

Figure 10. Gene Expression - Gene expression for several neural progenitor markers was determine via RT-qPCR normalized to the respective group control (n=6 per condition). Significant differences ($p<0.05$) between gene expression within the same experimental group are denoted with a pairwise lettering scheme.

demonstrated Oct4 and Sox2 were not strongly upregulated until day 6 and then continued to increase through day 12 (Figure 10). Nestin did not vary significantly over time until it was modestly upregulated on day 12.

Neurosphere Immunofluorescence

Protein localization can provide information about expression variations within cells or tissue structures. Colocalization of protein markers between three evaluated media formulations shows differences in nuclear distribution within cells and cellular distribution between cells within neurospheres (Figure 11). The degree of colocalization was evaluated by calculating Pearson correlation coefficients between each of the three fluorescent signals using single, independent data points from six to eight images per condition. Coefficient values ranged from 0.51 to 0.96 with higher numbers indication greater colocalization. An increase in Oct4 and Sox2 colocalization is seen within centrally located cells and in neurospheres induced with MSC media (A) as indicated by the increased yellow coloring (Figure 12). Optimal induction media (C) showed Oct4 colocalized with the blue nuclear stain throughout the neurosphere as indicated by cyan coloring. Finally, neurosphere induction without growth factors (B) showed the lowest amount of Sox2 colocalization within the nucleus indicated by a lower amount of purple coloring.

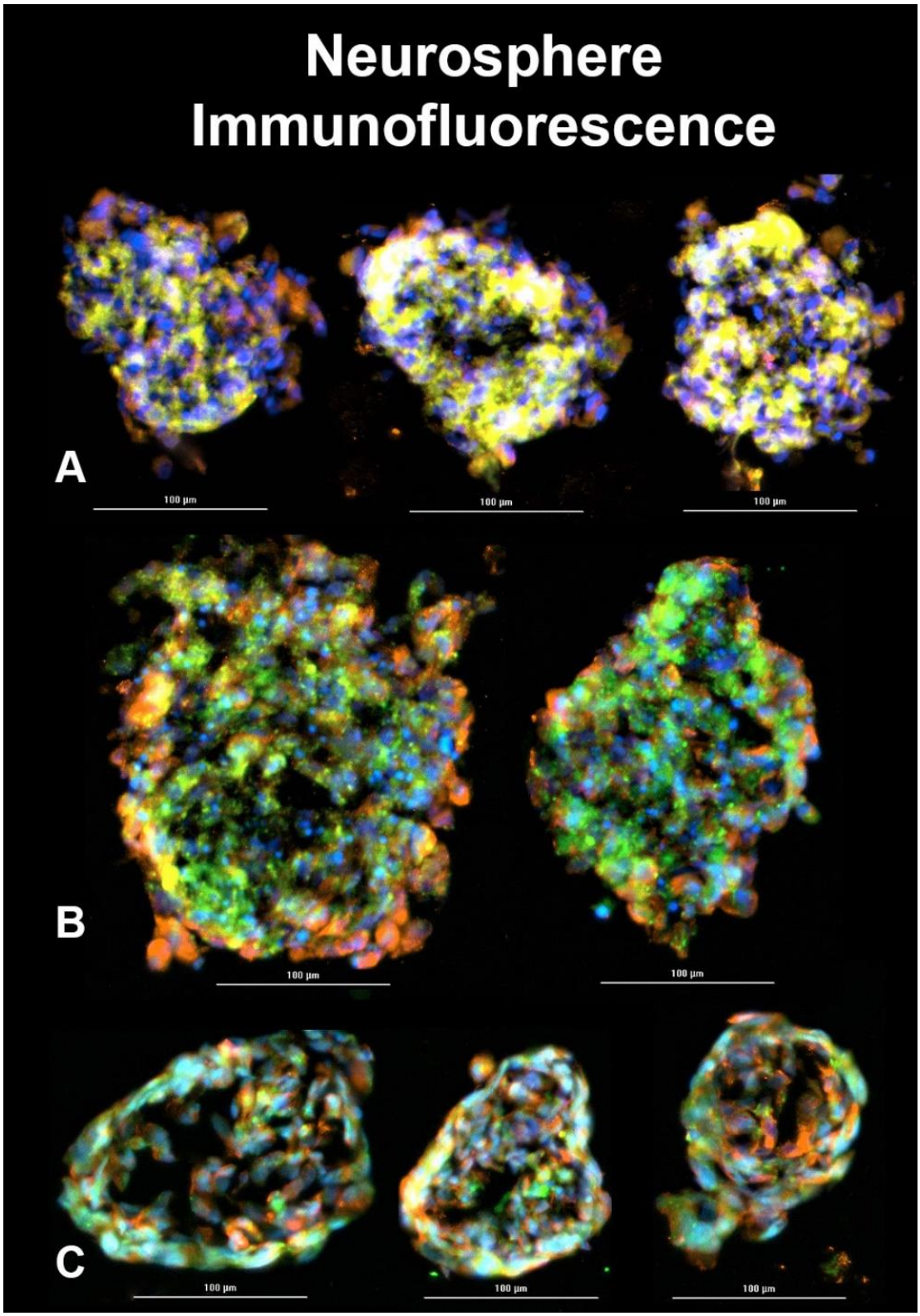

Figure 11. Immunofluorescence - Neurospheres induced with three induction medias (A - MSC Media Only, B - Neurosphere Media without GFs, C – Optimal Neurosphere Media) were compared for protein expression of two neuronal precursor markers. Green – Oct4, Red – Sox2, Blue – Hoechst. Bar represents 100 uM.

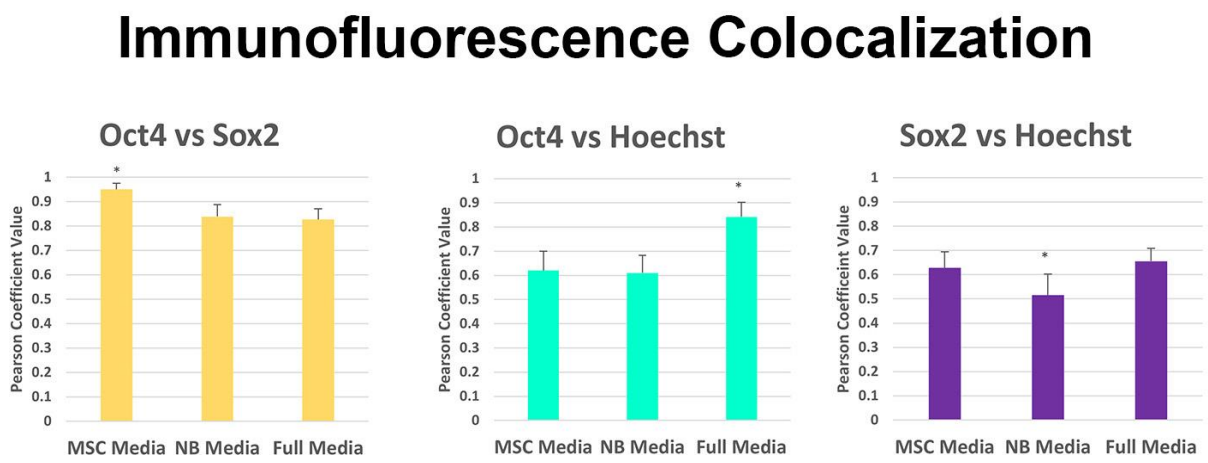

Figure 12. Colocalization – Pearson correlation coefficient values of colocalization were calculated with immunofluorescent images obtained after neurosphere induction using three induction medias (MSC Media Only, Neurobasal Media without GFs, Optimal or Full Neurosphere Media) (n=6 per condition). Statistically significant differences in colocalization of fluorescent staining markers are indicated with asterisks (* p<0.05).

Neuronal Differentiation

Neurospheres can enhance neuronal differentiation compared to MSCs. Dopaminergic neurons differentiated from neurospheres showed significantly higher expression of tyrosine hydroxylase (TH), a key dopamine precursor, than from MSCs (Figure 13). While other markers were not significantly different, the trends indicated neurospheres gene expression patterns were closer to those expected than neurons derived directly from MSCs. Immunofluorescence also revealed increase TH expression in neurospheres versus MSCs (Figure 14). While not indicated by gene expression, microtubule associated protein 2 (MAP2) expression was faintly observed near the nucleus of the neurosphere derived neurons but not those derived from MSCs. Dendrite projections were significantly longer in neurosphere derived neurons and exhibited a greater degree of bipolar formation (Figure 14). Schwann cell

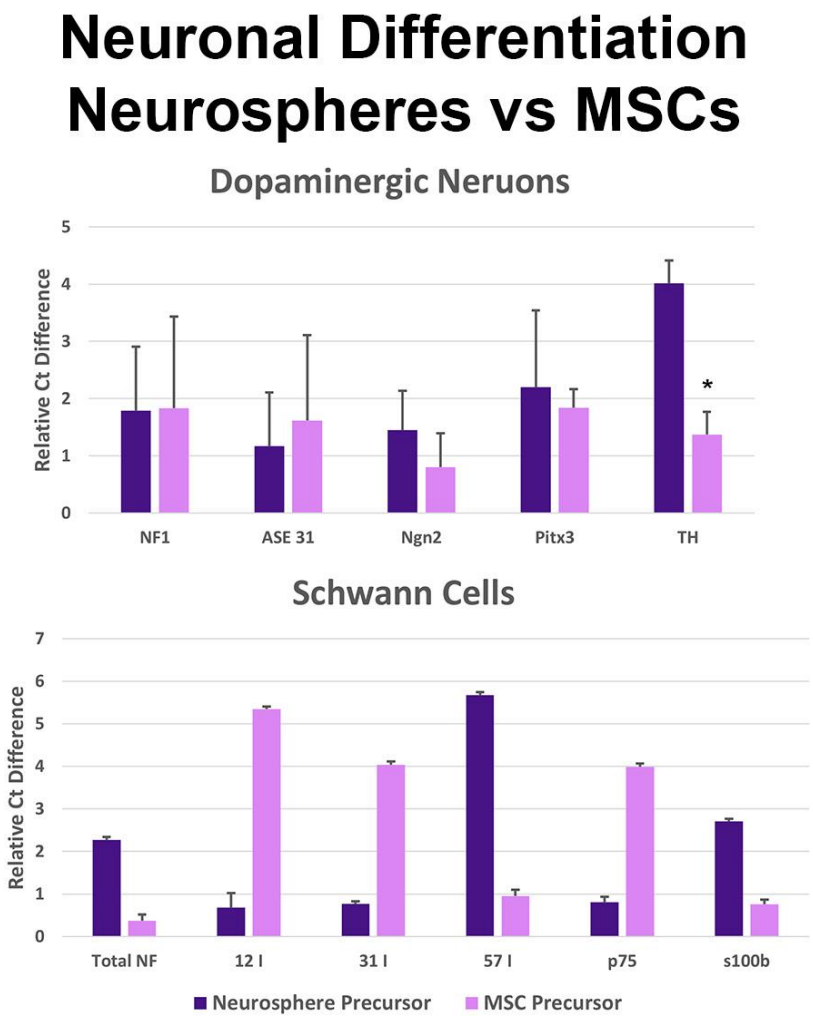

Figure 13. Neuronal Differentiation - Dopaminergic-like neurons (n=3) and Schwann cells (n=1) were differentiated from MSCs or neurospheres derived from MSCs. Gene expression was normalized to an undifferentiated MSC control. Statistically significant differences in gene expression are denoted with an asterisk for neurons (* p< 0.05). One replicate sample was assayed for each Schwann cell condition and error bars represent technical standard error and are all significantly different (p<0.05).

differentiated from neurospheres did not enhance the expected gene expression patterns except with respect to s100b (Figure 13). With respect to *NF1* expression, Schwann cells showed an increased expression of Total *NF1*, AIE12 and AIE 31. Neurospheres and neurons showed increased expression of AIE 12 only (Figure 15).

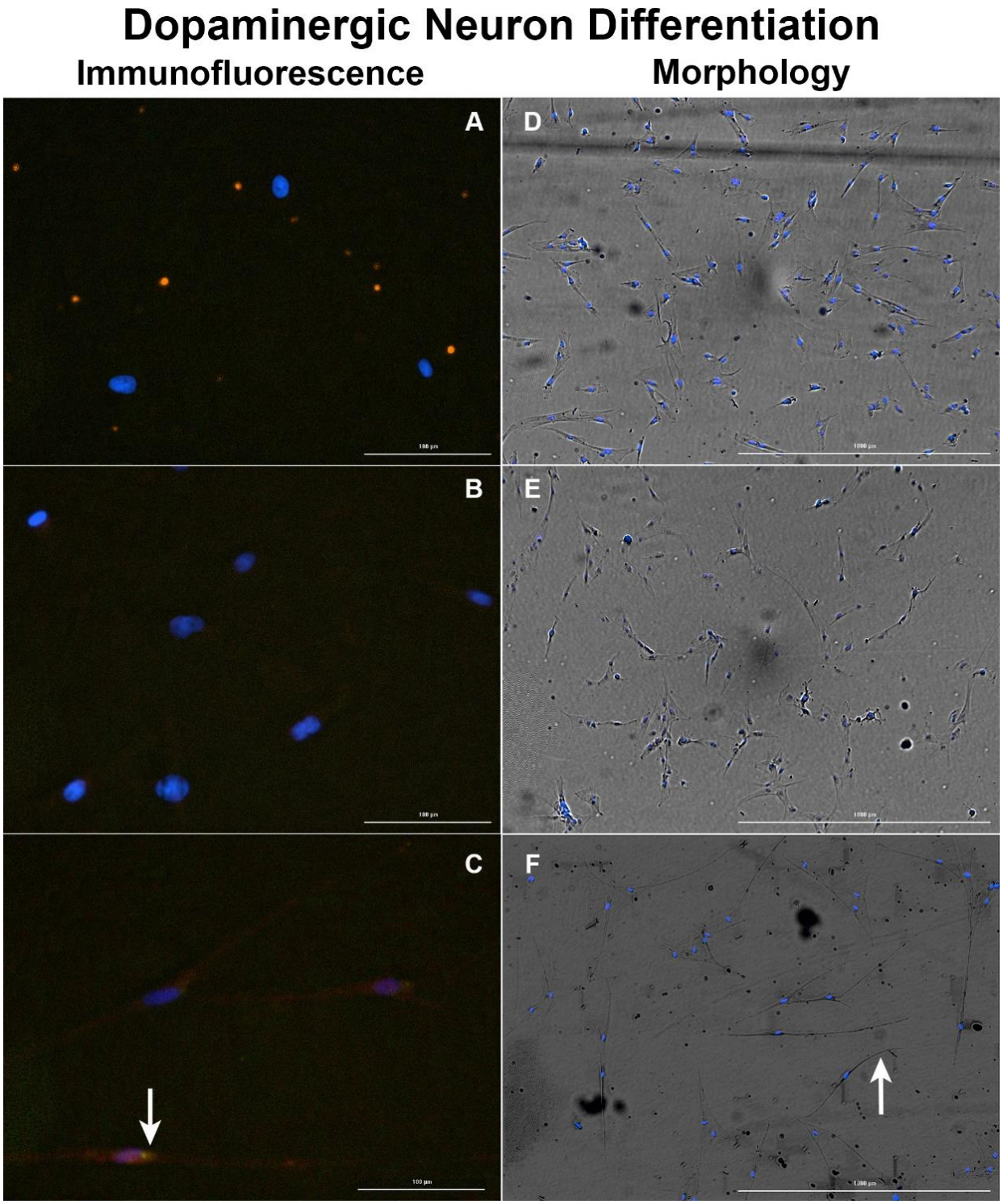

Figure 14. Neuron Morphology - Dopaminergic neurons differentiated from both MSCs and neurospheres were stained for MAP2 and TH expression. Left panel - 20x images merge fluorescent channels together (Green – MAP2; Red – TH; Blue – Hoechst). Right panel – 4x merge brightfield and Hoechst images. Arrow in C indicates distinct difference in nuclear MAP2 expression. Arrow in F indicates bipolar, axonal projection. (A,D – MSC control; B,E – Neurons from MSCs; C,F – Neurons from neurospheres)

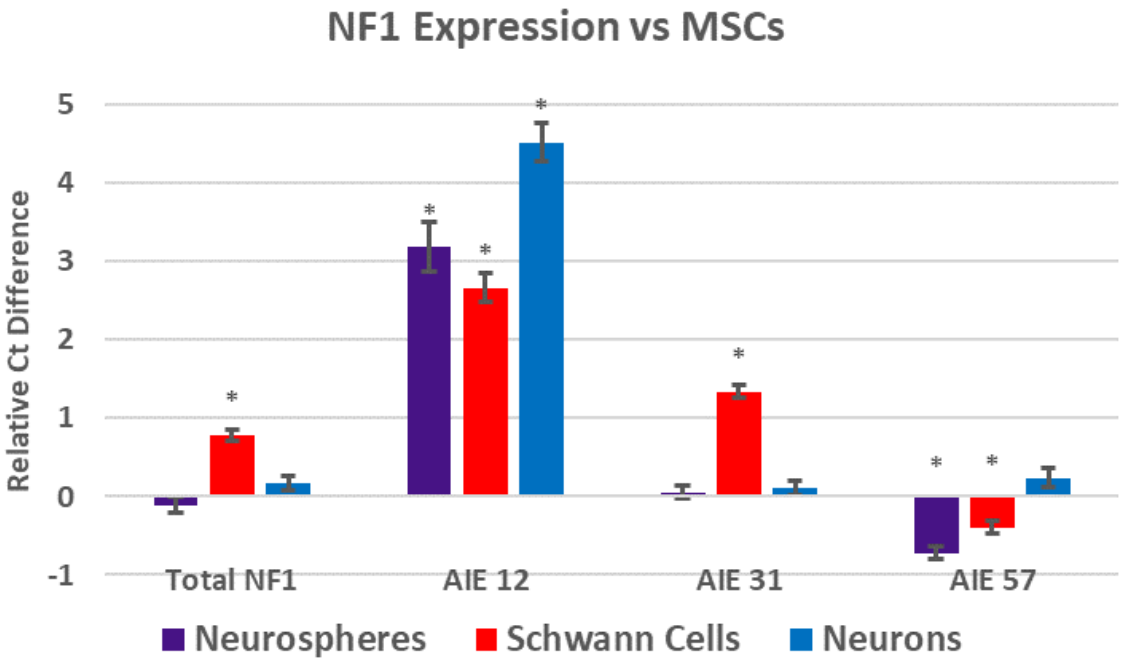

Figure 15. *NF1* ASE Expression - Neurospheres induced from MSCs, Schwann cells differentiated from MSCs, and dopaminergic neurons differentiated from neurospheres were assayed for mRNA expression levels of Total *NF1*, AIE 12, AIE 31, and AIE 57 (n=3 for each cell type). All values are relative to the undifferentiated and uninduced MSC control. Statistically significant gene expression relative to the MSC control is denoted with an asterisk ($p<0.05$).

2.5. Discussion

The neurosphere induction study determined an optimal protocol for inducing neurospheres and demonstrated the importance of proper media formulation, growth factor concentration, and induction time. An optimal neurosphere induction protocol for 50,000 adMSCs consists of using 500 uL of neurobasal medium with 1% B27, 1% N2, 20 ng/ml of EGF, 20 ng/mL bFGF, a 1% percent agarose gel coating a 24-well surface and cultured for 8 days with growth factors refreshed every 3 days. This protocol provides the greatest expression of key multipotent markers [204], appropriate localization of gene expression [205], and ideal sized neurospheres [206]. Further, this induction protocol was able to

enhance dopaminergic neuron differentiation of MSCs by increasing axonal projections, increasing mRNA expression of TH, and increasing protein expression of TH and MAP2. Longer differentiation periods may increase differentiation markers further. The results show that swine is a suitable model organism for the study of neurosphere induction and neural differentiation from adipose derived MSCs. Beyond basic science studies in cell development, research into therapeutic applications for cell transplantation could also benefit from these optimized protocols.

The expression of three well established markers of neural progenitors was used to validate neurosphere induction. Sox2 (SRY-related HMG-box gene 2) is linked with the inhibition of neuronal differentiation and has been shown to act as an important transcriptional factor to maintain the self-renewal capability of embryonic stem cell [207]. Oct4 (octamer-binding transcription factor 4), a known binding partner of Sox2, is also a key regulator essential for the maintenance of pluripotency and self-renewal of stem cells [205]. The intermediate filament protein Nestin (neuroectodermal stem cell marker) is widely accepted as a marker of neural stem cells and is found to be abundant in embryonic stem cell-derived progenitors that have the capability to develop into multi-lineages [208]. Expression of these markers in cells or tissues strongly suggests the presence of neural stem cells or cells with neurogenerative potential and is a primary benefit of neurosphere induction [209] [210].

This study shows media composition, growth factor concentration, and culture time all have significant effects on neurosphere induction and the expression of neural progenitor markers. Growing MSCs in suspension via agarose coating with growth factors or FBS was enough to significantly increase marker expression, with the N2 media formulation being slightly better overall. Conversely, the control induction media did not induce marker

expression as strongly when the cells were adhered to the plate surface. This could be due to the decreased cell-cell contact or due to the 3-D nature of suspension culture. 3-D culture is thought to better model the physiological influences of the *in vivo* environment [211, 212]. Media without bFGF did not significantly increase any of the markers while media without EGF increased all markers except Nestin. EGF and bFGF are known to increase the proliferation of MSCs and enhance the differentiation potential towards neural lineages, respectively [213]. While proliferation rates were not measured in this study, bFGF appears to influence neural progenitor markers expression more strongly. Doses both above and below the initial control dose of 10 ng/mL of each growth factor was shown to have positive induction effects as this significantly increased expression of all three markers. However, at the highest concentration of 40 ng/mL of growth factors a significant reduction in these markers was observed. Interestingly, media with no growth factors significantly increased gene expression. These patterns suggest a biphasic growth factor influence. This type of hormetic effect has not been reported for these growth factors but is frequently encountered in neuroscience [214]. Nerve growth factor, for example, displays a biphasic effect in neural progenitor cells in a similar range of concentrations [215]. Possible mechanisms for these effects include the presence of both high and low affinity receptors [216], dose dependent receptor expression and internalization [217], and/or interaction of competing internal pathways [218]. These results demonstrate the importance of precise growth factor concentration and is a key finding of this study.

Gene expression was also influenced by induction time in a positive manner. The longer the induction time, the greater the expression of neural progenitor markers. While three days was not enough time to increase all markers, they did all increase significantly by

six days. This suggests that neurosphere induction could reasonably be terminated at six days if a modest gene expression increase is the only criteria being considered.

Gene expression of Oct4 and Sox2 was generally modulated together and to a greater degree than Nestin. Oct4 and Sox2 have known interactions, so this is not unexpected. Nestin is known to increase during the early stages of neural differentiation and thus its expression may not be as pronounced during neurosphere induction, which is a de-differentiation or trans-differentiation process. Immunofluorescence indicated that Oct4 and Sox2 were highly colocalized overall, but to a significantly greater degree in neurospheres induced in normal MSC media. However, when optimal neurosphere media was used, Oct4 localized to the nucleus and decoupled from Sox2. This suggests that Oct4 localization plays a significant role in neural progenitor induction. It has been shown that nuclear localized activity of Oct4 is needed to induce cellular reprogramming [219]. Thus, nuclear localization of Oct4 in the optimal neurosphere media is important for neurosphere induction and cannot otherwise be determined simply by evaluating gene expression levels.

The increased expression of neural progenitor markers alone is not sufficient validation for the entire neurosphere as only portions of the cells may have this expression profile. Heterogenous neural progenitor populations are often produced during neurosphere induction if spheres become too large [220]. The maximum healthy neurosphere diameter has been determined to be about 250 μm, with larger sizes leading to cell necrosis within the center of the spheres [206]. This study shows that specific media composition and culture parameters help ensure acceptably sized neurospheres are produced. Spheres larger than 250 μm were produced in conditions that had no growth factors, had high levels of bFGF (40 ng/mL), and were induced for longer than 8 days. If gene expression alone was considered,

each of these conditions may appear to induce optimal neurospheres, however, given the heterogenous mixture and potential of necrotic core development, only the optimal neurosphere formulation determined in this study best fits all validation criteria. It should be noted that if large neurospheres are found prior to the final days of induction, sub-passaging the neurospheres through gentle enzymatic and mechanical dissociation is an acceptable way to maintain optimal induction and could be performed before this size threshold is surpassed [221].

Neurons can be difficult to culture from living tissue and usually require euthanizing the subject. Differentiating neurons from easily acquired stem cell sources could alleviate this difficulty. Dopaminergic neurons differentiated from optimally induced neurospheres also further validated the induction protocol. Compared to neurons differentiated from MSCs, neurosphere derived neurons displayed significantly greater levels of TH, an important dopamine precursor. These neurons also had higher expression of *NF1* AIE 12 but not AIE 31 or 57, as would be expected in cell with a dopaminergic phenotype. Immunofluorescence confirmed the increase in TH and demonstrated a weak nuclear signal of MAP2. While MAP2 was not detected in the RT-qPCR assay, this marker is associated with mature neurons and the differentiation process may need to be extended to detect significant changes in expression of this marker. Brightfield images of neurosphere derived neurons revealed significantly longer dendritic projections in a bipolar formation. This was distinct from the MSC derived neurons and undifferentiated MSCs which did not display these morphological phenotypes. Schwann cells were also differentiated from neurospheres and MSCs, however, the MSCs produced a better gene expression profile than the neurospheres. The Schwann cell differentiation protocol used in this study was initially

developed for MSCs and thus may not be taking advantage of the neurosphere induction. Other studies have shown neurospheres can be used for Schwann cell differentiation and future studies could be performed to compare these different protocols [196].

Having established a swine cell culture differentiation platform, these induction and differentiation protocols were used to evaluate *NF1* ASE expression of the various cell types. Compared to MSCs, *NF1* AIE 12 was upregulated in all of them, that is in neurospheres, Schwann cells and dopaminergic neurons. This ASE is associated with many neuronal cell types and particularly mature neurons. *NF1* AIE 31 was upregulated in Schwann cells and is congruent with known expression levels in human tissues. *NF1* AIE 57 is not associated with neuronal phenotypes and was only slightly decreased. These expression patterns of *NF1* further validates the platform as well as the translatability of swine cells for studying *NF1* ASE expression *in vitro*.

Animal models serve a valuable role in advancing research at a preclinical and basic science level. Tissue engineering platforms and cell-based therapeutics continue to be developed in relevant animal models and have led to expanded treatment strategies for a variety of medical conditions and diseases [222]. *In vitro* cell culture platforms are a critical component of this research pipeline and can be used to increase basic knowledge of the molecular and genetic mechanisms of disease. Adipose tissue is a particularly attractive sources for obtaining stem cells due to being easily accessible with minimally invasive procedures and retaining a high degree of multipotency [223]. When combined with scaffold biomaterials, these MSCs can be used for regenerating tissues like cartilage, tendons, ligaments, and bones, and can also enhance spinal cord rehabilitation following injury [174]. Enhanced characterization of adipose derived MSCs and further optimization of these tissue

culture protocols increase their value for many therapeutic and research applications. Mouse models have been used to study neurological conditions such as spinal cord injury and genetic diseases such as Neurofibromatosis Type 1, however, they have not shown the same efficacy in human preclinical trials due to translational limitations [224]. Using a model system that preserves key translational components increases the probability of success in clinical trials. Overall, this study provides validation for using swine cell culture protocols as a translatable platform to study human disease and develop potential therapies.

CHAPTER 3 -- *NF1* Alternatively Spliced Exon Regulatory Regions and Expression Patterns in Swine Tissues

3.1. Abstract

Neurofibromatosis type 1 (NF1) is a common monogenic disorder that can cause a variety of symptoms including skin lesions, cardiovascular abnormalities, skeletal deformations, and nervous system tumors, however, the mechanisms driving its complex presentation are largely unknown. Alternative splicing dysregulation is known to be involved with some aspects of tumorigenesis but has not been comprehensively studied in NF1 and may help explain the broad range of symptoms that are differentially manifest. Swine models have recently been developed to study NF1 and to serve as a translational platform for the evaluation of therapies, but it is not known if swine *NF1* expression is congruent to human. In this study, seven alternatively spliced exons (ASEs) homologous to human were identified in swine. Next, the mRNA expression levels of the ASEs were evaluated using RT-qPCR in several tissues from swine of two different ages. Finally, splicing regulatory regions for three ASEs were predicted and expression levels modulated *in vitro* using splice-switching oligonucleotides. RT-qPCR and Sanger sequencing of the swine ASE regions indicated six of the ASEs to be expressed in swine. ASE 13 was not found in any mRNA transcripts due to the addition of a single nucleotide in the otherwise homologous exonic sequence. *NF1* ASE expression profiles in different tissues revealed significant differences in ASE 12, 31, and 57, similar to those described in human. mRNA transcripts excluding *NF1* exons 4, 44, and 51 were also found to be expressed at low levels in all tissues with some statistically significant differences. Regulatory regions were identified for ASEs 12, 31, and 57 and splice-switching

oligonucleotides targeting these sites showed efficacy in modulating their expression levels in adipose-derived mesenchymal stem cells *in vitro*. This is the first report characterizing and detailing *NF1* ASE expression levels and regulatory regions in swine. These results help validate swine as a genetically congruent NF1 model and reveal novel insights into the complexities of *NF1* alternative splicing.

3.2. Introduction

NF1 is a complex genetic disorder typically diagnosed in childhood. It displays complete penetrance by adulthood and is pleiotropic with variable expressivity [225, 226]. Cutaneous manifestations are seen in up to 99% of patients and may include café au lait macules, axillary freckling, dermal lipomas and neurofibromas, or Lisch nodules [227] [228]. More severe symptoms include cognitive and learning dysfunction, bone deformations, cardiovascular disorders, and nervous system tumors. These nervous system tumors are often characterized as optic pathway gliomas, spinal neurofibromas, brain gliomas, or plexiform neurofibromas [229]. Plexiform neurofibromas can also transform into a malignant peripheral nerve sheath tumor which carry a very poor prognosis. NF1 patients have about a 15% greater chance of developing malignancies compared to the general population [2].

NF1 is caused by mutations in the *NF1* gene and over 3,000 different mutations have been clinically identified [113]. Despite a thorough description of the mutational profile, knowledge of specific mutations has not led to identification of strong genotype-phenotype correlations and thus had not been a very useful prognostic indicator or therapeutic guide [230]. However, a more generalized positive correlation between *NF1* splice-site mutations and the incidence of developing brain gliomas, including malignant peripheral nerve sheath

tumors has been found [127]. Given that nearly 30% of *NF1* genotypes are known to negatively influence proper *NF1* mRNA splicing, endogenous alternative splicing may also play a critical role in NF1 pathology [231]. A relatively high number of alternatively spliced genes are expressed in the central nervous system and splicing misregulation is increasingly implicated in many neurological disorders, including NF1 [122]. Splicing dysfunction is also seen in many cancer types, especially in pediatric populations [232].

Most human genes undergo natural exon skipping at some level through a process called alternative splicing to produce different isoforms of an mRNA transcript. Regulation of exon-exon splicing is mediated by spliceosome recognition of splicing regulatory regions within the gene. For ASEs, regulation of this activity is critical for maintaining proper balanced expression of mRNA isoforms. Manipulation of splicing, and particularly ASEs, can be accomplished using antisense oligonucleotides that target splicing regulatory elements, also known as splice-switching oligonucleotides (SSOs) [136]. SSOs have been used to therapeutic ends for a few genetic conditions but can also be used more generally to identify the regulatory regions involved in splicing.

Human *NF1* contains 61 exons and at least 7 of them are alternatively spliced in mature mRNA transcripts [85]. These ASEs, along with the other constitutively expressed exons, combine to form the various *NF1* mRNA isoforms and are differentially expressed in all human tissues. The four most commonly identified ASEs are denoted 11alt12, 12alt13, 30alt31, and 56alt57 [86]. These ASEs can also be referred to as a12 or ASE 12 instead of 11alt12, etc… Other less commonly studied ASEs include exon 4, 44, and 51 and are found to be excluded in some transcripts. For clarity, the nomenclature used in this work distinguishes the whole body of *NF1* ASEs further into two subcategories: alternatively

included exons (AIEs) and alternatively excluded exons (AEEs). In the conventional *NF1* nomenclature, AIEs are given a suffix or prefix to distinguish them from the other, more constitutively expressed exons, which are simply referred to by number. The AEEs are numbered regularly amongst the rest of the constitutively expressed exons and when referred to in the context of alternative splicing are prefaced with the phrase AEE indicating they are among the normally numbered exons but are being discussed in the context of its alternatively spliced nature. Most *NF1* AIEs have been characterized to some degree but it is unclear how these ASEs, apart from perhaps AIE 31 [96, 126, 233], contribute to the various phenotypes observed in NF1 patients. Shifts in the relative expression of neurofibromin isoforms in specific tissues caused *NF1* mutations may differentially influence the phenotypic presentation of the disease and have yet unknown implications in tumor development.

Beyond some characterization in human and mouse, *NF1* ASEs apart from ASE 31 have not been well studied. Only a couple of studies have examined the effects of *NF1* alternative splicing modulation or identified their associated splicing regulatory regions [123, 143]. SSOs can be used to modulate alternative splicing or correct dysfunctional splicing and provide an effective tool to study *NF1* alternative splicing in a very specific way. Inhibition can be achieved by targeting a known splice site to interfere with splicing protein interactions or disrupting secondary RNA structures [129]. Similarly, targeting splicing silencer sequences can be used to enhance or restore exon inclusion by blocking other splicing proteins or recruiting acting splice factors [130].

Studies using mouse models have helped reveal the role of splicing in neurological disease. However, studies have also revealed that pre-mRNA splicing of genes does not

occur as frequently in mice as it does in humans. In mice, splicing occurs in as few as 63% of genes while almost all human genes undergo alternative splicing [87]. Differences in alternative splicing between mice and humans may be why NF1 mouse models often display divergent phenotypes compared to humans [163]. Studies suggest the overall frequency of alternative splicing in swine closely resembles that in humans [152]. Several swine models of NF1 have been recently developed in hopes that these models will recapitulate the disorder in humans better than existing rodent models and thus offer a more translational platform for the development of novel therapies [1]. Identification and characterization of swine *NF1* ASEs will be important in further validating swine as a relevant translatable model for NF1 research.

NF1 alternative splicing may be able to explain some of the complexity of the NF1 phenotype. However, *NF1* ASE tissue distribution and expression is not precisely known. Splicing regulatory regions are also not well studied further limiting studies into the nature of *NF1* ASEs function impacts. Swine could be used as a genetically congruent animal model but *NF1* ASEs have not been identified or characterized in any way. Doing so would open the possibility of using swine as an in vivo model for studying *NF1* ASE SSOs. In this study, the homologues of human *NF1* ASEs and the local genomic regulatory regions involved in *NF1* alternative splicing are identified in swine. Tissue- and age-specific expression patterns of *NF1* mRNA transcripts in many tissues are characterized with comparison to those in humans. SSOs are also used to modulate *NF1* ASE splicing to demonstrate the involvement of the identified target region in alternative splicing and to show swine can be used to study *NF1* ASE SSOs.

3.3. Methods

Identification of *NF1* ASEs and mRNA Transcripts in Swine

Experiments involving animals were conducted under protocols approved by the University of Wisconsin-Madison Institutional Animal Care and Use Committee in accordance with published National Institutes of Health and United States Department of Agriculture guidelines. Genomic DNA from two breeds of swine (Wisconsin Miniature Swine® and Landrace x Duroc crossbreds) were purified from blood samples using the Wizard Genomic DNA Purification Kit (Promega). Human genome assembly (GRCh38.p10) was aligned with the swine genome assembly (Sscrofa11.1) and congruent *NF1* exons were identified and numbered in accordance with current *NF1* nomenclature [1, 86]. Primers (Table 1) were designed targeting the intronic regions surrounding these exons and PCR amplicons were made using Phusion High-Fidelity DNA Polymerase (ThermoFisher) and submitted for Sanger sequencing. AIEs were compared directly with those found in humans. AEEs were confirmed to be excluded by ascertaining the presence of an mRNA transcript sequence in multiple swine tissues that skips the targeted exon.

Quantification of Age- and Tissue-specific *NF1* ASE Expression

Swine aged 2 days (n=2 females, n=3 males) and 180 days (n=6 females) were euthanized by cardon dioxide asphyxiation or electrical stunning and exsanguination, respectively. Immediately following euthanasia, multiple tissues were excised, placed into DNA/RNAse-free microcentrifuge tubes, and snap frozen in liquid nitrogen to preserve mRNA transcripts. Tissues were generally selected based on having known associations to NF1 symptomatology (Figure 16). Isolation of mRNA was performed using one of two

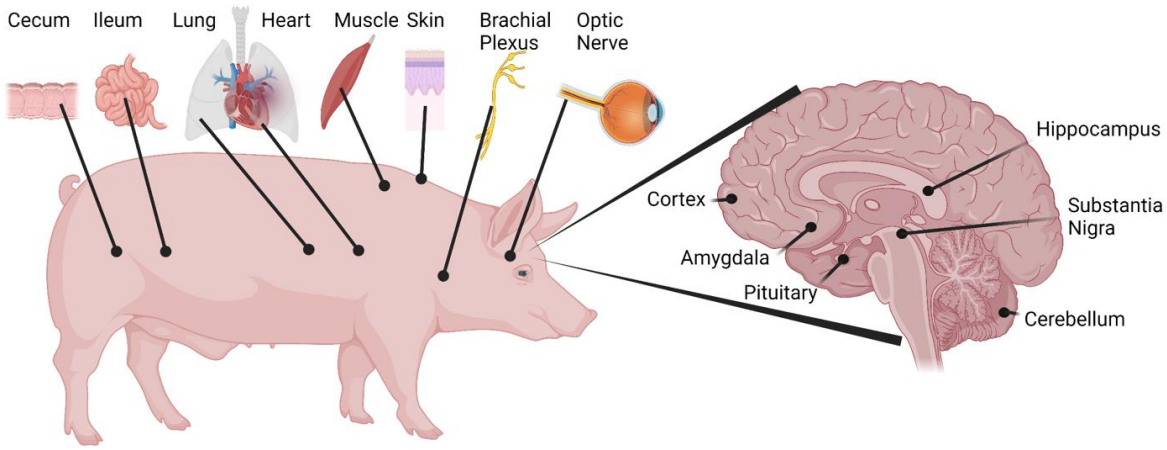

Figure 16. Swine Tissues - Diagram indicates general location of each tissue analyzed. Tissue taken from the amygdala region (temporal cortex) and substantia nigra region (midbrain) are approximations.

commercially available kits. Tissues taken from the brain (n=6) were processed with Fatty Tissue RNA Purification Kit (Norgen Biotek) and the tissues taken from the body and periphery (n=8) were processed with RNeasy Plus Universal Mini Kit (Qiagen) according to manufacturer's instructions. After qualitative and quantitative analysis with Nanodrop 2000 (ThermoFisher), cDNA libraries were created with the iScript™ cDNA Synthesis Kit (BioRad). RT-qPCR was performed with technical triplicates of each tissue sample to determine expression levels of each *NF1* ASE. Melt curves for each reaction were evaluated to ensure single peaks, or in the case of primer surrounding ASE regions, dual peaks were present. Primer design and scheme was modified based on previous publications detailing best practices for detecting ASE expression levels via RT-qPCR [234]. The modified primer scheme included a measure of redundancy to measure both *NF1* ASEs and Total *NF1* mRNA. This approach allowed for both absolute quantification and *NF1* ASE ratios to be determined (Figure 17). The primer sets used were as follows: 3 swine validated reference genes (PPIA, RPL4, TBP) [235], a primer set targeting the surrounding ubiquitously expressed exons for each ASE, and a primer set targeting either the AIE or the skipped AEE

product (Table 2). Standard curves were generated for each to determine primer efficiency values and ranges and to generate absolute copy numbers in post-hoc statistical analysis.

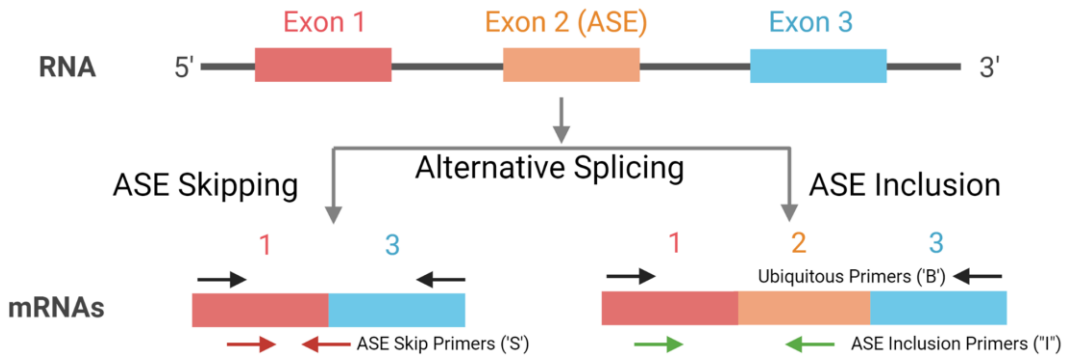

Figure 17. Primer Scheme - A generic schematic of primer design locations used to quantify ASE regions. Ubiquitous primers (denoted 'B' – both) lie on constitutively expressed exons and amplify targets located on all mRNA transcripts. ASE inclusion primers (green, 'I' – inclusion) only amplify targets that contain the intervening exon. ASE skip primers (red, 'S' – skip) only amplify targets that exclude the intervening exon.

Identification of *NF1* AIE Regulatory Regions

The secondary structure of each swine *NF1* AIE and surrounding 150 nucleotides was modeled using the Unified Nucleic Acid Folding and hybridization software package v3.9 [236]. The most energetically stable secondary structures (lowest Gibbs free energy values) were identified and partially open regions (not hydrogen bound to other RNA) were found. The Human Splicing Finder v3.0 was concurrently used to analyze potential splice silencer and enhancer genomic motifs [237]. Potential SSO binding targets between 20 and 30 nucleotides were chosen so as two fit two criteria: 1) it should bind to a partially open and partially closed region so as to have initial access via the open region but then to disrupt the secondary structure in the bound regions and 2) it should be located on an identified splicing motif that recruits splicing proteins or interferes with the exon junction. Binding affinity parameters for each potential SSO was then analyzed with RNAstructure software v5.8.1 to fit a set of criteria that maximizes efficacy in a physiological setting [238]. Ideally, SSOs were designed to be about 20 nucleotides long, to be without stretches of three or more

guanine or cytosine bases, to have a guanine-cytosine content of 40–60%, to have a melting temperature of >48°C. to have a free energy between 0 to –4 kcal/mol, and between 0 and -15 kcal/mol for SSO–SSO homodimers. NCBI BLAST was also used to ensure that the SSO designs did not have any significant predicted off-target interactions [134].

SSOs Synthesis and Modifications

The SSOs sequences derived using the above design process and best fitting all criteria were synthesized by Integrated DNA Technologies (IDT, Coralville, IA) with specific modifications (Table 3). The phosphodiester backbone was replaced with a phosphorothioated backbone and the 2′-hydroxyl group on the pentose ring was replaced with a 2'–O– methyl (2′–O–Me) group (Figure 18). The addition of a 2′–O–Me RNA nucleotides to inhibit ribonuclease and DNase digestion and the substitution of phosphorothioate on the ribose backbone to inhibit exonuclease and endonuclease digestion are very cost-effective and efficacious modifications [136]. SSO activity in cells is very low without these modifications due to degradation of both the SSO and pre-mRNA target.

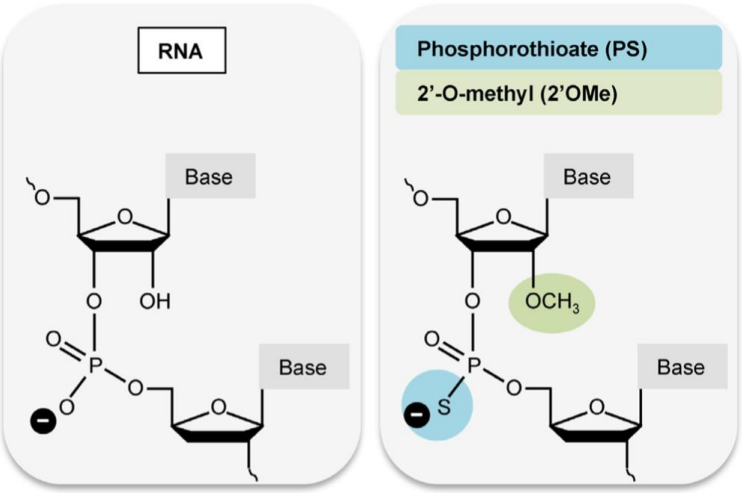

Figure 18. SSO Modifications - Structure of phosphorothioated backbone and 2'–O–methyl RNA base used to modify SSOs vs an unmodified RNA [136].

SSO Validation and Regulatory Element Confirmation

An artificial overexpression system was used to ensure sufficient detectable expression of each AIE in the *in vitro* cell culture platform [135]. For each *NF1* AIE, a minigene expression plasmid containing the AIE, neighboring exons, and intervening introns was created using Gibson Assembly® Master Mix Assembly (NEB) and the pTargeTTM Mammalian Expression Vector System (Promega, Madison, WI). The Neon® Transfection System (Thermo Fisher Scientific, Madison, WI) was then used to introduce the plasmids into primary adipose-derived MSCs from conventional swine. The plasmids also conferred neomycin resistance and allowed for purified selection of transfected cells. SSOs were then delivered into MSCs overexpressing the corresponding minigene plasmid, as well as into plasmid-free MSC controls using Lipofectamine® RNAiMAX Transfection Reagent (Thermo Fisher Scientific, Madison, WI). After two days, mRNA was isolated using the miRNeasy Mini Kit (Qiagen) and AIEs levels were quantified using the same RT-qPCR methods as described above.

3.4. Results

Seven *NF1* ASEs have been identified in the human genome assembly (GRCh38.p10): AIE 12, AIE 13, AIE 31, AIE 57, AEE 4, AEE 44, and AEE 51. Compared to Sanger sequences of swine DNA, AIE 12, 31, and 57 were identical homologues to human. AIE 13 had an insertion of a single adenosine nucleotide at the 8th position from the 5’ end (Figure 20). The Sscrofa11.1 assembly also indicated an adenosine nucleotide at this location and does not annotate this as an exonic region.

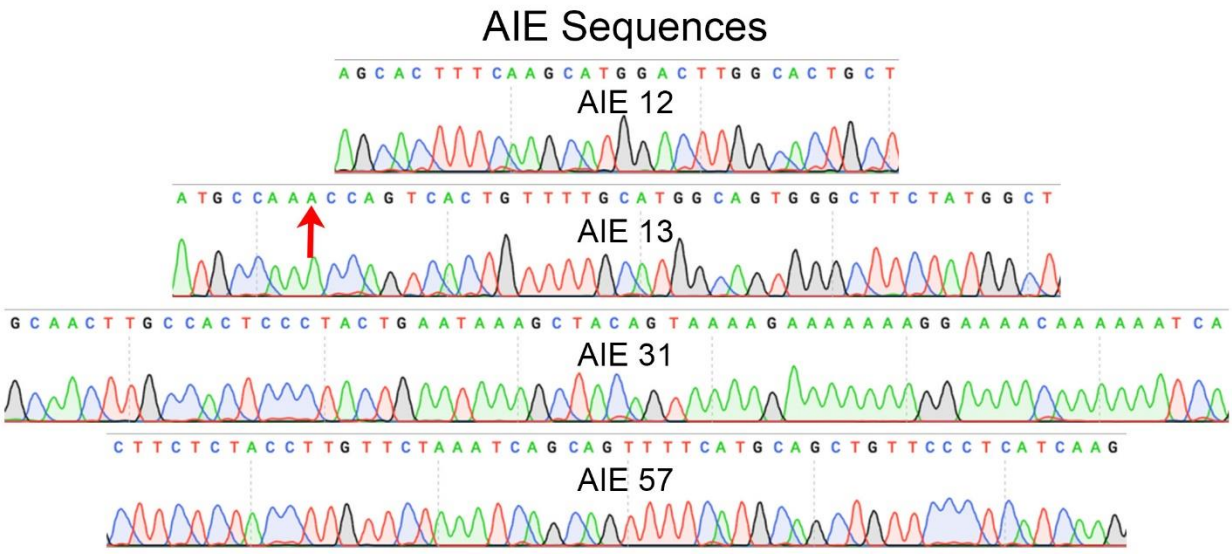

Figure 20. AIE Sequences - Sanger sequences of genomic DNA from *NF1* AIE regions. All regions are homologous to human except for AIE 13 which has an additional adenosine nucleotide indicated by the red arrow.

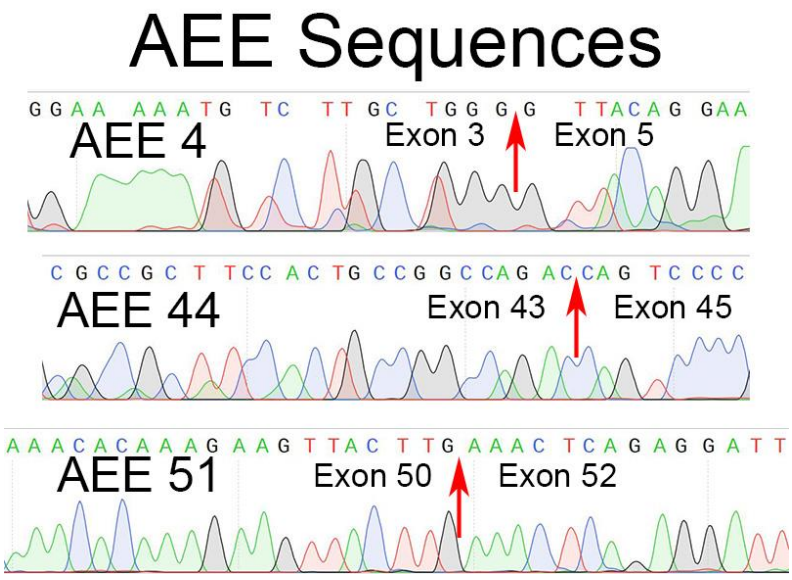

Figure 19. AEE Sequences - Sanger sequences of cDNA generated from mRNA transcripts taken from tissues of newborn swine. The regions sequenced are homologous to human. Exon-exon junctions are indicated by the red arrows.

The AEE sequences from cDNAs produced from RT-qPCR of newborn heart bridged the surrounding exons together at the expected junction sites (Figure 19). Further comparison of the AIEs and neighboring exons between the human and swine assemblies reveal nearly

homologous exons. Exon 3 and 51 are identical homologues. Exons 4, 5, 44, 45, and 50 have a total of 18 nucleotide substitutions. Exon 52 has an in-frame deletion of 3 base pairs and seven additional nucleotide substitutions.

Prior to assaying isolated mRNA from tissues samples, standard curves were generated for all primers (Figure 29). These provided a correction co-efficient for post-hoc statistical analysis of RT-qPCR data and indicated the working ranges the primers were valid for. The best fit line to the curves also served as a conversion equation so statistics could be performed in terms of total copy number instead of relative units. RT-qPCR samples from newborn heart, cortex, and ileum were analyzed with gel electrophoresis to verify expected band sizes were being produced by each primer (Figure 21). Primers surrounding AIE occasionally produced two visible bands, as two distinct amplicons were expected to be amplified.

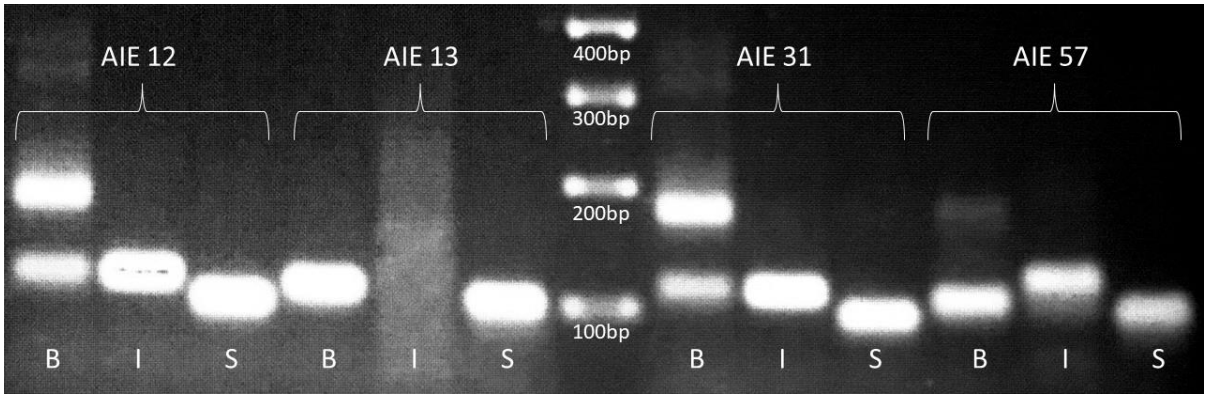

Figure 21. Gel electrophoresis of RT-qPCR products generated from newborn swine frontal cortex tissue. Bands represent size of amplicons and are at the expected locations relative to the ladder. Two bands are expected to be produce by 'B' primers as the inclusion or exclusion of the intervening AIE will change the amplicon size. No AIE 13 product was see using the 'I' primer and neither was a second band seen using the 'B' primer. No AIE 13 I band was seen in any tissue (data not shown).

Total *NF1* expression levels varied significantly between tissues and between different aged animals (Figure 22). Total *NF1* was significantly higher in adult lung and

illeum and lower in heart and skin. Between tissues in adult swine, total *NF1* was highest in heart followed by optic nerve and brachial plexus, then muscle and cortex, then illeum and cecum, and lowest in lung (Figure 23). In newborn tissues, total *NF1* was highest in optic nerve and brachial plexus, followed by ileum, lung, and cortex, then muscle and heart, and lowest in skin. Total NF1 was also higher in female nerves than male (Figure 22). Total AIE 12 was significantly higher in adult brachial plexus and lung than in newborn. Within both adult and newborn tissues, AIE 12 varied greatly and shared the same statistically significant trends, aside from brachial plexus and lung. Muscle, heart, and cortex was highest, followed by skin, then optic nerve, ileum and cecum (Figure 24). AIE 31 was significantly higher only in adult heart tissues relative to newborn. Within both adult and newborn tissues, ASE 31 varied in many tissues and shared the same statistically significant trends, aside from in heart. Optic nerve and brachial plexus was highest, followed by muscle, ileum, and cecum, then lung, skin and temporal cortex, and lowest in frontal cortex (Figure 25). AIE 57 was not significantly different between adult and newborn tissues. Within both adult and newborn tissues, only one significant trend was observed; heart and muscle had higher expression (Figure 26). In newborn tissues, AEE 4 was highest in cortex and brachial plexus, followed by optic nerve, muscle, ileum and lung, and lowest in heart. AEE 44 was not significantly different in any newborn tissues. AEE 51 was higest in optic nerve and brachial plexus, followed by muscle, heart, ileum and lung, and lowest in cortex tissue (Figure 27).

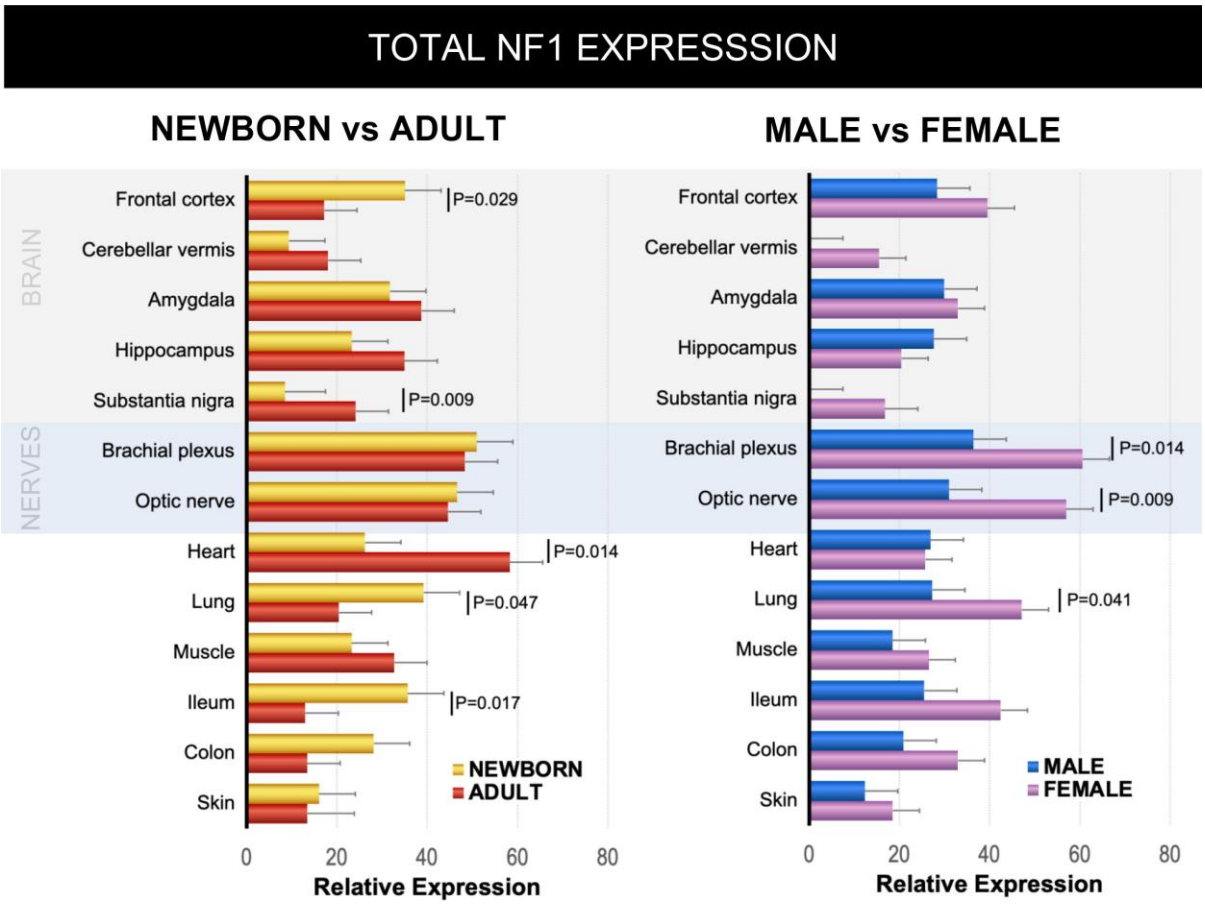

Figure 22. Total *NF1* Sex - RT-qPCR data expressed in terms of relative difference from the reference genes. Comparisons between age and sex are shown. Significant differences are denoted with a corresponding p value (p< 0.05).

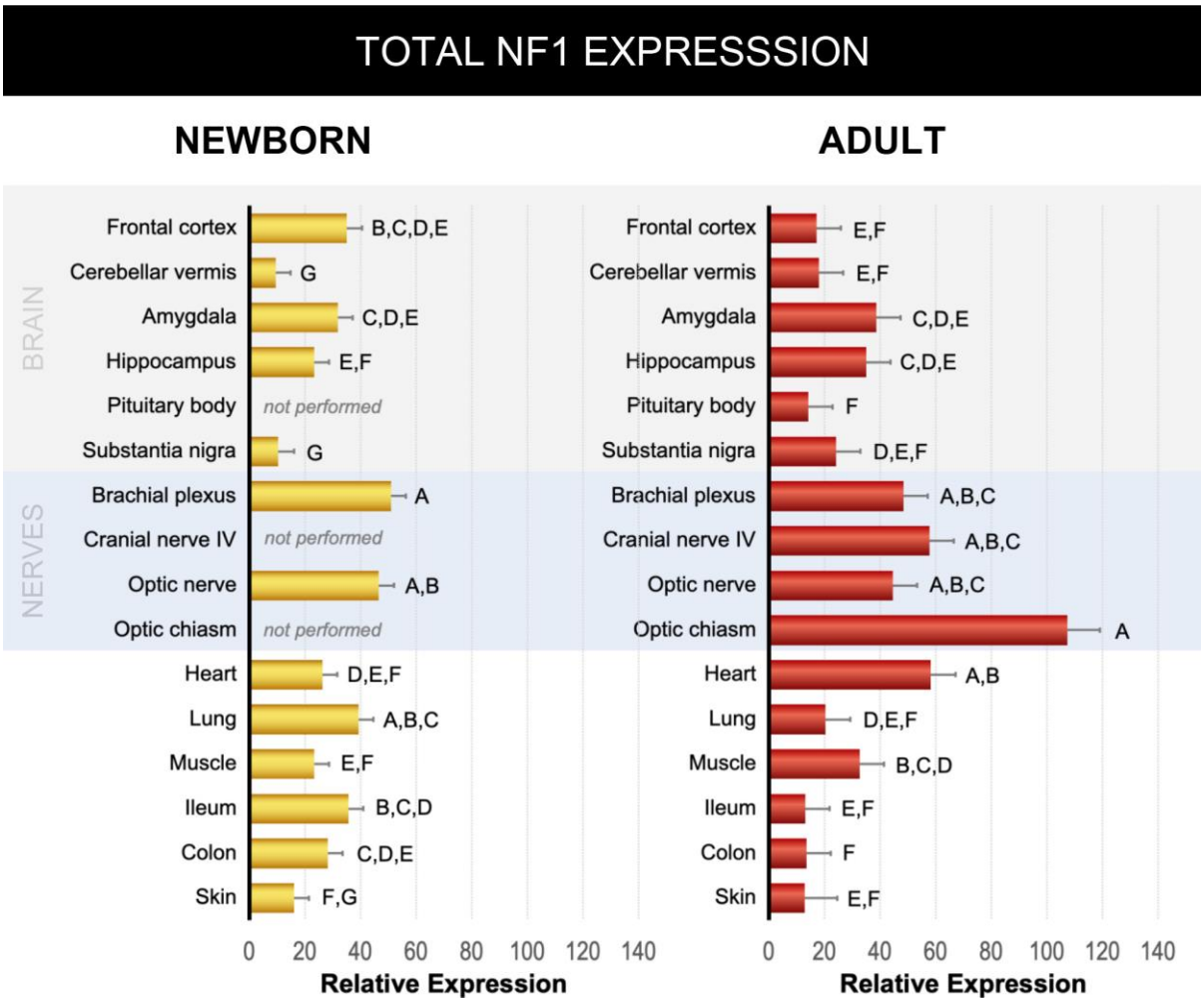

Figure 23. Total *NF1* Tissue - RT-qPCR data expressed in terms of relative difference from the reference genes. Comparisons between age and tissues are shown. Significant differences are denoted with a pairwise lettering scheme ($p < 0.05$).

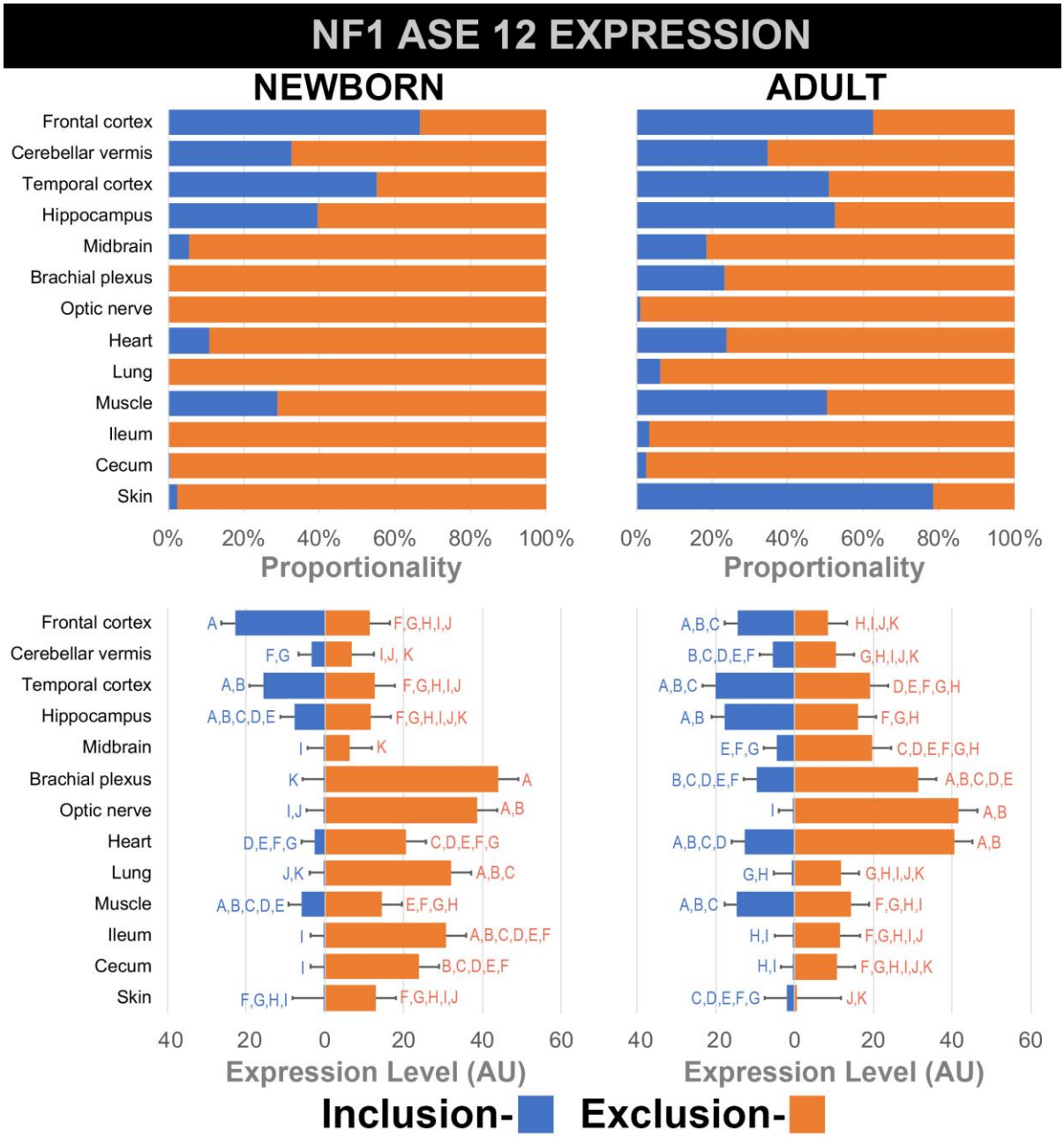

Figure 24. ***NF1*** **ASE 12 - RT-qPCR data expressed in terms of total copy number of transcripts. Significant differences (p<0.05) are denoted by pairwise lettering for comparisons between tissues from same-aged swine. Proportionality ratios are displayed using the same data as in the lower bar values and the sum of the AIE and AEE is converted to 100%**

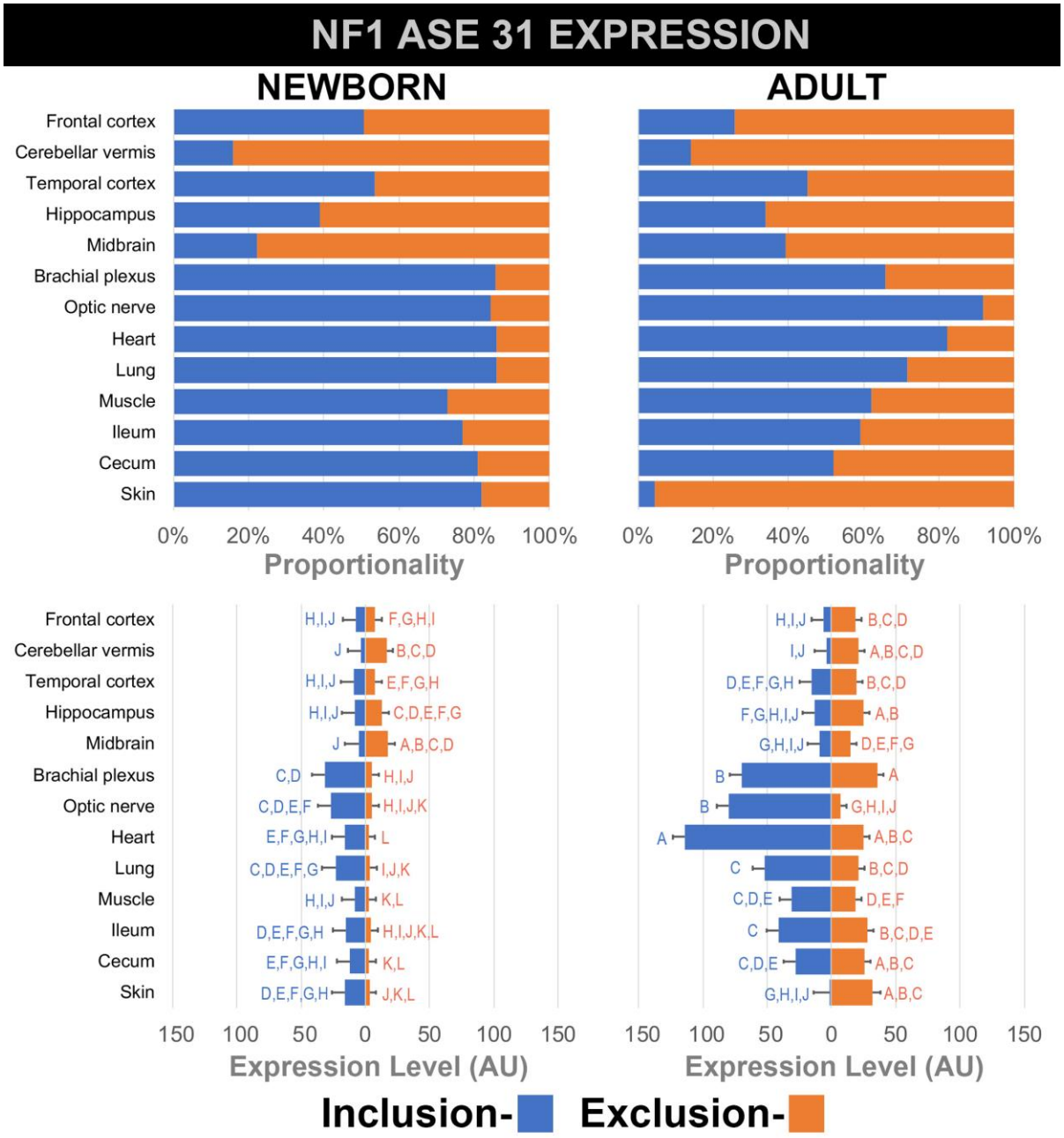

Figure 25. ***NF1*** **AIE 31 - RT-qPCR data expressed in terms of total copy number of transcripts. Significant differences (p<0.05) are denoted by pairwise lettering for comparisons between tissues from same-aged swine. Proportionality ratios are displayed using the same data as in the lower bar values and the sum of the AIE and AEE is converted to 100%**

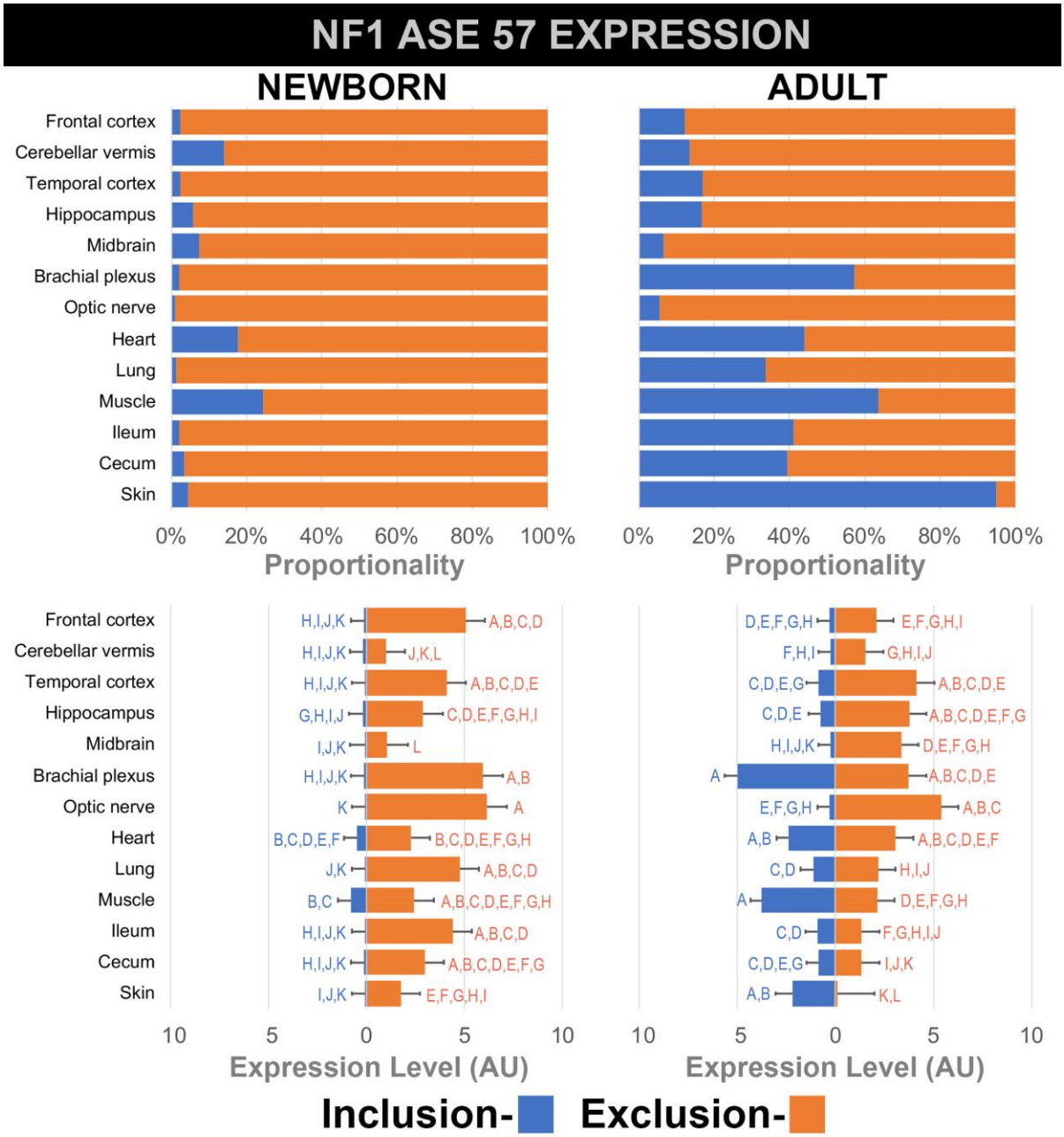

Figure 26. ***NF1*** **AIE 57 - RT-qPCR data expressed in terms of total copy number of transcripts. Significant differences (p<0.05) are denoted by pairwise lettering for comparisons between tissues from same-aged swine. Proportionality ratios are displayed using the same data as in the lower bar values and the sum of the AIE and AEE is converted to 100%**

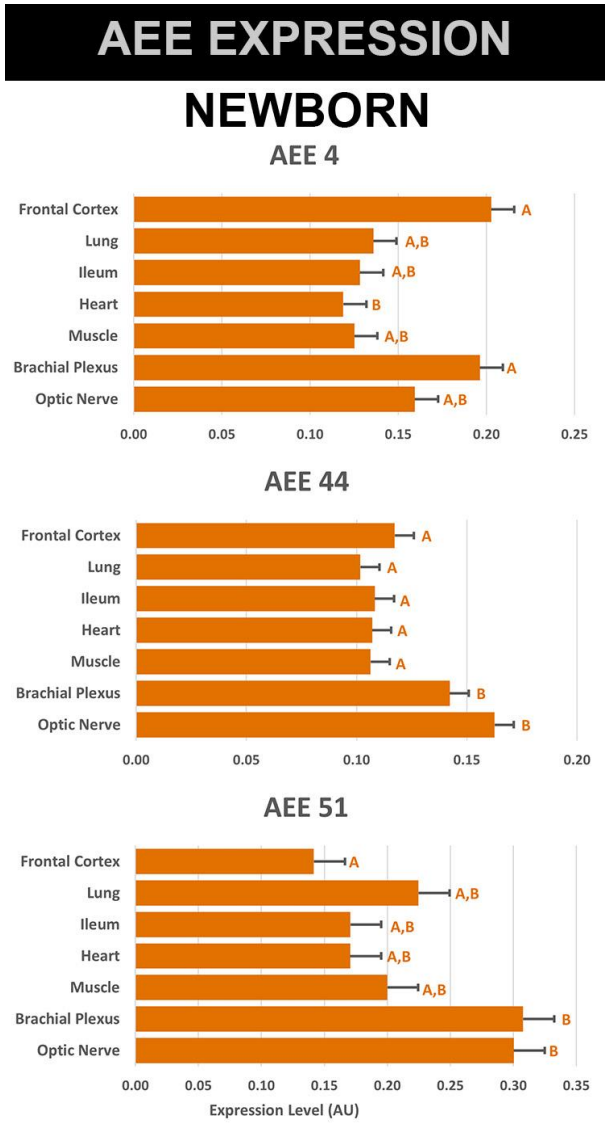

Figure 27. *NF1* AEEs - RT-qPCR data expressed in terms of total copy number of transcripts. Significant differences ($p<0.05$) are denoted by pairwise lettering for comparisons between tissues from same-aged swine. AEEs expression levels were compared only in newborn tissues (n=3).

Secondary pre-mRNA structures were generated for AIEs 12, 31 and 57 to evaluate potential SSO targets (Figure 30). SSOs were designed to meet specific criteria and were synthesized with the previously discussed modifications. Overexpression plasmids were created and confirmed to contain the appropriate insert by evaluating plasmid size with gel electrophoresis. Following transfection and puromycin slection of MSCs containing the

plasmid, RT-qPCR comparison of SSO transfected MSCs vs. control indicated that 5 of the 6 SSOs modulated AIE expression in a significant way. Each SSO that targeted a splice enhacing region showed a relatively large reduction in AIE inclusion: 2.5-fold reduction for AIE 12, 1.5-fold reduction for AIE 31, and a 6-fold reduction for AIE 57. SSOs targeting the inhibitory elements also showed efficacy in AIE 12 and 31. While significant, the increase in AIE was less than 1-fold higher. The SSO targeting the AIE 57 silencing site did not produce a increase in AIE 57 but had a toxic effect on the cell (Figure 28).

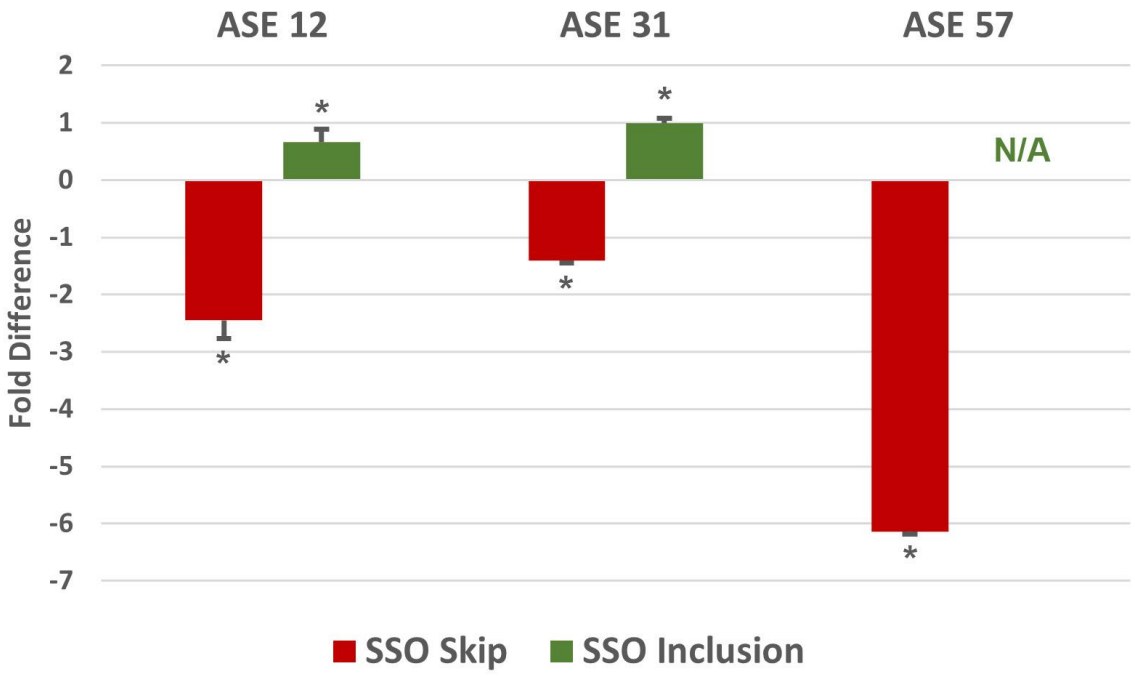

Figure 28. SSO Efficacy - Relative change of *NF1* AIE expression levels in minigene transfected MSCs following treatment with SSOs. Each ASE is normalized to an untreated control transfected with the respective minigene. AIE 57 Inclusion SSOs produced a toxic response in MSCs. All bars are significantly different from an untreated MSC control group ($p<0.05$).

3.5. Discussion

NF1 ASEs expression levels in newborn and adult swine tissues were compared to human to assess the translatability of swine for NF1 research and to establish a model for studying the role of *NF1* ASEs at a cellular level. The chosen tissues, including various brain, nerve, GI, muscle, and epithelial tissues, are known to be involved in many of the more prominent NF1 symptoms. Of particular focus is the myelinating tissues of the optic nerve and brachial plexus and neurons on the frontal and temporal cortex as these tissues are associated with neurofibroma formation and cognitive deficits, respectively. It remains poorly understood, however, what role *NF1* ASEs play in disease presentation. Establishing natural expression profiles for these key tissues provides solid basis from which to begin more complex studies in swine. Further, demonstrating the efficacy of SSOs as a tool to modulate *NF1* ASE expression provides an important means to evaluate the functional effects of *NF1* ASEs.

Swine was demonstrated to be genetically congruent with human with respect to both the genomic regions and tissues expression profiles. The results are concordant with known patterns of *NF1* ASE expression in corresponding human tissues and provide the first characterization of *NF1* ASE expression levels in swine. Genomic sequencing of three *NF1* AIEs indicated identical homology to human: AIE 12, 31, and 57. However, AIE 13 was not detected in any tissue. Further analysis showed that should this exonic region be included in a pre-mRNA transcript, the additional base pair would induce a frame shift and consequntly a premature stop codon producing a greatly truncated protein. While a truncated protein may have some physiological function, the total lack of detection of this product indicates it is not found in swine. Future studies may use SSOs in an attempt to force inclusion or genetically

modify cells without the additional nucleotide to study *NF1* AIE 13s effects. A simple phylogentic search of AIE 13 revealed that this sequence is completely conserved in all non-human primates and the domestic cat. It is also found in the genomic assemblies of the earthworm, golden eagle, vulture, brown kiwi, horse milkfish, asian fish, and rat, albeit with a number of base pair substituttions. Interestingly, multiple out-of-frame deletions are found in the homologous mouse and dog genomic region, and it is completly absent in zebrafish.

The detection of three *NF1* AEEs found in human is also significant as these AEEs have not been found in mouse [85]. AEEs were confirmed to be excluded in some *NF1* mRNA transcipts at a relatively low but significant level in all tissues assayed. Exon 51 was excluded most frequently, in up to 10% of the transcripts in optic nerve and brachial plexus tissues, but only in 0.5-3% of *NF1* mRNA in other tissues. Exon 44 was excluded in all tissues at a very low level, in 0.1-1.5 % of transcripts. Exon 4 was excluded with greatest frequency in brachial plexus and brain tissues, and at lowest frequency in heart tissues, varying from 3% to 0.25% respectively. It is unclear if human tissues have the same distribution of AEEs as swine because different tissues were evaluated in those other published reports. In one study, AEE 4 was found in 5% of blood and 2.3% of heart tissue and AEE 44 was found in 2.1% of muscle tissue transcripts. AEE 51 was found in 22% of liver, 15% of muscle, and 11% of kidney transcripts [85]. Overall trends appear to be congurent but more detailed analyis with additional tissues and with age-matched animals would need to be performed to confirm these expression profiles. Interestingly, the number of nucleotides that make up exons 4 and 44 in both swine and human is not divisible by three, suggesting that a frame shift and premature truncation stop codons would produce a truncated protein. One study showed that mRNA transcripts including these AEEs are in fact

polyadenylated and therefore likely to be trancribed into protein [85]. Whole transcriptome analysis could be used to determine the precise abundance and makeup of these *NF1* transcripts but may be challenging due to the difficulty of sequencing long mRNA transcripts.

Total *NF1* expression was higher in myelinating tissues and lowest in the cecum and skin. Most malignant NF1 tumors originate from myelin dense white matter and higher relative levels of AIE 31 was also found in these tissues. This AIE is known to influence Ras activity and is implicated in cancer [239]. Mutations influencing expression of AIE 31 are associated with increased activity of the Ras oncogene, however, there is no indication that *NF1* splicing mutations are concentrated at this region, suggesting that splicing alterations of other regions are also influential in inducing tumorigenic phenotypes. Human studies have reported that neurons lack AIE 31 expression and low detection levels were also found in brain tissue in the current study. AIE 12 was highest in cortical tissues, heart, and muscle. As these tissues are all dense with neurons or nerve endings, this was expected as is the case with human tissues. It is possible that this AIE is exclusive to neurons but pure homogenous cell culture would probably be needed to purify, grow, and isolate a sample of neurons. AIE 57 was highest in muscle and heart, as in humans, and its relative expression levels were low overall. Overall, the *NF1* AIE expression profile in swine tissues is similar to that in human.

Potential regulatory splice enhancing and inhibiting elements were identified for each of the three *NF1* AIEs and modified SSOs were designed targeting these six regions. All but one SSO showed efficay in modulating *NF1* AIE expression levels as predicted. This strongly suggests that the identified sites targeted by these SSO are involved in regulation of *NF1* alternative splicing. Reduction of AIEs was not complete when using the skipping SSOs

and may indicate other splice sites are also involved. Enhacement of AIEs was also rather modest, however, the process of inclusion is much more complex as the cell's endogenous machinery must be guided in the proper manner to facilitate this increase, whereas inhibiting AIE inclusion can simply invovle blocking the regulatory sequences or exon splice site from being accessed by the spliceosome. MSCs have a very high endogenous level of AIE 31 expression raising this level further may be prohibited by the cell. In the specific case of MSCs, an overexpression plasmid is not actually needed to increase AIE levels to a more easily detectable range, however, to be consistent in the experimental design one was used and a modest yet statistically significant increase was observed. It is possible that a cell needs to produce a certain ratio or absolute level of the *NF1* AIEs and the addition of the overexpression plasmids interferes with this regulatory feedback mechanism. Future studies will be done demonstrating the effects of these SSOs in the primary swine cell culture. The use of more robust SSO modifications like phosphorodiamidate morpholino oligomers (PMOs) may also increase efficacy. Indeed, a recently published study designed an SSO to enhance inclusion of *NF1* AIE 31 in an immortalized rat cell line using PMOs and used much lower doses. In agreement with this study, the identified regulatory regions were similar and the SSO both targeted very similar sequences. This suggests that splice site regulatory elements may also be conserved in humans, but further studies would need to be done to confirm this.

This is the first study to validate *NF1* ASE regulatory regions and compare *NF1* ASE expression levels in various swine tissues to human. The expression profiles revealed that swine are a valid translational model for the study of NF1 and *NF1* ASEs. Future studies may use genetically edited swine containing specific *NF1* mutations involving splicing. While

thousands of unique *NF1* mutations have been identified, very few genotype-phenotype correlations have been found. This inconsistency has elicited a deeper search to uncover the mechanisms governing this complex presentation of symptoms. Shifts in the relative expression of *NF1* ASEs in specific tissues caused by *NF1* mutations is suggested to influence the phenotypic presentation of the disease. Thus, it would reason that the restoration of the normal *NF1* ASE expression would prevent or attenuate the disease phenotype. To date, therapeutics that modulate *NF1* mRNA splicing have not been developed and no published studies have explored their effects *in vivo*. Only a few studies have even attempted to modulate *NF1* expression using SSOs [123] [143]. This study provides evidence that SSOs can be used to modulate *NF1* ASE expression in swine and provides a novel molecular technique that can be used to understand the role of *NF1* ASEs at different developmental stages and in different cell types. Further, this work opens the possibility that *NF1* SSOs may also be used with a therapeutic aim.

3.6 Supplementary Materials

NF1 ASE Region	Target	Primer Sequence	
AIE 12	For Sequencing	Forward	TTTTTACTTTTGCCAGTGTAATGAG
		Reverse	TGCATCCTTATGAATCCTAGTCG
	Surrounding Genomic Introns	Forward	TCGTCCACTGAGCCACTATG
		Reverse	CCAGAAGTCAGCTTCCCTTAC
AIE 13	For Sequencing	Forward	CCCTTAAACCTTTCCTTATGAACC
		Reverse	GCAAACTTCTCTGTCTGAACACC
	Surrounding Genomic Introns	Forward	GCATATGGCTTGGAAATGTG
		Reverse	GGGATAGACCACGATGGAAG
AIE 31	For Sequencing	Forward	TCAAGAACAATTATGTAAACACATGG
		Reverse	GGCCTTTGGGATAAATCAAAC
	Surrounding Genomic Introns	Forward	TGACAACATGGGGAACACAG
		Reverse	TGGACCCCTAGCTTGAGAAC
AIE 57	For Sequencing	Forward	AAGTTGAGCAATTGTTTGGTG
		Reverse	CAAACCACATACCCTCCTTTC
	Surrounding Genomic Introns	Forward	GCAGGTTCATCTGGAAGCTC
		Reverse	AGCCCGTATCAGTTACGTCTG
AEE 4	For Sequencing	Forward	TCTCTCTCAGTTGATTATATTGGAT
	Surrounding cDNA Exons	Forward	TTTGGAGAAGCTGCTGAAAA
		Reverse	TCCTGTAACCCCAGCAAGAC
AEE 44	For Sequencing	Forward	ACCAGTGGACAGAACTAGCC
	Surrounding cDNA Exons	Forward	TGAGAGATATTCCAACATGCA
		Reverse	CTCTCAAGTGCCTTTGGG
AEE 51	For Sequencing	Forward	ATGAGCTTGGACATGGGCC
	Surrounding cDNA Exons	Forward	AATCAGCCATGGTCCTCTCC
		Reverse	AAATCCTCTGAGTTTCAAGTAAC

Table 1. *NF1* ASE PCR Primers - Primer sequences used to amplify or sequence the genomic DNA for AIEs and the cDNA of mRNA transcripts for AEEs.

NF1 ASE Region	Target	Primer Sequence	
AIE 12	Ubiquitous Exons	Forward	CTGCCTGGCTCAAAATTCC
		Reverse	CTTAGGCCACCAATCTAATGC
	AIE Only	Forward	AAGCATGGACTTGGCACTG
		Reverse	ACAACCCTGGACTGCTTTATG
	AEE Only	Forward	GAATCATCACCAATTCTGCA
		Reverse	CACAACCCTGGACTGCTTTA
AIE 13	Ubiquitous Exons	Forward	TAAAGCAGTCCAGGGTTGTG
		Reverse	AGCTTCTTGTCTCCAGGTCTG
	AIE Only	Forward	TAAAGCAGTCCAGGGTTGTG
		Reverse	AGCCATAGAAGCCCACTG
	AEE Only	Forward	GGTGGCCTAAGATTGATGCTG
		Reverse	GTAAGACTCGGTGCCATTCG
AIE 31	Ubiquitous Exons	Forward	CATGCCATCATCAGCTCCTC
		Reverse	TGAGGGAAACGCTGGCTAAC
	AIE Only	Forward	CATGCCATCATCAGCTCCTC
		Reverse	TTATTCAGTAGGGAGTGGCAAG
	AEE Only	Forward	CTGTTTATACCAGGTGGTTAGCC
		Reverse	CATATGGTGAGACGATGGC
AIE 57	Ubiquitous Exons	Forward	GCAACTTCCCAGCATTCCC
		Reverse	CTTGGCTTGCGGATCCATG
	AIE Only	Forward	TTTCATGCAGCTGTTCCCTC
		Reverse	CTTGGCTTGCGGATCCATG
	AEE Only	Forward	GCATTCCCCAGGAATCG
		Reverse	CTTCTGCACTTGGCTTGC
AEE 4	Ubiquitous Exons	Forward	TCTCTCTCAGTTGATTATATTGGAT
		Reverse	ACATCAACATTGTCTTCTGAACA
	AEE Only	Forward	TTTGGAGAAGCTGCTGAAAA
		Reverse	TCCTGTAACCCCAGCAAGAC
AEE 44	Ubiquitous Exons	Forward	ACCAGTGGACAGAACTAGCC
		Reverse	AGAAGTGGTTGCAATTTGGT
	AEE Only	Forward	TGAGAGATATTCCAACATGCA
		Reverse	CTCTCAAGTGCCTTTGGG
AEE 51	Ubiquitous Exons	Forward	ATGAGCTTGGACATGGGCC
		Reverse	GAAGGGCTTGGATCTTCGGA
	AEE Only	Forward	AATCAGCCATGGTCCTCTCC
		Reverse	AAATCCTCTGAGTTTCAAGTAAC
PPIA	Exon-Exon Boundry	Forward	CACAAACGGTTCCCAGTTTT
		Reverse	TGTCCACAGTCAGCAATGGT
RPL4	Exon-Exon Boundry	Forward	AGGAGGCTGTTCTGCTTCTG
		Reverse	TCCAGGGATGTTTCTGAAGG
TBP	Exon-Exon Boundry	Forward	GATGGACGTTCGGTTTAGG
		Reverse	AGCAGCACAGTACGAGCAA

Table 2. Tissue RT-qPCR Primers - AEE only primers are located directly on the exon-exon junction based on the assembly data for the neighboring exons. Primers were biased longer towards the 5' end to minimize false priming. AIE primers are located centrally within the exon. Working concentration of all primer pairs were validated through a standard curve, melting temperature curves, and PCR gel electrophoresis to confirm expected performance.

NF1 ASE Region	Regulatory Target	Function	SSO Sequence
AIE 12	Enhancing Element	Skipping	UACAGCAGUGCCAAGUCCAUG
	Silencing Element	Inclusion	GUAGACAAAAAUAUUUCAC
AIE 31	Enhancing Element	Skipping	CUGAUUUUUUGUUUUCCUUUUUUUC
	Silencing Element	Inclusion	AGCAACAAAAACAAUG
AIE 57	Enhancing Element	Skipping	GGGAACAGCUGCAUGAAAA
	Silencing Element	Inclusion	GGAAGAAAAAACAAAAGUGAGUGG

Table 3. SSO Efficacy Designs - Sequences of SSOs targeting each regulatory element. All SSOs contained phosphorothioated backbones and 2′–O–Me groups throughout.

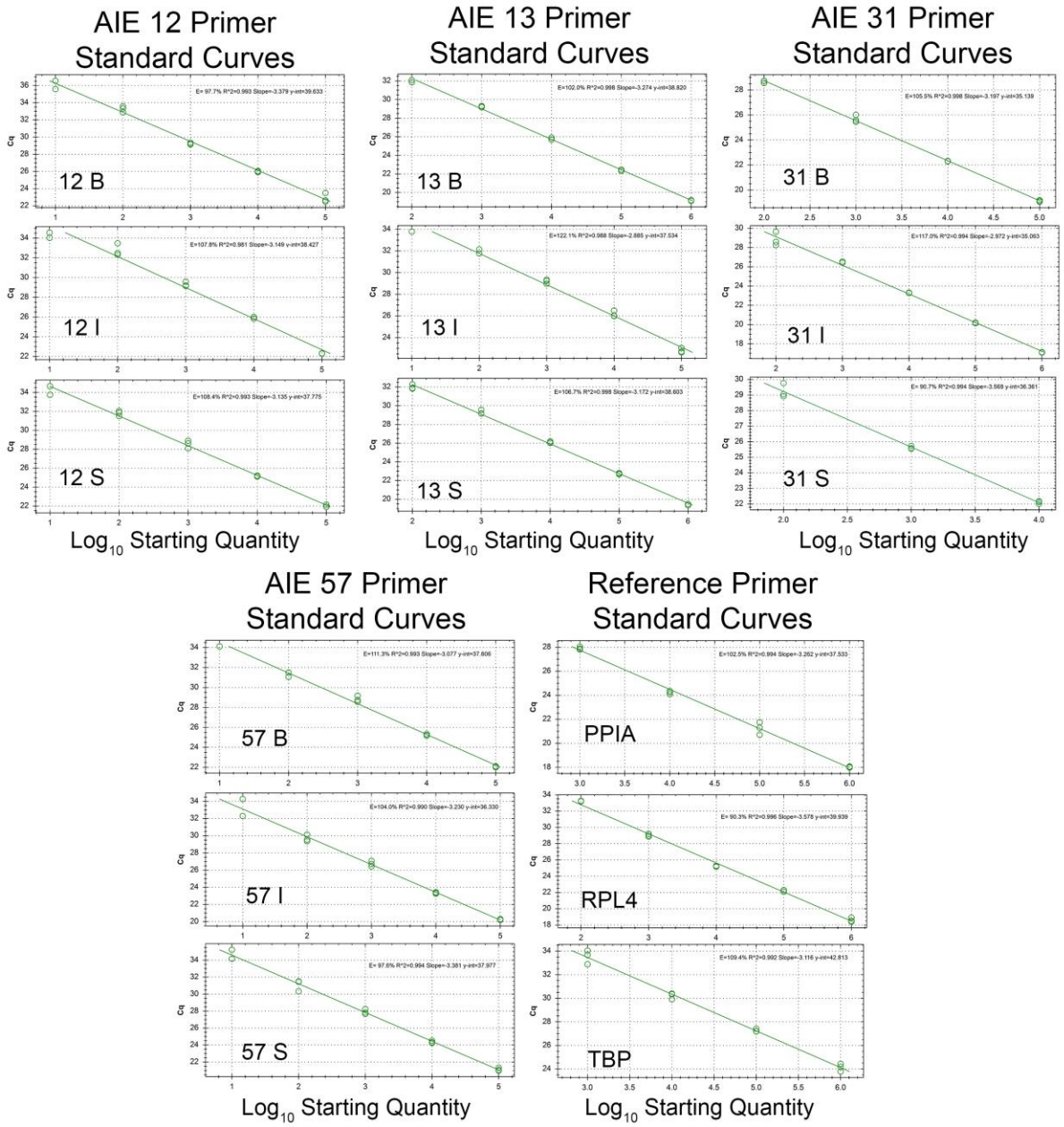

Figure 29. Standard Curves - Standard curves were generated for each RT-qPCR primer to determine efficiencies, working ranges, and a best fit line for deriving absolute copy numbers from raw Cq data. Serially diluted (1:10 dilution ratio) plasmid inserts were used for AIE primer standard curves. A serially diluted (1:10 dilution ratio) spike-in mixture of cDNA from newborn optic nerve and heart was used for reference gene standard curves.

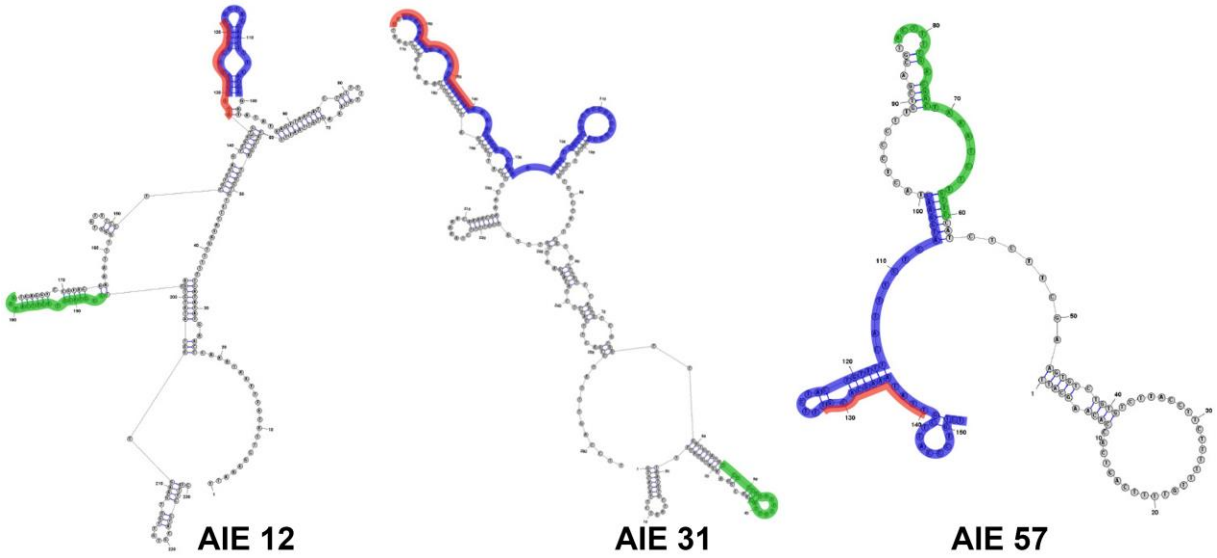

Figure 30. NF1 ASE mRNA Folding - Lowest energy folding structure predicted by RNAstructure software. Sequences included the target AIE and 100 bp of the surrounding intronic regions on each side. Blue highlights the AIE sequences. Red highlights the SSO inhibitory elements. Green highlights the SSO inclusion elements.

CHAPTER 4 -- Functional Effects of *NF1* Alternatively Spliced Exon Modulation in Differentiating Schwann Cells

4.1. Abstract

Neurofibromatosis Type 1 (NF1) is a complex genetic disorder that is closely linked to the development of a variety of cancers. Neurofibromas are the hallmark tumor associated with this disease and originate from the myelin sheath surrounding nerves. In the peripheral nervous system, these myelinating nerve support tissues are called Schwann cells and their transformation has been shown to be an important driver of NF1 tumorigenesis and therefore are a potential target for therapies. Alternative splicing dysregulation has been increasingly implicated in tumorigenesis. *NF1* splicing abnormalities are also disproportionately seen in NF1 patients. Splice-switching oligonucleotides (SSOs) can be used to modulate and even correct aberrant alternative splicing, however, this strategy has not been used in NF1. Prior work that has identified the splicing regulatory regions for several *NF1* alternatively spliced exons and validated corresponding SSOs that modulate their expression. However, functional effects of *NF1* alternatively spliced exon (ASE) modulation have not been reported. In the current study, SSOs targeting the splicing regulatory regions of three *NF1* ASEs were delivered to swine adipose-derived MSCs in a dose dependent manner to evaluate toxicity levels and determine the highest tolerated dose. Prior work has revealed Schwann cells have higher expression of *NF1* ASE 31 and modulation of it with SSOs may be a viable therapeutic strategy. Therefore, the SSO which promoted inclusion of *NF1* ASE 31 was used to demonstrate functional and ***potentially*** therapeutic effects in differentiating Schwann cells. In addition to WT MSCs, *NF1* +/- and *NF1* -/- MSCs were also used. Results indicated that

SSOs which increase *NF1* ASE 12 and 57 had a pronounced toxic effect on the MSCs at low doses. The other SSOs were tolerated at relatively high doses and indicates that increased *NF1* ASE 12 and 57 expression may have a detrimental effect in MSCs. Increasing *NF1* ASE 31 in MSCs and differentiating Schwann cell produced a decrease quantity of the active form of Ras and phosphorylated ERK1/2. It also had the effect of decreasing proliferation rates and increasing markers of Schwann cell maturity. Notably, these effects were only seen in cells that had at least one WT allele – it had no effect in *NF1* -/-cells. This is the first report linking *NF1* AIE modulation to Schwann cell development. Overall, these results show that SSOs can be used to modulate *NF1* ASE expression in a functionally relevant way and may have therapeutic applications targeting Schwann cell development. Future studies will explore the therapeutic potential of SSOs targeting other cell types within the tumor in NF1 patients prior to biallelic *NF1* inactivation.

4.2. Introduction

NF1 is characterized as an autosomal dominant disorder arising from mutations within the *NF1* gene. NF1 related tumors frequently originate in the myelinating tissues of the nervous system and often signify a poor prognosis depending on the type of tumor [54]. Tumors form with increased incidence on the dermis, in the brain, on cranial and peripheral nerves, and on the spinal cord. Some of these tumor types include lipomas, astrocytomas, brain and optic nerve gliomas, spinal and cutaneous neurofibromas, and plexiform neurofibromas. The latter of which have about a 15% chance of developing into malignant tumors compared to the general public [2]. Neurofibromas are heterogeneous tumors comprised of neoplastic Schwann cells and nonneoplastic fibroblasts, vascular endothelial

cells, and mast cells, as well as dense collagen [240]. While Schwann cells are clearly key drivers of neurofibroma formation, the specific role of *NF1* in this process is not known.

Human *NF1* contains 61 exons and at least 7 of them are alternatively spliced in mature mRNA transcripts [85]. These ASEs, along with the other constitutively expressed exons, combine to form the various *NF1* mRNA isoforms and are differentially expressed in all human tissues. The four most commonly identified ASEs are denoted 11alt12, 12alt13, 30alt31, and 56alt57 [86]. These ASEs can also be referred to as a12 or ASE 12 instead of 11alt12, etc… Other less commonly studied ASEs include exon 4, 44, and 51 and are found to be excluded in some transcripts. For clarity, the nomenclature used in this work distinguishes the whole body of *NF1* ASEs further into two subcategories: alternatively included exons (AIEs) and alternatively excluded exons (AEEs). In the conventional *NF1* nomenclature, AIEs are given a suffix or prefix to distinguish them from the other, more constitutively expressed exons, which are simply referred to by number. The AEEs are numbered regularly amongst the rest of the constitutively expressed exons and when referred to in the context of alternative splicing are prefaced with the phrase AEE indicating they are among the normally numbered exons but are being discussed in the context its alternatively spliced nature.

All of these ASEs potentially have a role in disease presentation and severity but only AIE 31 has been studied to this end [241]. This ASE is located directly in the GTPase activating protein related domain and is known to regulate Ras activity and consequently several downstream pathways. [233] Ras activity is directly related to cell proliferation and has been strongly associated with NF1 tumors [242]. Myelinating tissues including Schwann cells have a relatively high expression of AIE 31 and are often the tumorigenic cell of origin

in neurofibromas [51] and are strongly influenced by *NF1* +/- cells in the microenvironment [240]. Therefore, modulating *NF1* AIE 31 could have great therapeutic potential in tumorigenesis or tumor development.

Antisense oligonucleotides have recently been used to correct dysfunctional mRNA splicing in spinal muscular atrophy and Duchenne's' muscular dystrophy [243, 244]. They can also be used to modulate endogenous splicing and are referred to as splice-switching oligonucleotides (SSOs). By designing SSOs targeting specific sites on the mRNA, exon inclusion or exclusion can be induced. SSO-mediated exon inclusion can be achieved by targeting a splicing silencer sequence (exonic or intronic), disrupting secondary RNA inhibitory structures, or recruiting splice factors. Conversely, natural or cryptic exon skipping can be achieved by targeting a known splice site or splice enhancer element. While these aspects make SSOs a versatile tool for correcting splicing dysfunction, they also make ideal therapeutics because they are easy to synthesize, they are highly target-specific, they can gain access to many cell types in the body without requiring any additional packaging or unique delivery methods, they are well tolerated, their mechanism of action can be predicted based on their design, they can be designed to target patient-specific mutations, and the effects of a single injection can modulate splicing for up to a year in some tissues [136]. Given these favorable qualities and the successful precedence in treating other diseases, SSOs are very amenable for studying *NF1* alternative splicing. Using SSOs first as a tool to further understand the role of alternative splicing in NF1 could then be translated into a treatment with therapeutic potential for NF1 patients to correct splicing mutations.

MSCs are multipotent cells commonly used for *in vitro* cell culture studies. Protocols for differentiating MSCs into Schwann cells have also been well established, including in

swine. They can also be obtained from a variety of tissues such as bone marrow, peripheral blood, and adipose. These factors make them a good choice to evaluate SSOs in this translational swine cell culture platform. Several swine models of NF1 have been recently developed in hopes that these models will recapitulate the disorder in humans better than existing rodent models and thus offer a more translational platform for the development of novel therapies [1]. With respect to the seven ASEs identified in human, swine has completely homologous genomic DNA to six of them, the exception being AIE 13. Only three of the *NF1* ASEs have been found in rodents [85] and studies have also shown mouse models do not present as many of the complex NF1 phenotypes as swine do [87]. These reasons justify the use of swine as a platform for studying NF1 in a translationally relevant manner.

SSO previously designed for use in NF1 swine ASE modulation were used. Briefly, *NF1* AIE regulatory regions were identified and SSO designed to either enhance or inhibit inclusion of the target AIE. For the 3 AIEs of interest in swine, six unique SSOs in total were used. MSCs taken from conventional and genetically edited NF1 swine were isolated and differentiated into Schwann cells using established protocols. SSOs were first applied to conventional MSCs to determine dosing and viability curves. Finally, SSO were applied to MSCs from all swine genotypes while being differentiated into Schwann cells to demonstrate functional effects downstream from *NF1* mRNA splicing. The results have provided rationale for further SSO studies using primary tumor cells obtained from NF1 swine models or in other tumorigenic cell types such as fibroblasts or mast cells.

4.3. Methods

SSO Dosing and Viability

Six SSOs were modified to have phosphorothioated backbones and 2'–O– methyl (2′–O–Me) RNA bases and synthesized by Integrated DNA Technologies (IDT, Coralville, IA) (Table 4). The efficacy of SSO activity in cells is very low without these modifications due to degradation of both the SSO and pre-mRNA target. The addition of 2′–O–Me RNA nucleotides on the ends of SSOs inhibit ribonuclease and DNase digestion and the substitution of phosphorothioate on the ribose backbone inhibits exonuclease and endonuclease digestion [136]. Serial dilutions of SSOs were prepared on a logarithmic scale with the highest dose being 4000 nM and the lowest dose 2.5 nM, in addition to a 0 nM and untreated control. WT MSCs were seeded from a single pool of homogenous cells at a density of 1,500 cells per well. SSOs were delivered into MSCs using RNAiMAX Reagent (ThermoFisher) according to the manufacturer's recommendations for 96-well plates. After four days, images were taken of each well and ImageJ software used to count the number of surviving cells. Follow-up experiments used an SSO shown to have efficacy in increasing *NF1* AIE 31 (Inc31) and was administered at a concentration of 500 nM.

Adipose-derived MSC Harvest

MSCs from wild-type and genetically edited NF1 swine were isolated according to established protocols [200]. *NF1* genotypes included *NF1* AIE 31 +/-, *NF1* AIE 31 -/-, and *NF1* Trunc +/- (Figure 31). *NF1* AIE 31 +/- and -/- alleles have a genomic deletion of the AIE 31 exon. *NF1* Trunc +/- and -/- alleles have a single nucleotide deletion in exon one resulting in a premature stop codon and greatly truncated protein. Clonal *NF1* Trunc -/-

population of MSCs were derived from *NF1* Trunc +/- MSCs using a CRISPR/Cas9 plasmid construct (IDT, Coralville, IA) delivered with the Neon® Transfection System (Thermo Fisher Scientific). After single cell sorting, robust growing clonal populations were confirmed with Sanger sequencing and used along with the other MSC genotypes for cell culture experiments. Cryopreserved samples were maintained for each original genotype and MSCs passaged greater than 8 times were not used for experiments.

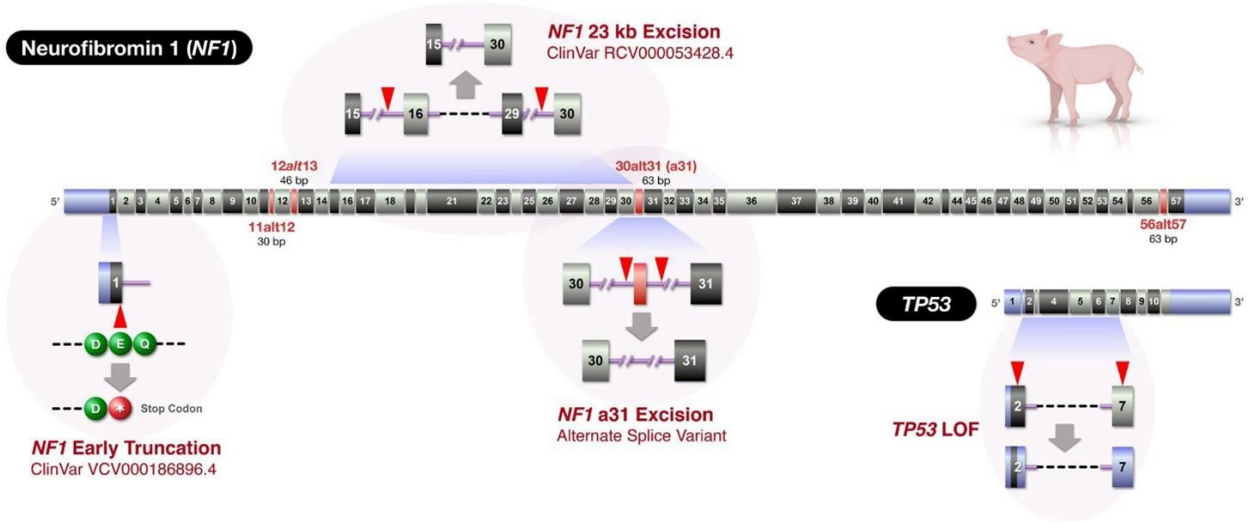

Figure 31. *NF1* Genotypes – Schematic diagrams representing the mutations in genetically edited swine. *NF1* Early Truncation and *NF1* a31 Excision are represented in the current study [1].

Functional Assays in MSCs and Schwann cells

Proliferation rates and Ras activity was determined for both MSCs and differentiated Schwann cells for each of the five genotypes. MSCs from each of the five genotypes were first treated with SSO Inc31 in two replicate 6-wells containing 100,000 cells using RNAiMAX Reagent. A separate untreated control was also made for each genotype. The following day MSCs from one 6-well were used to seed a 96-well plate at a density of 1,500 cells per well in six replicate wells. The plates were incubated with the BioSpa Live Cell Analysis System (Biotek) and imaged every 4 hours with the Cytation 5 Cell Imaging Multi-

Mode Reader (Biotek). Cell counts were performed using an included software program and statistical analysis was performed determining the average growth rate constants from a best fit exponential growth curve. After 3 days, cells from the other 6-well plate were assayed with the Ras G-LISA Activation Assay Kit (Cytoskeleton, Inc) and again compared with the untreated controls to determine the total amount of active Ras.

Each unique line of MSCs was also differentiated into Schwann cells using a series of differentiation medias in duplicate 6-wells [202]. After 14 days, mRNA was extracted from one 6-well using the miRNeasy Mini Kit (Qiagen) according to manufacturer's protocols. After qualitative and quantitative analysis with Nanodrop 2000 (ThermoFisher), cDNA libraries were created with the iScript™ cDNA Synthesis Kit (BioRad). RT-qPCR was performed with technical triplicates of each tissue sample to determine expression levels of each *NF1* ASEs and markers of Schwann cell maturity. The primer sets used were as follows: 3 validated references genes (PPIA, RPL4, TBP), a primer set targeting *NF1* AIE 31, and primers targeting genes upregulated in differentiating Schwann cells (Table 5). Cells from the other 6-well were assayed for Ras activity as described above.

SSO Inc31 Administration During Schwann Cell Differentiation

The same five lines of MSCs were again seeded into 6-wells and differentiated into Schwann cells while being administered SSO Inc31 on Day 0, 4, 8, and 12 of differentiation. A proliferation assay compared the untreated Schwann cells control group to the SSO treatment group over the last 3 days of differentiation as previously described. On Day 14 of differentiation, gene expression and Ras activation assays were performed and compared with the untreated controls.

4.4. Results

Efficacy and cell viability assays were performed to determine the optimal SSO concentration for use in MSCs. The first assay used an SSO that induced skipping of AIE 31 and showed that concentrations of 125 nM produced detectable effects and this increased linearly with higher concentrations (Figure 32). However, cell viability decreased

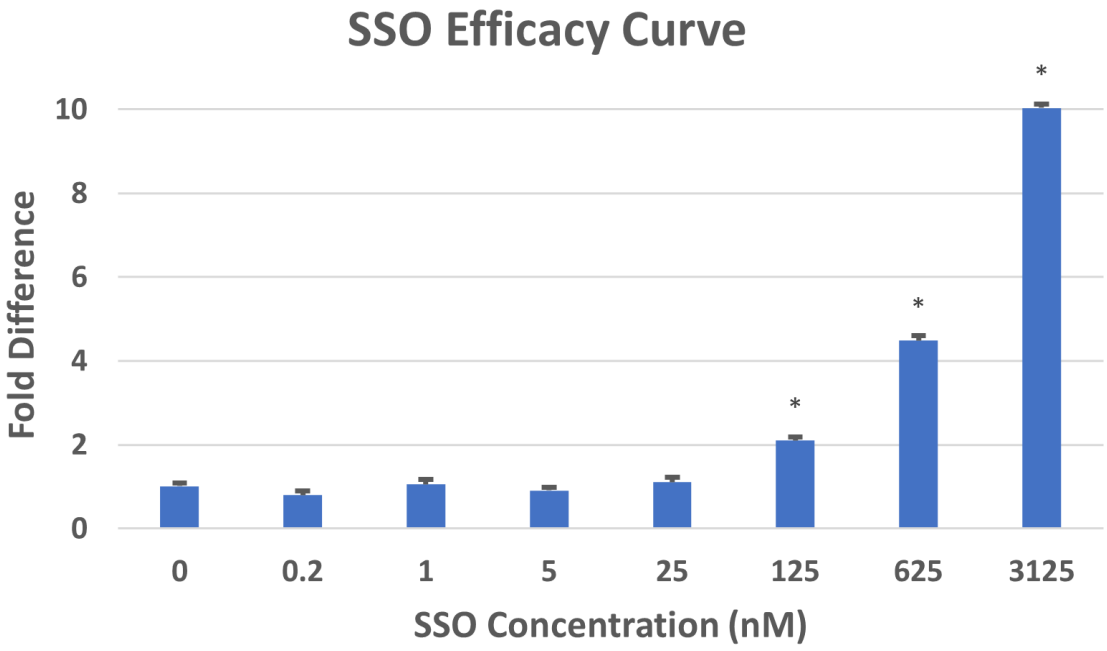

Figure 32. Efficacy Curve – Increasing concentrations of SSO AIE 31 Skip in MSCs after 2 days. Significant differences from the untreated 0 nM control are indicated with an asterisk ($p<0.05$).

significantly at high concentrations, so a viability assay was performed to determine the highest tolerated concentration for each SSO. The cell survival assay indicated MSCs tolerate SSOs at doses up to 40 nM delivered with RNAiMAX, while doses of 4000 nM dramatically reduced MSC viability after four days. Maximum viable dosing was determined for each of the six SSOs and is indicated by the highest dose above the graphical trendline (Figure 33). SSOs designed to inhibit AIE expression were generally well tolerated by the MSCs as compared to SSOs designed to enhance AIE expression. The exception to this trend was SSO

targeting AIE 31, which was tolerated at relatively high doses as well. SSOs targeting AIE 12 and 57 both demonstrated loss of viability at 100 nM doses. All other SSO doses retained MSC viability exceeding doses 640 nM or higher. SSO Inc31 was the focus of subsequent studies and 500 nM dosing was chosen to maximize efficacy while minimizing potential toxicity issues, especially given repeated dosing regimens.

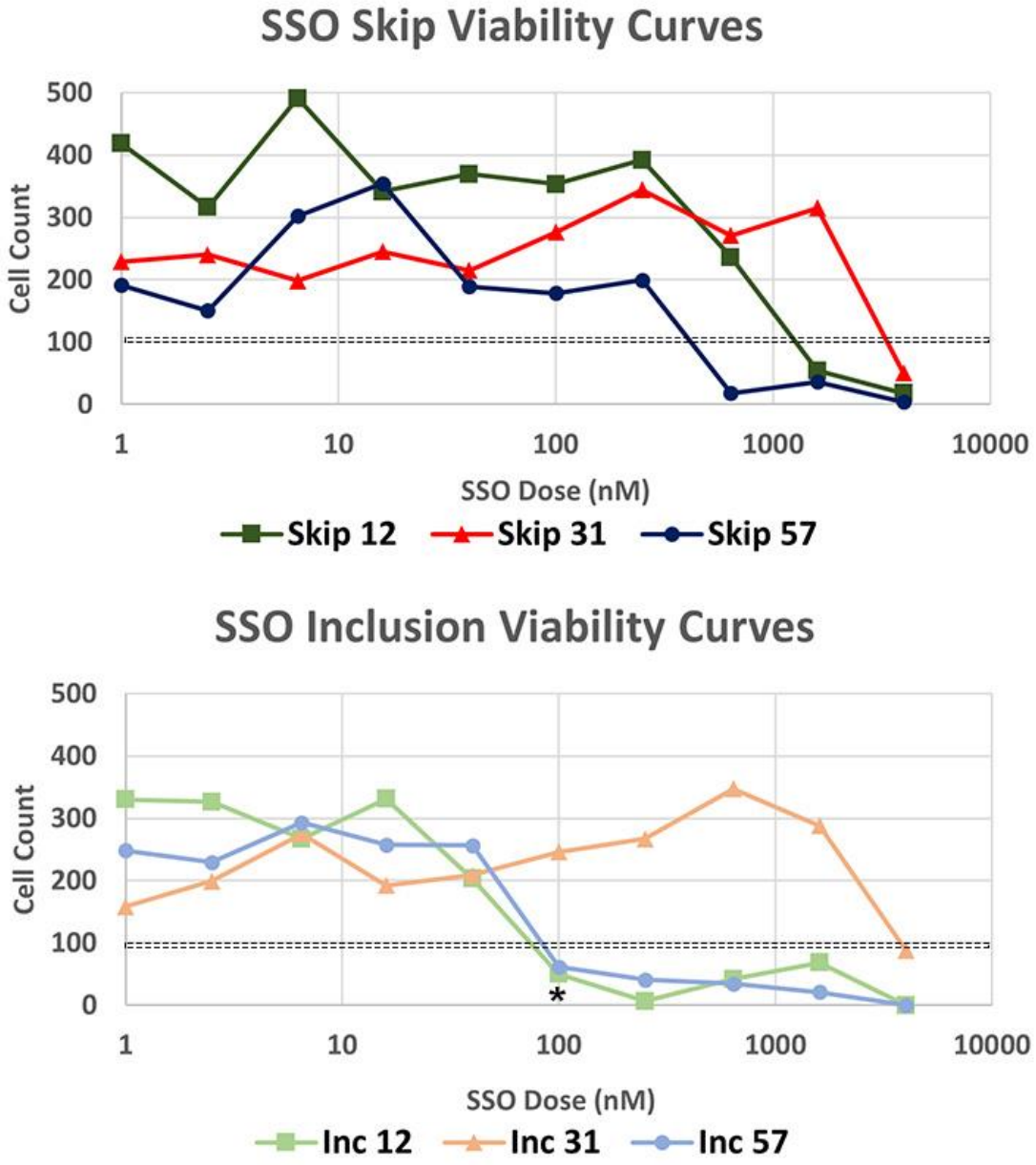

Figure 33. Viability Curves - SSOs administered to MSCs at various concentrations and counted after 4 days. SSO Inc 12 and 57 decreased cell viability at relatively low doses (indicated by asterisk), suggesting a negative mechanistic effect of forced exon inclusion in this cell type.

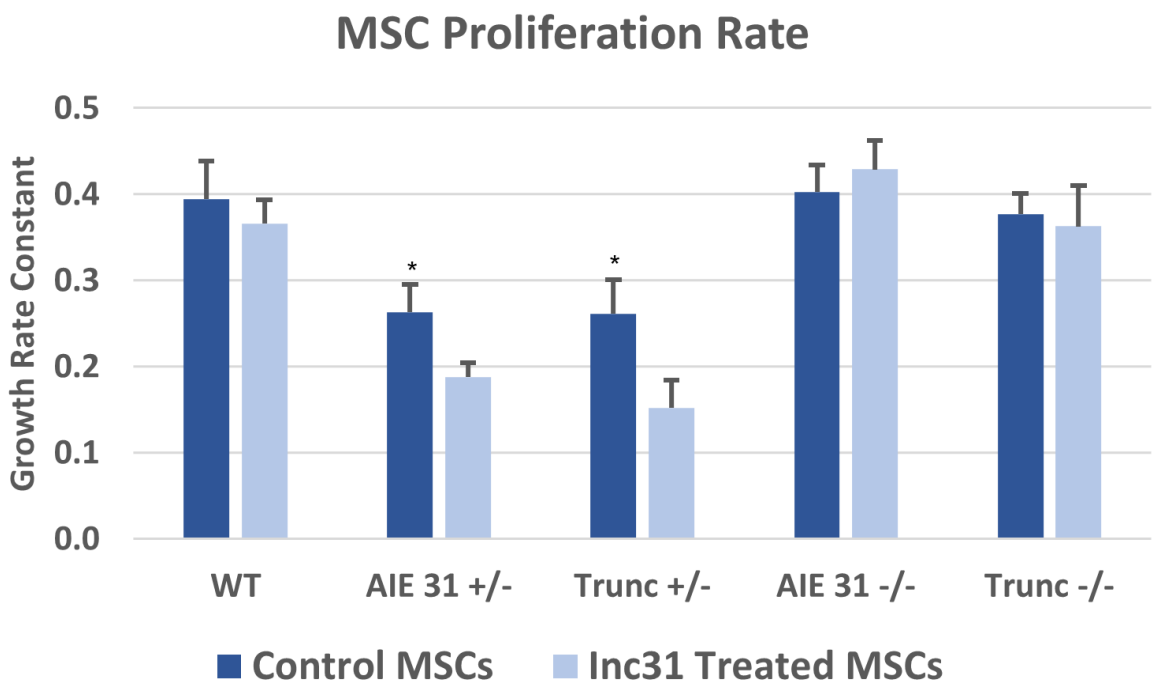

Figure 34. MSC SSO Proliferation – Proliferation rate growth constant of MSCs over a 3-day period following treatment with SSO Inc 31. Growth rate constants were calculated assuming an exponentially fit curve y(t)=ae^(kt). Significance between control and treatment groups indicated by * (p<0.05).

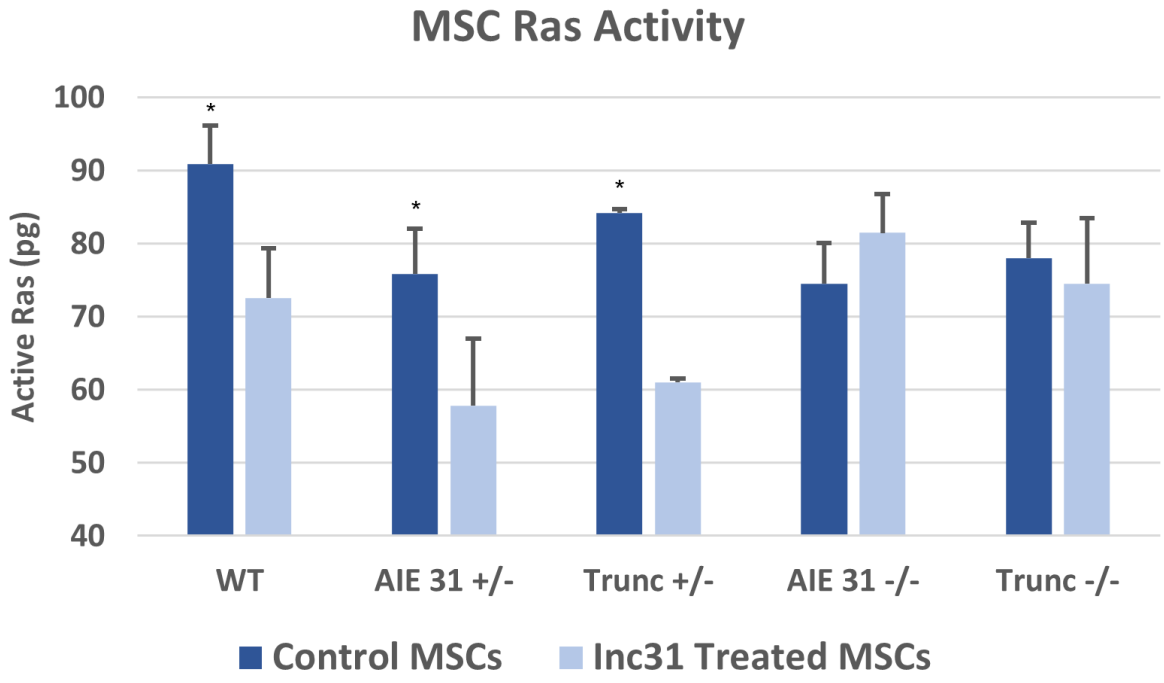

Figure 35. MSC SSO Ras – Active bound Ras quantified with standardize ELISA assay. Error bars represent technical duplicates. Significance between control and treatment groups indicated by * (p<0.05).

MSCs administered a single dose of SSO Inc31 produced significant changes in MSC proliferation and Ras activity in multiple genotypes. These changes generally trended together. Ras activity was reduced in WT, AIE 31 +/-, and Trunc +/- cells while proliferation was reduced in AIE 31 +/- and Trunc +/- cells (Figure 34, 35). Proliferation and Ras activity were statistically unchanged in both AIE -/- and Trunc -/- cells. This result was expected in *NF1* -/- cell lines as no functional target is present in the mutated alleles. It should be noted that due to the nature of the *NF1* Trunc -/- mutation, mRNA product is still detectable, even though any protein produced would be truncated before translation of the first exon is completed.

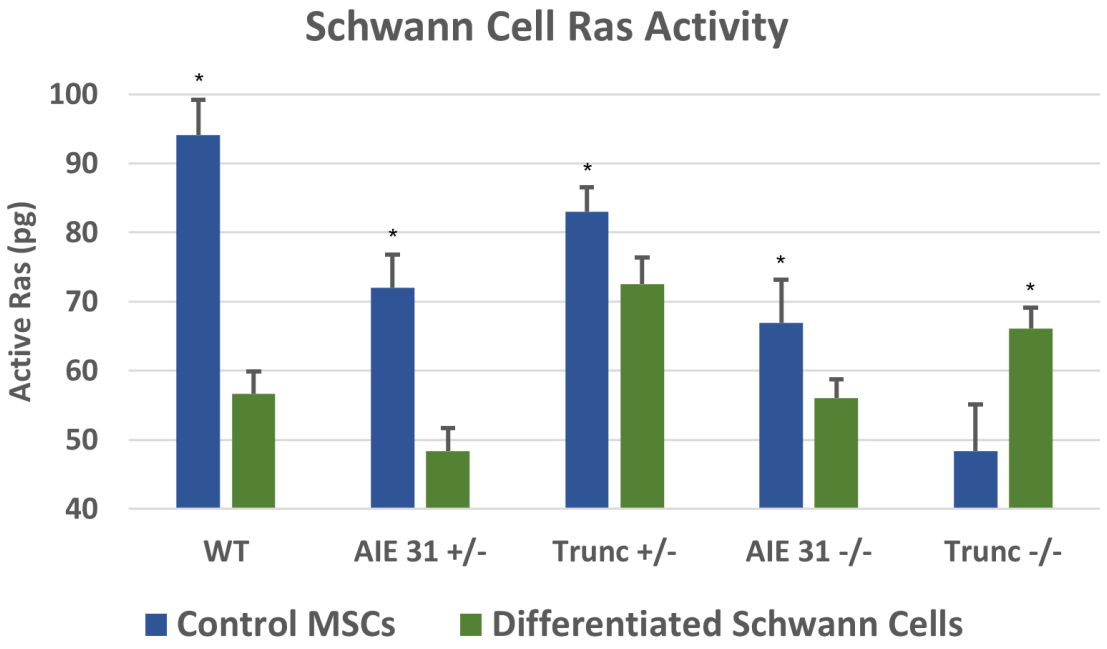

Figure 36. Schwann Ras – Active bound Ras quantified with standardize ELISA assay. Error bars represent technical duplicates. Significance between control and treatment groups indicated by * ($p<0.05$).

MSCs differentiating into Schwann cells show decreased Ras activity among all genotypes except *NF1* Trunc -/-, which show an increase in Ras activity (Figure 36). RT-qPCR revealed that this cell line did not upregulate markers associated with Schwann cell differentiation as the other cell lines did (Figure 37). Additionally, it did not show a

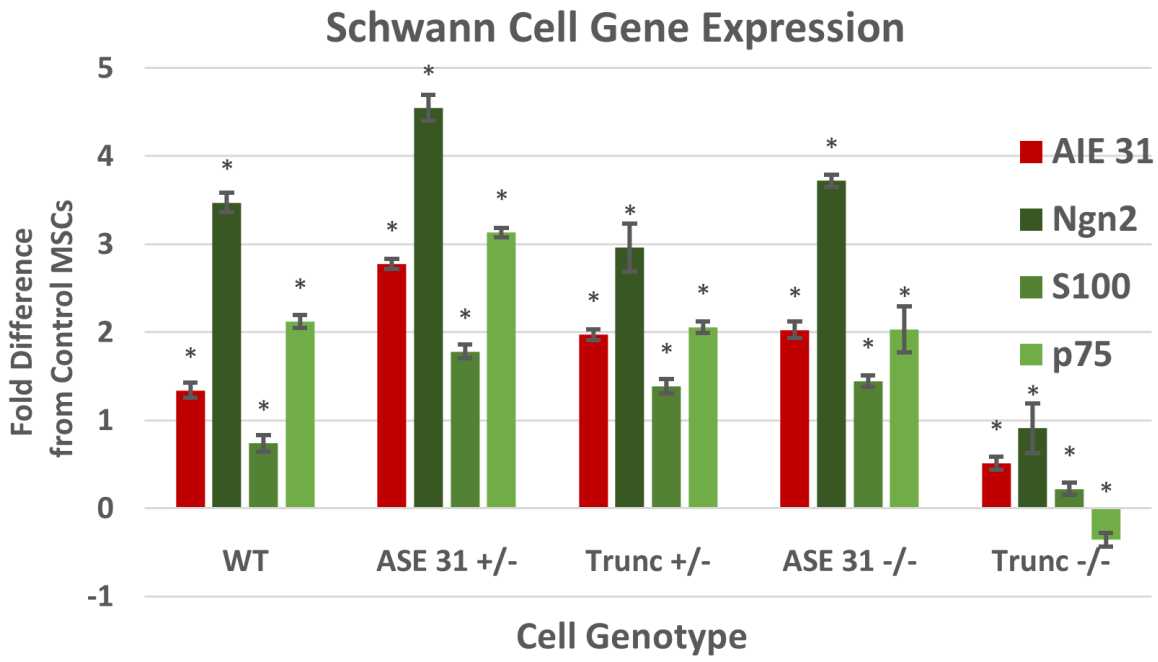

Figure 37. Schwann RT-qPCR – Gene expression of *NF1* AIE 31 and Schwann markers determined by RT-qPCR assay. Each genotype represents relative change vs its undifferentiated MSC control. Error bars represent standard deviation of technical triplicates. All bars are significantly different from its respective undifferentiated MSC control ($p<0.05$).

significant increase in AIE 31. These results suggest that Schwann cell differentiation of MSCs is characterized by a decrease in Ras activity and an increase in *NF1* AIE 31 and that *NF1* Trunc -/- MSCs do not differentiate into mature Schwann cells as the other cell lines. Differentiating Schwann cells that are concurrently transfected with SSO a31 Inc show enhanced expression of Schwann cell markers in cell lines that have functional targets but not in *NF1* AIE 31 -/- or *NF1* Trunc -/- Schwann cells, as compared to their respective untreated control Schwann cells (Figure 40). Ras activity and proliferation rates were also significantly decreased in WT and *NF1* AIE 31 +/- cells administered SSO Inc31, beyond the decrease associated with just Schwann differentiation (Figure 38, 39). These results show that SSO Inc31 enhanced Schwann cell differentiation and maturity through increasing expression of *NF1* AIE 31.

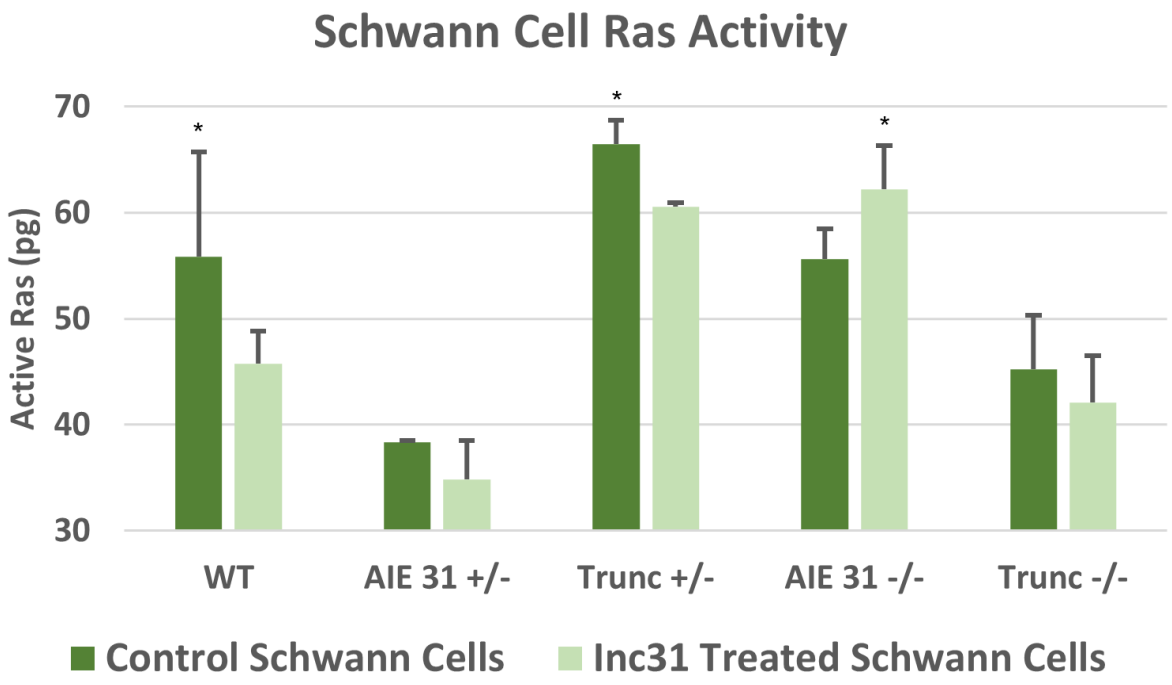

Figure 38. Schwann SSO Ras – Active bound Ras quantified with standardize ELISA assay. Error bars represent standard deviation of technical duplicates. Significance between control and treatment groups indicated by * ($p<0.05$).

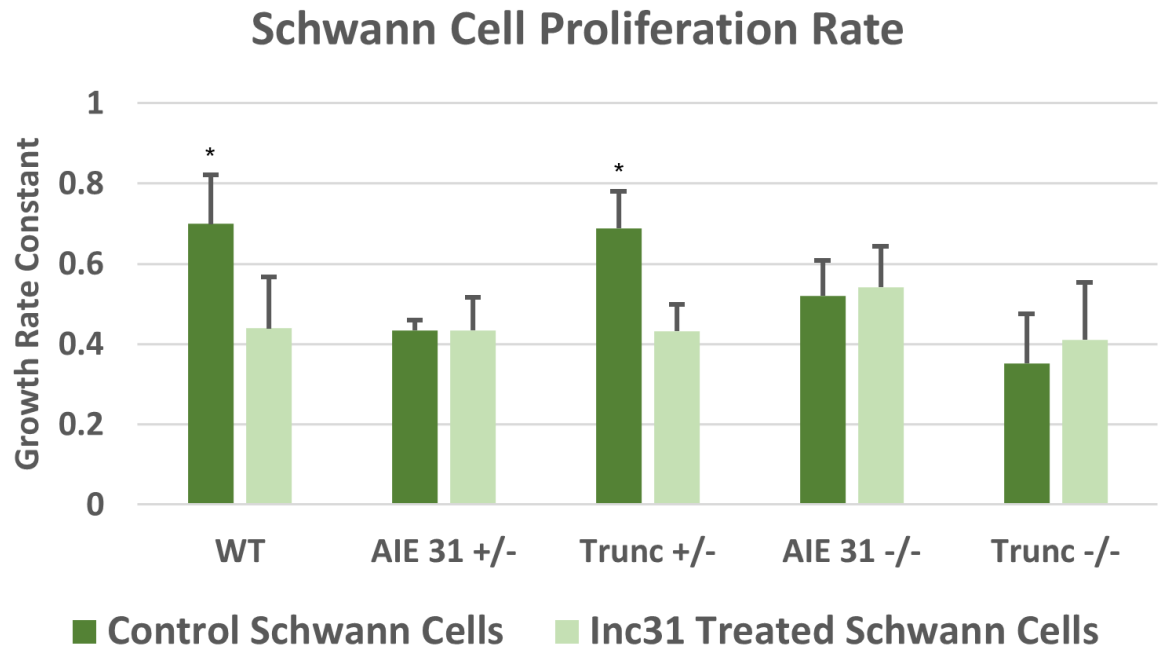

Figure 39. Schwann SSO Proliferation – Proliferation rate constant of MSCs over a 3 day period following treatment with SSO Inc 31. Growth rate constants were calculated assuming an exponentially fit curve y(t)=ae^(kt). Significance between control and treatment groups indicated by * ($p<0.05$).

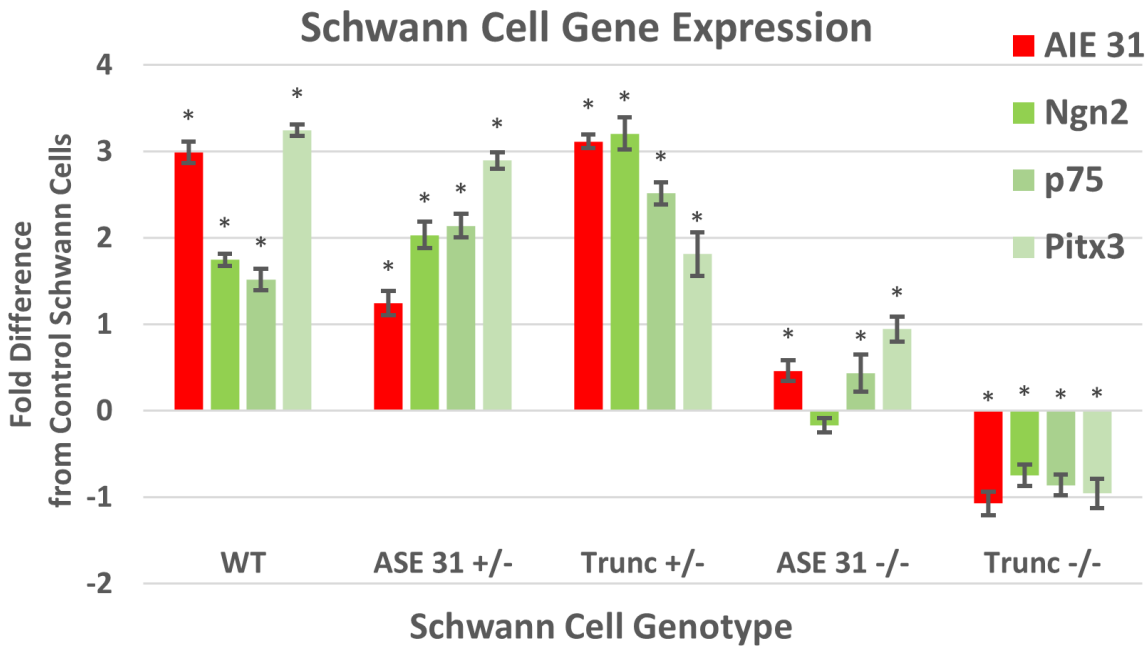

Figure 40. Schwann SSO RT-qPCR – Gene expression of *NF1* AIE 31 and Schwann markers determined by RT-qPCR assay. Each genotype represents relative change vs its untreated differentiated control. Error bars represent standard deviation of technical triplicates. All bars except one are significantly different from its respective untreated Schwann cell control ($p<0.05$).

4.5. Discussion

This is the first study to link *NF1* ASE modulation via SSOs to Schwann cell development. It has shown that SSOs can be used to modulate *NF1* AIE 31 expression in a functionally relevant way and may have therapeutic applications through targeting Schwann cell differentiation. This study has also shown that *NF1* ASEs in NF1 -/- cells cannot be modulated, however, a single functional allele is sufficient to elicit a functional response. SSOs could be used to target *NF1* +/- cells in the tumor microenvironment, as these cells are known to drive neurofibroma development.

Previous studies showed that SSOs can modulate *NF1* ASEs in a targeted manner, but optimized SSO concentrations were not used. This study found that higher concentrations of SSO produce greater ASE modulation. However, cell viability also decreases at higher

concentrations so a balance needed to be found to maximize efficacy. The viability curve for SSO Inc31 indicated concentrations as high as 1250 nM were tolerated by MSCs and significantly increased *NF1* AIE 31 in MSCs 2 days after administration. Previous studies have shown that that a single dose is not sufficient to produce detectable differences in *NF1* AIE 31 expression 14 days later in MSCs or differentiating Schwann cells. Therefore, serial doses of SSO Inc31were delivered throughout the differentiation process and significant increases in *NF1* AIE 31 were detected while cell viability was maintained. A single dose of 2000 nM SSO Inc31 would have likely been detrimental to cell viability but when spread over 14 days it was tolerated. The decay rate or half-life of these modified SSOs is not known but the previous results indicate that physiological activity significantly declines between 4 and 14 days. Different modifications can increase the duration of this activity and some reports have shown that SSOs can remain effective for months in some tissues *in vivo*. Further studies could be performed to optimize the dosing regimen for maximum efficacy but would likely need to be determined for any given cell type and SSO modification.

While MSCs have clear advantages for the current studies, but they also come with some limitations. The *NF1* ASE expression profile of swine indicates that AIE 12 and 57 are found at very low levels in MSCs. Consequently, a relatively small change in expression may have outsized influences on the cells and may induce an apoptotic or other toxic response. The cell viability assay suggests the SSOs that increase AIE 12 and 57 do elicited a specific negative response in MSCs. Testing these SSOs in cell types known to have higher expression of their associated *NF1* ASE may prove to be a more efficacious approach of evaluating their functional activities. Prior studies in this lab have shown that using an artificial minigene overexpression system to increase the target mRNA in MSCs can be used

to evaluate SSO efficacy and that SSO efficacy is consistently increased at higher doses, even if detrimental to the overall health of the cell. Using an overexpression system, however, doesn't reflect the true state of the biological system and other cell types would need to be used to evaluate SSO functional downstream effects. Fortunately, MSCs and Schwann cells do express AIE 31 at a high level and are well suited for evaluating SSO modulation targeting this ASE.

NF1 AIEs have been previously characterized in Schwann cells and compared to MSCs. *NF1* AIE 12, while very low in MSCs, increases in Schwann cells. *NF1* AIE 31 is expressed at high levels in MSCs and increases further in Schwann cells while *NF1* AIE 57 is very low in MSCs and decreases slightly in Schwann cells. It has been well established that *NF1* AIE 31 is upregulated in Schwann cells and is important for fine-tuning Ras activity. These results show that differentiating Schwann cells also show an increase in AIE 31 in swine cell culture. Further, treatment with SSO Inc31 in both MSCs and differentiating Schwann cells causes functional downstream effects in both Ras activity and proliferation rate. SSO Inc31 also increases the expression of Schwann markers in differentiating Schwann cells. The coordinated rise in *NF1* AIE 31 and Schwann cell markers suggests this ASE is linked to Schwann cell development and its suppression may be detrimental to normal activity. One recent report has linked NF1 AIE 31 modulation to Ras activity in developing neurons, but this is the first report showing this AIE also is associated directly with expression of neuronal markers in differentiating Schwann cells. Proliferation rate and Ras activation are known to be linked together and their dysregulation is often associated with a tumorigenic phenotype. Attenuating their activities may be a viable therapeutic

strategy in NF1 tumor, or any tumor with enhanced Ras activity or Schwann cell involvement, by increasing *NF1* AIE 31 with SSOs.

Several previously published studies have shown an association between the expression of *NF1* AIE 31 and Ras activity and have attributed this relationship to its location within the GRD domain of neurofibromin. These studies have also shown that inclusion of *NF1* AIE 31 produces an increase in proliferation and Ras activation, contrary to what the current study indicates [245]. Most of these prior studies on *NF1* AIE 31 were performed in rodent models, and it is possible swine *NF1* AIE 31 has a different biological effect in this culture platform due to subtle differences in the protein or in the way the Ras pathway signals in swine. Different cell types could also be influenced in uniquely different ways by *NF1* AIE 31. *NF1* AIE 31 expression is remarkably different in neurons compared to Schwann cells and many of the prior *NF1* AIE 31 studies have looked primarily at neurons. Given the low expression in neurons, other cellular mechanisms may become more dominant. Some of these studies have also looked at immortalized cell lines but this too may cause unknown changes in the Ras signaling pathway and therefore changes in *NF1* AIE 31 may not be the same in a normal physiological state. Further studies in other species, in different primary cell types, and with additional assays may illuminate this notable difference in differentiating swine Schwann cells.

SSO Inc31 has consistent functional effects upon MSCs and the Schwann differentiation process only in WT and *NF1* +/- cell lines indicating that cell lines that must have at least one normal *NF1* allele to be amenable to SSO modulation. The two *NF1* homozygous cells lines, *NF1* AIE 31 -/- and *NF1* Trunc -/-, either lack an mRNA target or the functionality to express neurofibromin and show little or even negative changes in

Schwann cell markers, Ras activity, and proliferation rates following SSO Inc31 treatment. MSC cell lines show similar trends when treated with this SSO. In addition to confirming the need for a WT allele to function, these data also demonstrate that SSO Inc31 is acting in a specific, targeted manner by eliminating the possibility that SSO delivery is simply decreasing Ras activity and proliferation rate generally. The cell of origin in neurofibromas are thought to be Schwann cells that have lost *NF1* heterozygosity and would therefore not respond to SSO treatment. However, recent studies have strongly implicated the microenvironment in the development and progression of neurofibroma growth. This *NF1* microenvironment is made up of supporting cells such as fibroblasts, mast cells, and macrophages. Importantly, these cells typically retain *NF1* heterozygosity in neurofibromas making them potential cell targets of SSOs. Patients with heterogeneous *NF1* mutations could benefit from SSO therapy to enhance *NF1* AIE 31 expression in the microenvironment and reduce or even prevent Schwann cell tumorigenic activity. Overall, this work provides strong rationale to further pursue SSO therapies targeting this *NF1* ASE using preclinical NF1 swine models. Future studies may explore the therapeutic potential of SSOs targeting cell types within the NF1 tumor microenvironment.

4.6 Supplementary Materials

NF1 ASE Region	Regulatory Target	Function	SSO Sequence
AIE 12	Enhancing Element	Skipping	UACAGCAGUGCCAAGUCCAUG
	Silencing Element	Inclusion	GUAGACAAAAAUAUUUCAC
AIE 31	Enhancing Element	Skipping	CUGAUUUUUUGUUUUCCUUUUUUUC
	Silencing Element	Inclusion	AGCAACAAAAACAAUG
AIE 57	Enhancing Element	Skipping	GGGAACAGCUGCAUGAAAA
	Silencing Element	Inclusion	GGAAGAAAAAACAAAAGUGAGUGG

Table 4. SSO Viability Designs - Sequences of SSO for each regulatory element. All SSOs contained phosphorothioated backbones and 2′–O–Me groups throughout.

NF1 ASE Region	Target	Primer Sequence	
AIE 31	Surrounding Exons	Forward	CATGCCATCATCAGCTCCTC
		Reverse	TGAGGGAAACGCTGGCTAAC
	AIE Only	Forward	CATGCCATCATCAGCTCCTC
		Reverse	TTATTCAGTAGGGAGTGGCAAG
PPIA	Exon-Exon Boundry	Forward	CACAAACGGTTCCCAGTTTT
		Reverse	TGTCCACAGTCAGCAATGGT
RPL4	Exon-Exon Boundry	Forward	AGGAGGCTGTTCTGCTTCTG
		Reverse	TCCAGGGATGTTTCTGAAGG
TBP	Exon-Exon Boundry	Forward	GATGGACGTTCGGTTTAGG
		Reverse	AGCAGCACAGTACGAGCAA
Ngn2	Exon-Exon Boundry	Forward	CTGAGTAGCAGCGGAGACAG
		Reverse	CGGACTGGCAGGAGATAAAG
S100	Exon-Exon Boundry	Forward	GGGACAAGCACAAGCTGAAG
		Reverse	TCCATGACTTTGTCCACGAC
p75	Exon-Exon Boundry	Forward	TGCTGCTGCTGCTGCTC
		Reverse	AGGTTGCAGGCTTTGCAG
Pitx3	Exon-Exon Boundry	Forward	CAAGGGCCAAGAGCACAG
		Reverse	CTTCTTCAGCGAGCCGTCTT

Table 5. Neuronal RT-qPCR Primers - Primers used for RT-qPCR of swine tissue culture. All primers span an early exon-exon junction.

CHAPTER 5 – Discussion and Future Directions

5.1. Current Medical Care

Medical care for NF1 patients begins with a diagnosis and continues with surveillance for complications or other new manifestations [246]. Medical costs for NF1 pediatrics patients average nearly $20,000 per year and can be much higher if surgical interventions are indicated [247]. Aside from tumors, areas that are routinely evaluated include neurological abnormalities like learning deficits, seizures, or neuropathy, bone abnormalities such as scoliosis or osteoporosis, psychosocial issues, and cardiovascular problems [248]. Should any of these be identified, therapies are aimed at treating symptoms as very few NF1-centric therapeutics exist at this time.

Cancer Therapies

Tumor treatment for NF1 patients has traditionally been based on the presentation, histology, and molecular characteristics of the tumor. Tumors can be resected and adjuvant treatments like chemotherapy and radiotherapy can be used, although radiotherapy is sometimes avoided due to the potential to cause a second hit mutation in *NF1* heterogeneous cells. More recently, several therapeutics have been adapted and created specifically for *NF1* type tumors because of a greater understanding of the molecular pathology of NF1. Imatinib was among the first therapies and has shown some success in treating plexiform neurofibromas [249]. Sirolimus and rapamycin, both mTOR inhibitors, also frequently exhibit positive responses [250]. For MPNST cell lines, certain classes of drugs have shown the most promise in preclinical trials, namely inhibitors of Raf, MEK, PI3K/mTOR, and Pak [251]. This has resulted in the first NF1-centric cancer drug, selumetanib, a MEK inhibitor,

to be approved by the FDA [252]. It is geared towards pediatric patients with inoperable plexiform neurofibromas but is used more broadly for many NF1 tumors [253]. Other MEK inhibitors are currently in clinical trials.

Interventional Strategies

Nutritional and other preventative strategies for NF1 are not formally written into guidelines. However, there have been studies to suggest that certain practices can be beneficial. Docosahexaenoic acid (DHA) has been shown to inhibit MPNST growth at high doses in mouse models and promote apoptosis *in vitro* [254]. Many NF1 patients, particularly children, can present with reduced muscle mass and other motor functions. NF1 mouse models exhibit impaired long-chain fatty acid metabolism in muscle tissues which is corrected by an increased medium-chain fatty acid diet and reduction of long-chain fatty acids [255]. Progesterone receptors are found on a large majority of all neurofibromas, in both males and females, and may warrant consideration of antiprogestins as a treatment or preventative measure [256]. Pregnancy has also been shown to increase neurofibroma growth, while the post-partum period decreases it [257].

Developing Treatments

Current treatments for NF1 are very limited and often inadequate for the many NF1 patients seeking medical care. While an increased awareness within the medical community of this disease helps in directing patients to the proper facilities and physicians, there is still a great need for NF1-centric therapies. Understanding the causative role that *NF1* has in disease development has become central to developing targeted therapies. This has also led to

identifying *NF1* as a central tumor suppressor in many other cancer types. Finding suitable therapeutic targets for NF1 may have benefits more broadly in cancer treatment. This fact further highlights the importance of elucidating the complex mechanisms surrounding the function of this gene. The results of this current work have provided a foundation and rationale for future tissue-, cell-, and molecular- level experiments to facilitate the development of a therapy for NF1.

5.2. Future Directions

Tumor Microenvironment

The tumor microenvironment has been strongly implicated in driving NF1 tumorigenesis. *NF1* heterogeneity has been shown to influence cells directly and indirectly as it modifies the cellular microenvironment. *NF1* +/- fibroblasts' ability to properly orient themselves in their environment is impaired [91]. *NF1* heterogeneity of mast cells and fibroblasts are also important mediators of *NF1* -/- Schwann cells' initiation of plexiform neurofibroma development [63]. In mice, neurofibromas originating from *NF1*-/- Schwann cells require an *NF1* +/- microenvironment or tumors will not form [148]. Optic nerve glioma formation in mice are also dependent on *NF1* heterogeneity in the tumor microenvironment [119].

SSOs are not able to modulate *NF1* ASE expression in *NF1*-/- cells, however, SSOs are capable of modulating *NF1* ASE expression in *NF1* +/- cells in a manner consistent with or greater than a comparable WT cell. In a co-culture system, *NF1* +/- fibroblasts could be grown together with *NF1* -/- Schwann cells to evaluate the tumorigenic role of fibroblasts. Then, SSOs could be administered to attenuate this tumorigenic activity by targeting *NF1*

ASEs in fibroblasts. Preliminary results have shown SSO are capable of modulating *NF1* ASE levels in fibroblasts (Figure 41). Similar cell culture methodologies and functional assays as used in this work could be adapted for this experiment. Additionally, primary mast cells obtained from available GE swine could also be used in this co-culture system.

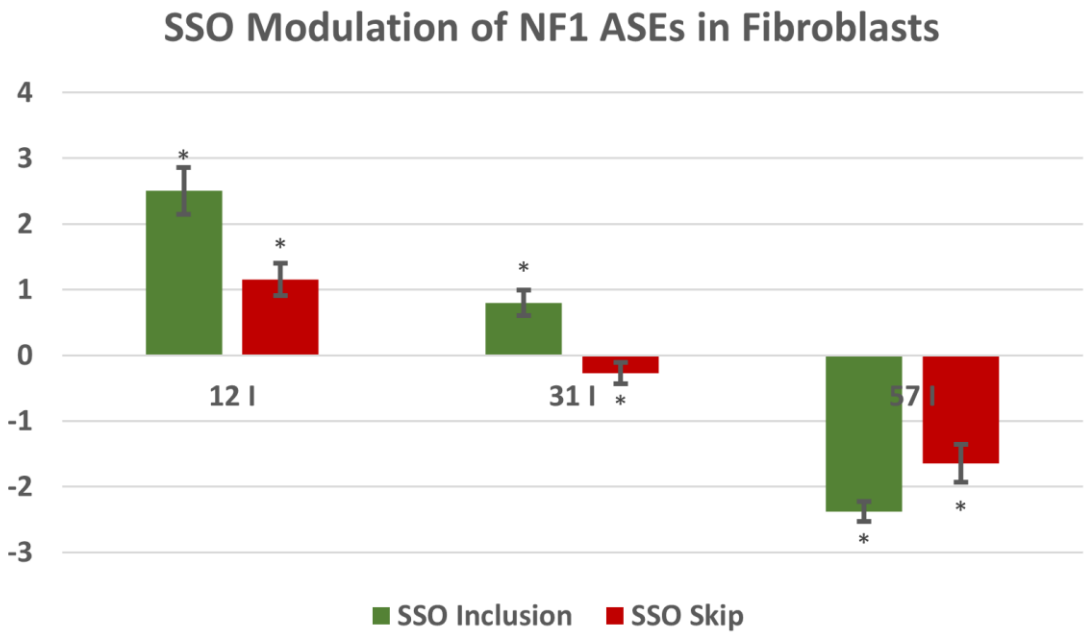

Figure 41. SSO Fibroblast Efficacy – SSOs administered to fibroblasts in the same manner as MSCs from the previous studies. SSO Skip 12 appears to increase ASE 12, but the Ct value is beyond the working range of the primers and cannot be meaningfully reduced (>37 Ct value). SSO Inc 57 again showed toxic effects. All bars are significantly different from an untreated MSC control group ($p<0.05$).

Full mRNA Transcript Sequencing

Total RNA sequencing would be valuable to further elucidate the *NF1* isoforms present in various tissues and may shed further insights into the nature of some tissue specific pathologies. The results of the current studies determined expression levels of each *NF1* ASE as an isolated entity. An unresolved question concerning mRNA transcripts remains. In what combinations are *NF1* ASEs expressed? For example, if ASE 12 is included, does that exclude ASE 57? Is there any relationship between expression of ASEs? These questions can

only be definitively answered with whole transcriptome analysis of *NF1* mRNA. Additionally, data generated in adult swine tissues using primers spanning the entire ASE 31 region gave inconsistent results when compared to other primers designed to detect constitutively expressed *NF1* mRNA. This suggests some additional splicing events may be occurring in this region. Whole transcriptome analysis would be able to identify any other alternatively spliced exons or splicing events that are perhaps unique to swine [258].

Sequencing of large mRNA transcripts is challenging and likely the reason these studies have not been undertaken. To overcome this challenge, two swine tissue samples used in this study, from the frontal cortex and heart, were prepared for *NF1* transcript analysis. Prior to analysis with PacBio, a few important steps were taken. Total mRNA from the cryopreserved tissues of interest was isolated once again but also treated with DNase. Each sample was submitted for mRNA analysis with the Agilent RNA 6000 Nano Kit to evaluate mRNA integrity, with RIN numbers above 7 indicating good condition. Importantly, degradation must be minimal to confidently proceed with whole transcript sequencing. Three approaches were used to sequence. The first using a standard Iso-Seq Express protocol that amplifies all mRNA, a second process that uses the standard reverse transcriptase process but then uses an *NF1* selective primer for cDNA amplification, and a third process that uses a UMI-tagged primer in the reverse transcriptase reaction and then uses the *NF1* selective primer for cDNA amplification. The *NF1* specific selection steps were performed to maximize the abundance of *NF1* cDNA to the point where PacBio can be used but also hedging to ensure enough cDNA was present to create a library, typically at least 80 ng. The libraries generated are currently awaiting analysis.

In situ hybridization

NF1 ASE expression levels were determined for whole tissue samples taken from swine. Each of these samples is, to some degree, a heterogenous mixture. While the tissue of interest is hopefully the predominant one, other tissue types are present and thus included in the total mRNA samples isolated. One solution to this probably would be to do single cell RNA sequencing. This would be able to distinguish expression levels for *NF1* between individual cells. There are some drawbacks to this approach, however, aside from cost. Separating tissues into a single cell constitution can be difficult as many different enzymes are likely needed and even then, some cell type may remain attached to the tissue matrix. These processes must also be done on live cells and the procedure is likely to change mRNA expression. Some questions therefore remain. Are isolated cell types within a given tissue responsible for the predominant changes noted in *NF1* ASE expression? Are some expression differences being diluted out because too few cells are contained within the sample? Apart from single-cell RNA sequencing, another approach that also avoids the potential pitfalls as mentioned before could be used to answer these questions. *In situ* hybridization is a histological technique used to label, or probe, tissues for specific RNA or DNA sequences and has been used to label whole transcript *NF1* mRNA [259]. Chemical or radiolabeled probes would be designed to target each ASE region and then used on snap-frozen, cryosectioned tissues, along with tissue specific probes, to determine which cells expressed the abundance of any given ASE. This approach would produce semi-quantitative visual data; however, it could also be used to determine intra-cellular localization of the ASEs in a way sequencing cannot. Custom *in situ* hybridization service can be contracted by a variety of companies. Bio-Techne has generated BaseScope probe designs for swine ASE 12, 31,

and 57 and would be able to perform this analysis. It should be noted that antibodies have not been created for specific NF1 isoforms. Should they be developed in the future, these could be used on these same tissues and offer the additional advantage of intra-cellular protein localization analysis, which would provide greater physiologically relevant information than mRNA localization.

DNA Methylation of ASE Regions

Methylation of DNA is an inheritable epigenetic mark associated with CpG sites on DNA and is a regulator of many cellular processes including transcription, X-chromosome inactivation, and cellular differentiation, among many others. Methylation acts as a local repressor to the binding of other molecules, so if the promoter region of a gene is methylated, its transcription will be repressed. *NF1* promoter region methylation has been characterized but, in at least one comprehensive study, no evidence for its role in tumor development was indicated [260]. *NF1* has over 5000 other sites within the gene that may undergo methylation, including near ASE, however, this has not been explored. It's estimated that 22% of ASE are regulated by DNA methylation and regulated by way of at least three different distinct protein communication pathways [261].

DNA methylation detection is frequently performed using bisulfite genomic sequencing analysis. In this technique, bisulfate treatment of DNA converts cytosines into uracil residues unless they are methylated. A subsequent PCR reaction will recognize uracil as thymine and is run along with an untreated DNA strand. Following a sequencing reaction, the two samples are compared to determine locations of methylation [262]. The function of these identified methylation marks could then be studied using a CRISPR/dCas9 system.

This system can be used to achieve both selective methylation or passive demethylation of targeted CpG sites under a broad range of conditions [263]. These approaches in combination could be applied to *NF1* ASE regions under experimental conditions or in different animal tissues, similarly to that conducted in the presented body of work.

In vivo SSO Delivery in Swine

The efficacy of *NF1* specific SSOs *in vitro* has been established in this work. They can modify *NF1* ASEs in a selective manner thereby modulating downstream cellular activity. It remains to be seen, however, how well these SSOs perform *in vivo*. One of the greatest challenges to SSO therapy is delivering them to targeted tissues and many additional factors must be taken into account [264]. Basic pharmacokinetics, the biodistribution profile, toxicity and dosing regimens, and off-target interactions are clearly important. The blood brain barrier limits the transport of many pharmaceuticals, including oligonucleotides. Bypassing this using intrathecal injection is possible but also carriers many additional risks. Complexing SSOs with agents like nanoparticles can assist in targeting tissues but this can also further exclude their entry though the vascular endothelial barrier and are more likely to be taken up by immune cells. Many other SSO modifications and packaging systems could be employed but must be evaluated in swine first before true therapeutic SSO therapy can prudently be attempted. Establishing delivery methodology will be critical in advancing development of SSO therapies, not only in the animal models, but also for administration to patients.

NF1 Splicing-Mutation Swine Models

NF1 swine models are currently being validated as a translational model at many institutions. The current aims are usually to show that swine present NF1 symptomatology and molecular pathology sufficiently like human. Confirmation of this will open a new translational pipeline for the discovery and pre-clinical testing of new therapies. The next generation of GE NF1 swine could be designed to harbor *NF1* mutations on recognized regulatory splice sites anywhere on the *NF1* gene, although mutations homologous to one of the many splice-altering regions seen in humans would be preferred. SSO could then be adapted to correct the aberrant splicing and be validated *in vivo* before being moved into clinical trials. As genetically engineering swine becomes more efficient and economical, creating swine with these genotypes could take priority over producing NF1 swine that simply display NF1 sequelae.

5.3. Conclusions

The research undertaken in this body of work has further established that NF1 swine models represent the phenotypic complexity observed in NF1 patients. Swine effectively models *NF1* alternative splicing in humans and can be used to evaluate SSO modulation of *NF1* ASEs. This work has established a translationally relevant NF1 cell culture platform to study NF1. This is the first report comparing *NF1* ASE expression levels and regulatory regions in swine to human. It is also the first report linking *NF1* AIE modulation to Schwann cell development. These results have provided rationale for future studies using SSOs to correct other *NF1* splicing defects using swine as a model. Other novel findings from this research include identifying a single base pair addition in the ASE 13 region in swine,

demonstrating many statistically significant differences in *NF1* ASE expression with respect to tissue and age, and demonstrating that enhancing *NF1* ASE 31 inclusion in differentiating Schwann cells and MSCs reduces Ras activity and proliferation rate. *NF1* ASEs may prove to be a critical component dictating NF1 complexity and further elucidation of their functional roles will be greatly facilitated by NF1 swine models.

BIBLIOGRAPHY

1. Rubinstein, C.D., et al., *Assessment of Mosaicism and Detection of Cryptic Alleles in CRISPR/Cas9-Engineered Neurofibromatosis Type 1 and TP53 Mutant Porcine Models Reveals Overlooked Challenges in Precision Modeling of Human Diseases.* Front Genet, 2021. **12**: p. 721045.
2. Rasmussen, S.A., Q. Yang, and J.M. Friedman, *Mortality in neurofibromatosis 1: an analysis using U.S. death certificates.* Am J Hum Genet, 2001. **68**(5): p. 1110-8.
3. Genetic and Rare Diseases Information Center, N. *Neurofibromatosis*. 2022; Available from: https://rarediseases.info.nih.gov/.
4. Uusitalo, E., et al., *Incidence and mortality of neurofibromatosis: a total population study in Finland.* J Invest Dermatol, 2015. **135**(3): p. 904-906.
5. Zanca, A. and A. Zanca, *Antique illustrations of neurofibromatosis.* Int J Dermatol, 1980. **19**(1): p. 55-8.
6. Choulant, L., *Graphische incunabeln für naturgeschichte und medicin. Enthaltend geschichte und bibliographie der ersten naturhistorischen und medicinischen drucke des XV und XVI. jahrhunderts, welche mit illustrirenden abbildungen versehen sind. Nebstnachträgen zu des verfassers Geschichte und bibliographie der anatomischen abbildung*. 1858, Leipzig,: R. Weigel. xx, 168 p.
7. Riccardi, V.M., *Von Recklinghausen neurofibromatosis.* N Engl J Med, 1981. **305**(27): p. 1617-27.
8. Collins, F.S., et al., *Progress towards identifying the neurofibromatosis (NF1) gene.* Trends Genet, 1989. **5**(7): p. 217-21.
9. Williams, V.C., et al., *Neurofibromatosis type 1 revisited.* Pediatrics, 2009. **123**(1): p. 124-33.
10. Lobo, I., *Same genetic mutation, different genetic disease phenotype.* Nature Education, 2008. **1 (1): 64**.
11. Health, N.I.o., *Neurofibromatosis. Conference statement. National Institutes of Health Consensus Development Conference.* Arch Neurol, 1988. **45**(5): p. 575-8.
12. Spurlock, G., et al., *SPRED1 mutations (Legius syndrome): another clinically useful genotype for dissecting the neurofibromatosis type 1 phenotype.* J Med Genet, 2009. **46**(7): p. 431-7.
13. Colley, A., D. Donnai, and D.G. Evans, *Neurofibromatosis/Noonan phenotype: a variable feature of type 1 neurofibromatosis.* Clin Genet, 1996. **49**(2): p. 59-64.
14. Nava, C., et al., *Cardio-facio-cutaneous and Noonan syndromes due to mutations in the RAS/MAPK signalling pathway: genotype-phenotype relationships and overlap with Costello syndrome.* J Med Genet, 2007. **44**(12): p. 763-71.
15. Kontaridis, M.I., et al., *PTPN11 (Shp2) mutations in LEOPARD syndrome have dominant negative, not activating, effects.* J Biol Chem, 2006. **281**(10): p. 6785-92.
16. Allanson, J.E., et al., *Watson syndrome: is it a subtype of type 1 neurofibromatosis?* J Med Genet, 1991. **28**(11): p. 752-6.
17. Hebron, K.E., E.R. Hernandez, and M.E. Yohe, *The RASopathies: from pathogenetics to therapeutics.* Dis Model Mech, 2022. **15**(2).

18. Kehrer-Sawatzki, H. and D.N. Cooper, *Challenges in the diagnosis of neurofibromatosis type 1 (NF1) in young children facilitated by means of revised diagnostic criteria including genetic testing for pathogenic NF1 gene variants.* Hum Genet, 2022. **141**(2): p. 177-191.
19. Le, C. and P.M. Bedocs, *Neurofibromatosis*, in *StatPearls*. 2022: Treasure Island (FL).
20. Garty, B.Z., A. Laor, and Y.L. Danon, *Neurofibromatosis type 1 in Israel: survey of young adults.* J Med Genet, 1994. **31**(11): p. 853-7.
21. Legius, E., et al., *Revised diagnostic criteria for neurofibromatosis type 1 and Legius syndrome: an international consensus recommendation.* Genetics in Medicine, 2021. **23**(8): p. 1506-1513.
22. Khoury, M.J., L.L. McCabe, and E.R. McCabe, *Population screening in the age of genomic medicine.* N Engl J Med, 2003. **348**(1): p. 50-8.
23. Center, M.C. *Neurofibromatosis Screening*. 2018; Available from: https://moffitt.org/cancers/neurofibromatosis/diagnosis/screening/.
24. Sabbagh, A., et al., *NF1 molecular characterization and neurofibromatosis type I genotype-phenotype correlation: the French experience.* Hum Mutat, 2013. **34**(11): p. 1510-8.
25. Nunley, K.S., et al., *Predictive value of cafe au lait macules at initial consultation in the diagnosis of neurofibromatosis type 1.* Arch Dermatol, 2009. **145**(8): p. 883-7.
26. Senthilkumar, V.A. and K. Tripathy, *Lisch Nodules*, in *StatPearls*. 2022: Treasure Island (FL).
27. Ragge, N.K., et al., *Images of Lisch nodules across the spectrum.* Eye (Lond), 1993. **7 (Pt 1)**: p. 95-101.
28. Friedman, J., *Neurofibromatosis 1*. GeneReviews, 2019.
29. Upadhyaya, M., *The Molecular Biology of Neurofibromatosis Type 1*. Colloquium Series on Genomic and Molecular Medicine, 2014.
30. Dulai, S., et al., *Decreased bone mineral density in neurofibromatosis type 1: results from a pediatric cohort.* J Pediatr Orthop, 2007. **27**(4): p. 472-5.
31. Wu, X., et al., *Neurofibromin plays a critical role in modulating osteoblast differentiation of mesenchymal stem/progenitor cells.* Hum Mol Genet, 2006. **15**(19): p. 2837-45.
32. Friedman, J.M., et al., *Cardiovascular disease in neurofibromatosis 1: report of the NF1 Cardiovascular Task Force.* Genet Med, 2002. **4**(3): p. 105-11.
33. Oderich, G.S., et al., *Vascular abnormalities in patients with neurofibromatosis syndrome type I: clinical spectrum, management, and results.* J Vasc Surg, 2007. **46**(3): p. 475-484.
34. Greene, J.F., Jr., J.E. Fitzwater, and J. Burgess, *Arterial lesions associated with neurofibromatosis.* Am J Clin Pathol, 1974. **62**(4): p. 481-7.
35. Huffman, J.L., et al., *Neurofibromatosis and arterial aneurysms.* Am Surg, 1996. **62**(4): p. 311-4.
36. Bizzarri, C. and G. Bottaro, *Endocrine implications of neurofibromatosis 1 in childhood.* Horm Res Paediatr, 2015. **83**(4): p. 232-41.
37. Diggs-Andrews, K.A. and D.H. Gutmann, *Modeling cognitive dysfunction in neurofibromatosis-1.* Trends Neurosci, 2013. **36**(4): p. 237-47.

38. Hofman, K.J., et al., *Neurofibromatosis type 1: the cognitive phenotype.* J Pediatr, 1994. **124**(4): p. S1-8.
39. Descheemaeker, M.J., et al., *Behavioural, academic and neuropsychological profile of normally gifted Neurofibromatosis type 1 children.* J Intellect Disabil Res, 2005. **49**(Pt 1): p. 33-46.
40. Thompson, H.L., et al., *Speech-language characteristics of children with neurofibromatosis type 1.* Am J Med Genet A, 2010. **152A**(2): p. 284-90.
41. Huijbregts, S., *Cognitive-behavioral phenotype or comorbid disorder? The case of attention-deficit-hyperactivity disorder in neurofibromatosis type 1.* Dev Med Child Neurol, 2012. **54**(10): p. 873-4.
42. Omrani, A., et al., *HCN channels are a novel therapeutic target for cognitive dysfunction in Neurofibromatosis type 1.* Mol Psychiatry, 2015. **20**(11): p. 1311-21.
43. Hegedus, B., et al., *Neurofibromatosis-1 regulates neuronal and glial cell differentiation from neuroglial progenitors in vivo by both cAMP- and Ras-dependent mechanisms.* Cell Stem Cell, 2007. **1**(4): p. 443-57.
44. Anastasaki, C., et al., *Elucidating the impact of neurofibromatosis-1 germline mutations on neurofibromin function and dopamine-based learning.* Hum Mol Genet, 2015. **24**(12): p. 3518-28.
45. Landry, J.P., et al., *Comparison of Cancer Prevalence in Patients With Neurofibromatosis Type 1 at an Academic Cancer Center vs in the General Population From 1985 to 2020.* JAMA Netw Open, 2021. **4**(3): p. e210945.
46. Nascimento, R., et al., *Arm malignant peripheral nerve sheath tumour: a rare clinical presentation.* BMJ Case Rep, 2019. **12**(8).
47. Rozza-de-Menezes, R.E., et al., *Prevalence and clinicopathological characteristics of lipomatous neurofibromas in neurofibromatosis 1: An investigation of 229 cutaneous neurofibromas and a systematic review of the literature.* J Cutan Pathol, 2018. **45**(10): p. 743-753.
48. Ortonne, N., et al., *Cutaneous neurofibromas: Current clinical and pathologic issues.* Neurology, 2018. **91**(2 Suppl 1): p. S5-S13.
49. Pummi, K.P., et al., *Tight junction proteins and perineurial cells in neurofibromas.* J Histochem Cytochem, 2006. **54**(1): p. 53-61.
50. Riccardi, V.M., *Cutaneous manifestation of neurofibromatosis: cellular interaction, pigmentation, and mast cells.* Birth Defects Orig Artic Ser, 1981. **17**(2): p. 129-45.
51. Le, L.Q., et al., *Cell of origin and microenvironment contribution for NF1-associated dermal neurofibromas.* Cell Stem Cell, 2009. **4**(5): p. 453-63.
52. Jouhilahti, E.M., et al., *The development of cutaneous neurofibromas.* Am J Pathol, 2011. **178**(2): p. 500-5.
53. Duong, T.A., et al., *Mortality associated with neurofibromatosis 1: a cohort study of 1895 patients in 1980-2006 in France.* Orphanet J Rare Dis, 2011. **6**: p. 18.
54. Wu, L.L., Q., *Therapeutic targets for malignant peripheral nerve sheath tumors.* Future Neurology, 2019. **14**(1).
55. Upadhyaya, M., et al., *The spectrum of somatic and germline NF1 mutations in NF1 patients with spinal neurofibromas.* Neurogenetics, 2009. **10**(3): p. 251-63.

56. Listernick, R., et al., *Late-onset optic pathway tumors in children with neurofibromatosis 1.* Neurology, 2004. **63**(10): p. 1944-6.
57. Diggs-Andrews, K.A., et al., *Sex Is a major determinant of neuronal dysfunction in neurofibromatosis type 1.* Ann Neurol, 2014. **75**(2): p. 309-16.
58. Fisher, M.J., et al., *Gender as a disease modifier in neurofibromatosis type 1 optic pathway glioma.* Ann Neurol, 2014. **75**(5): p. 799-800.
59. Peltonen, S., et al., *Pediatric malignancies in neurofibromatosis type 1: A population-based cohort study.* Int J Cancer, 2019. **145**(11): p. 2926-2932.
60. Warrington, N.M., et al., *The cyclic AMP pathway is a sex-specific modifier of glioma risk in type I neurofibromatosis patients.* Cancer Res, 2015. **75**(1): p. 16-21.
61. Upadhyaya, M., et al., *Germline and somatic NF1 gene mutations in plexiform neurofibromas.* Hum Mutat, 2008. **29**(8): p. E103-11.
62. Staser, K., F.C. Yang, and D.W. Clapp, *Pathogenesis of plexiform neurofibroma: tumor-stromal/hematopoietic interactions in tumor progression.* Annu Rev Pathol, 2012. **7**: p. 469-95.
63. Yang, F.C., K. Staser, and D.W. Clapp, *The plexiform neurofibroma microenvironment.* Cancer Microenviron, 2012. **5**(3): p. 307-10.
64. Martin, E., et al., *Neurofibromatosis-associated malignant peripheral nerve sheath tumors in children have a worse prognosis: A nationwide cohort study.* Pediatr Blood Cancer, 2020. **67**(4): p. e28138.
65. Thomas, L., et al., *Molecular heterogeneity in malignant peripheral nerve sheath tumors associated with neurofibromatosis type 1.* Hum Genomics, 2012. **6**: p. 18.
66. Agaimy, A., N. Vassos, and R.S. Croner, *Gastrointestinal manifestations of neurofibromatosis type 1 (Recklinghausen's disease): clinicopathological spectrum with pathogenetic considerations.* Int J Clin Exp Pathol, 2012. **5**(9): p. 852-62.
67. Stewart, W., et al., *Gastric carcinoid: germline and somatic mutation of the neurofibromatosis type 1 gene.* Fam Cancer, 2007. **6**(1): p. 147-52.
68. Wang, S., et al., *miR-107 regulates tumor progression by targeting NF1 in gastric cancer.* Sci Rep, 2016. **6**: p. 36531.
69. Gutmann, D.H., J.G. Gurney, and K.M. Shannon, *Juvenile xanthogranuloma, neurofibromatosis 1, and juvenile chronic myeloid leukemia.* Arch Dermatol, 1996. **132**(11): p. 1390-1.
70. Eisfeld, A.K., et al., *NF1 mutations are recurrent in adult acute myeloid leukemia and confer poor outcome.* Leukemia, 2018. **32**(12): p. 2536-2545.
71. Gutmann, D.H., et al., *Loss of neurofibromatosis type I (NF1) gene expression in pheochromocytomas from patients without NF1.* Genes Chromosomes Cancer, 1995. **13**(2): p. 104-9.
72. Brems, H., et al., *Mechanisms in the pathogenesis of malignant tumours in neurofibromatosis type 1.* Lancet Oncol, 2009. **10**(5): p. 508-15.
73. Maani, N., et al., *NF1 Patients Receiving Breast Cancer Screening: Insights from The Ontario High Risk Breast Screening Program.* Cancers (Basel), 2019. **11**(5).
74. Pearson, A., et al., *Inactivating NF1 Mutations Are Enriched in Advanced Breast Cancer and Contribute to Endocrine Therapy Resistance.* Clin Cancer Res, 2020. **26**(3): p. 608-622.

75. Marrero, D., et al., *The neurofibromin 1 type I isoform predominance characterises female population affected by sporadic breast cancer: preliminary data.* J Clin Pathol, 2012. **65**(5): p. 419-23.
76. Johnson, M., et al., *Surgical dilemma of the management of breast cancer in a patient with neurofibromatosis: case report and a review of the literature.* J Surg Case Rep, 2020. **2020**(10): p. rjaa365.
77. Lupton, C.J., et al., *The cryo-EM structure of the human neurofibromin dimer reveals the molecular basis for neurofibromatosis type 1.* Nat Struct Mol Biol, 2021. **28**(12): p. 982-988.
78. Hajra, A., et al., *DNA sequences in the promoter region of the NF1 gene are highly conserved between human and mouse.* Genomics, 1994. **21**(3): p. 649-52.
79. Haeussler, J., et al., *Tumor antigen HuR binds specifically to one of five protein-binding segments in the 3'-untranslated region of the neurofibromin messenger RNA.* Biochem Biophys Res Commun, 2000. **267**(3): p. 726-32.
80. Cawthon, R.M., et al., *cDNA sequence and genomic structure of EV12B, a gene lying within an intron of the neurofibromatosis type 1 gene.* Genomics, 1991. **9**(3): p. 446-60.
81. Cawthon, R.M., et al., *Identification and characterization of transcripts from the neurofibromatosis 1 region: the sequence and genomic structure of EVI2 and mapping of other transcripts.* Genomics, 1990. **7**(4): p. 555-65.
82. Viskochil, D., et al., *The gene encoding the oligodendrocyte-myelin glycoprotein is embedded within the neurofibromatosis type 1 gene.* Mol Cell Biol, 1991. **11**(2): p. 906-12.
83. Bergoug, M., et al., *Neurofibromin Structure, Functions and Regulation.* Cells, 2020. **9**(11).
84. Pan, Q., et al., *Deep surveying of alternative splicing complexity in the human transcriptome by high-throughput sequencing.* Nat Genet, 2008. **40**(12): p. 1413-5.
85. Vandenbroucke, I., et al., *Quantification of NF1 transcripts reveals novel highly expressed splice variants.* FEBS Lett, 2002. **522**(1-3): p. 71-6.
86. Anastasaki, C., PhD, et al., *UPDATED NOMENCLATURE FOR HUMAN AND MOUSE NEUROFIBROMATOSIS TYPE 1 GENES.* Neurol Genet, 2017.
87. Lee, Y. and D.C. Rio, *Mechanisms and Regulation of Alternative Pre-mRNA Splicing.* Annu Rev Biochem, 2015. **84**: p. 291-323.
88. Fleming, V.A., et al., *Alternative splicing of the neurofibromatosis type 1 pre-mRNA is regulated by the muscleblind-like proteins and the CUG-BP and ELAV-like factors.* BMC Mol Biol, 2012. **13**: p. 35.
89. Shilyansky, C., Y.S. Lee, and A.J. Silva, *Molecular and cellular mechanisms of learning disabilities: a focus on NF1.* Annu Rev Neurosci, 2010. **33**: p. 221-43.
90. Sherekar, M., et al., *Biochemical and structural analyses reveal that the tumor suppressor neurofibromin (NF1) forms a high-affinity dimer.* J Biol Chem, 2020. **295**(4): p. 1105-1119.
91. Kaufmann, D., et al., *Partial Blindness to Submicron Topography in NF1 Haploinsufficient Cultured Fibroblasts Indicates a New Function of Neurofibromin in Regulation of Mechanosensoric.* Mol Syndromol, 2012. **3**(4): p. 169-79.

92. Naschberger, A., et al., *The structure of neurofibromin isoform 2 reveals different functional states.* Nature, 2021. **599**(7884): p. 315-319.
93. Yan, W., et al., *Structural Insights into the SPRED1-Neurofibromin-KRAS Complex and Disruption of SPRED1-Neurofibromin Interaction by Oncogenic EGFR.* Cell Rep, 2020. **32**(3): p. 107909.
94. Raso, E., *Splice variants of RAS-translational significance.* Cancer Metastasis Rev, 2020. **39**(4): p. 1039-1049.
95. Escobar-Hoyos, L.F., et al., *Altered RNA Splicing by Mutant p53 Activates Oncogenic RAS Signaling in Pancreatic Cancer.* Cancer Cell, 2020. **38**(2): p. 198-211 e8.
96. Costa, R.M., et al., *Learning deficits, but normal development and tumor predisposition, in mice lacking exon 23a of Nf1.* Nat Genet, 2001. **27**(4): p. 399-405.
97. Feng, L., et al., *PKA phosphorylation and 14-3-3 interaction regulate the function of neurofibromatosis type I tumor suppressor, neurofibromin.* FEBS Lett, 2004. **557**(1-3): p. 275-82.
98. Izawa, I., N. Tamaki, and H. Saya, *Phosphorylation of neurofibromatosis type 1 gene product (neurofibromin) by cAMP-dependent protein kinase.* FEBS Lett, 1996. **382**(1-2): p. 53-9.
99. D'Angelo, I., et al., *A novel bipartite phospholipid-binding module in the neurofibromatosis type 1 protein.* EMBO Rep, 2006. **7**(2): p. 174-9.
100. Leondaritis, G., L. Petrikkos, and D. Mangoura, *Regulation of the Ras-GTPase activating protein neurofibromin by C-tail phosphorylation: implications for protein kinase C/Ras/extracellular signal-regulated kinase 1/2 pathway signaling and neuronal differentiation.* J Neurochem, 2009. **109**(2): p. 573-83.
101. Mangoura, D., et al., *Phosphorylation of neurofibromin by PKC is a possible molecular switch in EGF receptor signaling in neural cells.* Oncogene, 2006. **25**(5): p. 735-45.
102. Cichowski, K., et al., *Dynamic regulation of the Ras pathway via proteolysis of the NF1 tumor suppressor.* Genes Dev, 2003. **17**(4): p. 449-54.
103. Bergoug, M.C.M., Fabienne Godin, Michel Doudeau, Iva Sosic, Marcin Suskiewicz, Béatrice Vallée, Hélène Bénédetti, *Noncanonical structural requirements of neurofibromin SUMOylation reveal a folding-deficiency of several pathogenic mutants.* bioRxiv, 2021.
104. Anastasaki, C. and D.H. Gutmann, *Neuronal NF1/RAS regulation of cyclic AMP requires atypical PKC activation.* Hum Mol Genet, 2014. **23**(25): p. 6712-21.
105. Hannan, F., et al., *Effect of neurofibromatosis type I mutations on a novel pathway for adenylyl cyclase activation requiring neurofibromin and Ras.* Hum Mol Genet, 2006. **15**(7): p. 1087-98.
106. Lau, N., et al., *Loss of neurofibromin is associated with activation of RAS/MAPK and PI3-K/AKT signaling in a neurofibromatosis 1 astrocytoma.* J Neuropathol Exp Neurol, 2000. **59**(9): p. 759-67.
107. Downward, J., *Targeting RAS signalling pathways in cancer therapy.* Nat Rev Cancer, 2003. **3**(1): p. 11-22.

108. Banerjee, S., et al., *Neurofibromatosis-1 regulates mTOR-mediated astrocyte growth and glioma formation in a TSC/Rheb-independent manner.* Proc Natl Acad Sci U S A, 2011. **108**(38): p. 15996-6001.
109. Keng, V.W., et al., *PTEN and NF1 inactivation in Schwann cells produces a severe phenotype in the peripheral nervous system that promotes the development and malignant progression of peripheral nerve sheath tumors.* Cancer Res, 2012. **72**(13): p. 3405-13.
110. Uhlen, M., et al., *Proteomics. Tissue-based map of the human proteome.* Science, 2015. **347**(6220): p. 1260419.
111. Barron, V.A. and H. Lou, *Alternative splicing of the neurofibromatosis type I pre-mRNA.* Biosci Rep, 2012. **32**(2): p. 131-8.
112. Gutmann, D.H., et al., *Expression of the neurofibromatosis 1 (NF1) isoforms in developing and adult rat tissues.* Cell Growth Differ, 1995. **6**(3): p. 315-23.
113. Koczkowska, M., et al., *Genotype-Phenotype Correlation in NF1: Evidence for a More Severe Phenotype Associated with Missense Mutations Affecting NF1 Codons 844-848.* Am J Hum Genet, 2018. **102**(1): p. 69-87.
114. Fahsold, R., et al., *Minor lesion mutational spectrum of the entire NF1 gene does not explain its high mutability but points to a functional domain upstream of the GAP-related domain.* Am J Hum Genet, 2000. **66**(3): p. 790-818.
115. Messiaen, L.M., et al., *Exhaustive mutation analysis of the NF1 gene allows identification of 95% of mutations and reveals a high frequency of unusual splicing defects.* Hum Mutat, 2000. **15**(6): p. 541-55.
116. Consoli, C., et al., *Gonosomal mosaicism for a nonsense mutation (R1947X) in the NF1 gene in segmental neurofibromatosis type 1.* J Invest Dermatol, 2005. **125**(3): p. 463-6.
117. Gutmann, D.H., *Exploring the genetic basis for clinical variation in neurofibromatosis type 1.* Expert Rev Neurother, 2016. **16**(9): p. 999-1001.
118. Bajenaru, M.L., et al., *Neurofibromatosis 1 (NF1) heterozygosity results in a cell-autonomous growth advantage for astrocytes.* Glia, 2001. **33**(4): p. 314-23.
119. Bajenaru, M.L., et al., *Optic nerve glioma in mice requires astrocyte Nf1 gene inactivation and Nf1 brain heterozygosity.* Cancer Res, 2003. **63**(24): p. 8573-7.
120. Daginakatte, G.C. and D.H. Gutmann, *Neurofibromatosis-1 (Nf1) heterozygous brain microglia elaborate paracrine factors that promote Nf1-deficient astrocyte and glioma growth.* Hum Mol Genet, 2007. **16**(9): p. 1098-112.
121. Brosseau, J.P., et al., *NF1 heterozygosity fosters de novo tumorigenesis but impairs malignant transformation.* Nat Commun, 2018. **9**(1): p. 5014.
122. Vuong, C.K., D.L. Black, and S. Zheng, *The neurogenetics of alternative splicing.* Nat Rev Neurosci, 2016. **17**(5): p. 265-81.
123. Pros, E., et al., *Antisense therapeutics for neurofibromatosis type 1 caused by deep intronic mutations.* Hum Mutat, 2009. **30**(3): p. 454-62.
124. Jang, M.A., et al., *Identification and characterization of NF1 splicing mutations in Korean patients with neurofibromatosis type 1.* J Hum Genet, 2016. **61**(8): p. 705-9.
125. Wimmer, K., et al., *Extensive in silico analysis of NF1 splicing defects uncovers determinants for splicing outcome upon 5' splice-site disruption.* Hum Mutat, 2007. **28**(6): p. 599-612.

126. Eisenbarth, I., et al., *Analysis of an alternatively spliced exon of the neurofibromatosis type 1 gene in cultured melanocytes from patients with neurofibromatosis 1.* Arch Dermatol Res, 1995. **287**(5): p. 413-6.
127. Alkindy, A., et al., *Genotype-phenotype associations in neurofibromatosis type 1 (NF1): an increased risk of tumor complications in patients with NF1 splice-site mutations?* Hum Genomics, 2012. **6**: p. 12.
128. Hernandez-Imaz, E., et al., *Functional Analysis of Mutations in Exon 9 of NF1 Reveals the Presence of Several Elements Regulating Splicing.* PLoS One, 2015. **10**(10): p. e0141735.
129. Siva, K., G. Covello, and M.A. Denti, *Exon-skipping antisense oligonucleotides to correct missplicing in neurogenetic diseases.* Nucleic Acid Ther, 2014. **24**(1): p. 69-86.
130. Lorson, C.L. and E.J. Androphy, *An exonic enhancer is required for inclusion of an essential exon in the SMA-determining gene SMN.* Hum Mol Genet, 2000. **9**(2): p. 259-65.
131. Urban, E. and C.R. Noe, *Structural modifications of antisense oligonucleotides.* Farmaco, 2003. **58**(3): p. 243-58.
132. Shimo, T., et al., *Design and evaluation of locked nucleic acid-based splice-switching oligonucleotides in vitro.* Nucleic Acids Res, 2014. **42**(12): p. 8174-87.
133. Moulton, J.D. and S. Jiang, *Gene knockdowns in adult animals: PPMOs and vivo-morpholinos.* Molecules, 2009. **14**(3): p. 1304-23.
134. Aartsma-Rus, A., *Overview on AON design.* Methods Mol Biol, 2012. **867**: p. 117-29.
135. Disterer, P., et al., *Development of therapeutic splice-switching oligonucleotides.* Hum Gene Ther, 2014. **25**(7): p. 587-98.
136. Havens, M.A. and M.L. Hastings, *Splice-switching antisense oligonucleotides as therapeutic drugs.* Nucleic Acids Res, 2016. **44**(14): p. 6549-63.
137. Wan, J., *Antisense-mediated exon skipping to shift alternative splicing to treat cancer.* Methods Mol Biol, 2012. **867**: p. 201-8.
138. Bauman, J., N. Jearawiriyapaisarn, and R. Kole, *Therapeutic potential of splice-switching oligonucleotides.* Oligonucleotides, 2009. **19**(1): p. 1-13.
139. Geary, R.S., *Antisense oligonucleotide pharmacokinetics and metabolism.* Expert Opin Drug Metab Toxicol, 2009. **5**(4): p. 381-91.
140. Rigo, F., P.P. Seth, and C.F. Bennett, *Antisense oligonucleotide-based therapies for diseases caused by pre-mRNA processing defects.* Adv Exp Med Biol, 2014. **825**: p. 303-52.
141. Syed, Y.Y., *Eteplirsen: First Global Approval.* Drugs, 2016. **76**(17): p. 1699-1704.
142. Corey, D.R., *Nusinersen, an antisense oligonucleotide drug for spinal muscular atrophy.* Nat Neurosci, 2017. **20**(4): p. 497-499.
143. Biayna, J., et al., *Using antisense oligonucleotides for the physiological modulation of the alternative splicing of NF1 exon 23a during PC12 neuronal differentiation.* Scientific Reports, 2021. **11**(1).
144. Guo, H.F., et al., *A neurofibromatosis-1-regulated pathway is required for learning in Drosophila.* Nature, 2000. **403**(6772): p. 895-8.

145. Chao, R.C., et al., *Therapy-induced malignant neoplasms in Nf1 mutant mice.* Cancer Cell, 2005. **8**(4): p. 337-48.
146. Jacks, T., et al., *Tumour predisposition in mice heterozygous for a targeted mutation in Nf1.* Nat Genet, 1994. **7**(3): p. 353-61.
147. Brannan, C.I., et al., *Targeted disruption of the neurofibromatosis type-1 gene leads to developmental abnormalities in heart and various neural crest-derived tissues.* Genes Dev, 1994. **8**(9): p. 1019-29.
148. Zhu, Y., et al., *Neurofibromas in NF1: Schwann cell origin and role of tumor environment.* Science, 2002. **296**(5569): p. 920-2.
149. Yang, F.C., et al., *Neurofibromin-deficient Schwann cells secrete a potent migratory stimulus for Nf1+/- mast cells.* J Clin Invest, 2003. **112**(12): p. 1851-61.
150. Walters, E.M., et al., *Swine models, genomic tools and services to enhance our understanding of human health and diseases.* Lab Animal, 2017. **46**(4): p. 167-172.
151. Schomberg, D.T., et al., *Miniature Swine for Preclinical Modeling of Complexities of Human Disease for Translational Scientific Discovery and Accelerated Development of Therapies and Medical Devices.* Toxicol Pathol, 2016. **44**(3): p. 299-314.
152. Nygard, A.B., et al., *A study of alternative splicing in the pig.* BMC Res Notes, 2010. **3**: p. 123.
153. Hanna, A.S., et al., *Brachial plexus anatomy in the miniature swine as compared to human.* J Anat, 2022. **240**(1): p. 172-181.
154. Schook, L.B., et al., *A Genetic Porcine Model of Cancer.* PLoS One, 2015. **10**(7): p. e0128864.
155. Mohiuddin, M.M., et al., *Progressive genetic modifications of porcine cardiac xenografts extend survival to 9 months.* Xenotransplantation, 2022: p. e12744.
156. Isakson, S.H., et al., *Genetically engineered minipigs model the major clinical features of human neurofibromatosis type 1.* Commun Biol, 2018. **1**: p. 158.
157. White, K.A., et al., *A porcine model of neurofibromatosis type 1 that mimics the human disease.* JCI Insight, 2018. **3**(12).
158. Uthoff, J., et al., *Longitudinal phenotype development in a minipig model of neurofibromatosis type 1.* Sci Rep, 2020. **10**(1): p. 5046.
159. Khanna, R., et al., *Assessment of nociception and related quality-of-life measures in a porcine model of neurofibromatosis type 1.* Pain, 2019. **160**(11): p. 2473-2486.
160. Rothschild, M.F., A. Ruvinsky, and C.A.B. International., *The genetics of the pig*. 2nd ed. 2011, Wallingford, Oxfordshire, UK: CABI. x, 507 p.
161. Perlman, R.L., *Mouse models of human disease An evolutionary perspective.* Evolution Medicine and Public Health, 2016(1): p. 170-176.
162. Nygard, A.B., et al., *Investigation of tissue-specific human orthologous alternative splice events in pig.* Anim Biotechnol, 2010. **21**(4): p. 203-16.
163. Li, K., et al., *Mice with missense and nonsense NF1 mutations display divergent phenotypes compared with human neurofibromatosis type I.* Dis Model Mech, 2016. **9**(7): p. 759-67.

164. Andersen, M.L. and L.M.F. Winter, *Animal models in biological and biomedical research - experimental and ethical concerns.* An Acad Bras Cienc, 2019. **91**(suppl 1): p. e20170238.
165. Keele, K.D., *Three Early Masters of Experimental Medicine-Erasistratus, Galen and Leonardo da Vinci.* Proc R Soc Med, 1961. **54**(7): p. 577-88.
166. Bustad, L.K. and R.O. McClellan, *Swine in biomedical research.* Science, 1966. **152**(3728): p. 1526-30.
167. Ericsson, A.C., M.J. Crim, and C.L. Franklin, *A brief history of animal modeling.* Mo Med, 2013. **110**(3): p. 201-5.
168. Davidson, M.K., J.R. Lindsey, and J.K. Davis, *Requirements and selection of an animal model.* Isr J Med Sci, 1987. **23**(6): p. 551-5.
169. Swindle, M.M., et al., *Swine as models in biomedical research and toxicology testing.* Vet Pathol, 2012. **49**(2): p. 344-56.
170. Schomberg, D.T., et al., *Translational Relevance of Swine Models of Spinal Cord Injury.* J Neurotrauma, 2016.
171. Gerrity, R.G., et al., *Diabetes-induced accelerated atherosclerosis in swine.* Diabetes, 2001. **50**(7): p. 1654-65.
172. Bohan, A.E., et al., *The proliferation and differentiation of primary pig preadipocytes is suppressed when cultures are incubated at 37 degrees Celsius compared to euthermic conditions in pigs.* Adipocyte, 2014. **3**(4): p. 322-32.
173. Gun, G. and W.A. Kues, *Current progress of genetically engineered pig models for biomedical research.* Biores Open Access, 2014. **3**(6): p. 255-64.
174. Williams, K.J., R.A. Godke, and K.R. Bondioli, *Isolation and culture of porcine adipose tissue-derived somatic stem cells.* Methods Mol Biol, 2011. **702**: p. 77-86.
175. Feisst, V., S. Meidinger, and M.B. Locke, *From bench to bedside: use of human adipose-derived stem cells.* Stem Cells Cloning, 2015. **8**: p. 149-62.
176. Langhof, H., et al., *Preclinical efficacy in therapeutic area guidelines from the U.S. Food and Drug Administration and the European Medicines Agency: a cross-sectional study.* Br J Pharmacol, 2018. **175**(22): p. 4229-4238.
177. Singh, V.K. and T.M. Seed, *How necessary are animal models for modern drug discovery?* Expert Opin Drug Discov, 2021. **16**(12): p. 1391-1397.
178. Arrizabalaga, J.H. and M.U. Nollert, *Properties of porcine adipose-derived stem cells and their applications in preclinical models.* Adipocyte, 2017. **6**(3): p. 217-223.
179. Friedrich, J., et al., *Spheroid-based drug screen: considerations and practical approach.* Nat Protoc, 2009. **4**(3): p. 309-24.
180. Cheng, L.S., et al., *Optimizing neurogenic potential of enteric neurospheres for treatment of neurointestinal diseases.* J Surg Res, 2016. **206**(2): p. 451-459.
181. Pellegatta, S., et al., *Neurospheres enriched in cancer stem-like cells are highly effective in eliciting a dendritic cell-mediated immune response against malignant gliomas.* Cancer Res, 2006. **66**(21): p. 10247-52.
182. Achilli, T.M., J. Meyer, and J.R. Morgan, *Advances in the formation, use and understanding of multi-cellular spheroids.* Expert Opin Biol Ther, 2012. **12**(10): p. 1347-60.

183. Larson B., H.S., Hannah Gitschier2, Alexandra Wolff3, Wini Luty3, *Image-based Analysis of a Human Neurosphere Stem Cell Model for the Evaluation of Potential Neurotoxicants.* 2016.
184. Jensen, J.B. and M. Parmar, *Strengths and limitations of the neurosphere culture system.* Mol Neurobiol, 2006. **34**(3): p. 153-61.
185. Yang, E., et al., *Generation of neurospheres from human adipose-derived stem cells.* Biomed Res Int, 2015. **2015**: p. 743714.
186. Fu, L., et al., *Derivation of neural stem cells from mesenchymal stemcells: evidence for a bipotential stem cell population.* Stem Cells Dev, 2008. **17**(6): p. 1109-21.
187. Feng, N., et al., *Generation of highly purified neural stem cells from human adipose-derived mesenchymal stem cells by Sox1 activation.* Stem Cells Dev, 2014. **23**(5): p. 515-29.
188. Mung, K.L., et al., *Rapid and efficient generation of neural progenitors from adult bone marrow stromal cells by hypoxic preconditioning.* Stem Cell Res Ther, 2016. **7**(1): p. 146.
189. Radtke, C., et al., *Peripheral glial cell differentiation from neurospheres derived from adipose mesenchymal stem cells.* Int J Dev Neurosci, 2009. **27**(8): p. 817-23.
190. Lim, J.H., et al., *Evaluation of gene expression and DNA copy number profiles of adipose tissue-derived stromal cells and consecutive neurosphere-like cells generated from dogs with naturally occurring spinal cord injury.* Am J Vet Res, 2017. **78**(3): p. 371-380.
191. Jahanbazi Jahan-Abad, A., et al., *Curcumin attenuates harmful effects of arsenic on neural stem/progenitor cells.* Avicenna J Phytomed, 2017. **7**(4): p. 376-388.
192. Kang, S.K., et al., *Neurogenesis of Rhesus adipose stromal cells.* J Cell Sci, 2004. **117**(Pt 18): p. 4289-99.
193. Wang, Y., et al., *Hypoxia promotes dopaminergic differentiation of mesenchymal stem cells and shows benefits for transplantation in a rat model of Parkinson's disease.* PLoS One, 2013. **8**(1): p. e54296.
194. Zhao, M.T., et al., *Porcine skin-derived progenitor (SKP) spheres and neurospheres: Distinct "stemness" identified by microarray analysis.* Cell Reprogram, 2010. **12**(3): p. 329-45.
195. Yin, F., et al., *Spontaneous differentiation of porcine neural progenitors in vitro.* Cytotechnology, 2011. **63**(4): p. 363-70.
196. Xu, Y., et al., *Neurospheres from rat adipose-derived stem cells could be induced into functional Schwann cell-like cells in vitro.* BMC Neurosci, 2008. **9**: p. 21.
197. Liard, O., et al., *Adult-brain-derived neural stem cells grafting into a vein bridge increases postlesional recovery and regeneration in a peripheral nerve of adult pig.* Stem Cells Int, 2012. **2012**: p. 128732.
198. Denham, M. and M. Dottori, *Neural differentiation of induced pluripotent stem cells.* Methods Mol Biol, 2011. **793**: p. 99-110.
199. Hofrichter, M., et al., *Comparative performance analysis of human iPSC-derived and primary neural progenitor cells (NPC) grown as neurospheres in vitro.* Stem Cell Res, 2017. **25**: p. 72-82.
200. Chen, Y.J., et al., *Isolation and Differentiation of Adipose-Derived Stem Cells from Porcine Subcutaneous Adipose Tissues.* J Vis Exp, 2016(109): p. e53886.

201. Singh, M., et al., *Synergistic Effect of BDNF and FGF2 in Efficient Generation of Functional Dopaminergic Neurons from human Mesenchymal Stem Cells.* Sci Rep, 2017. **7**(1): p. 10378.
202. Sun, X., et al., *Differentiation of adipose-derived stem cells into Schwann cell-like cells through intermittent induction: potential advantage of cellular transient memory function.* Stem Cell Res Ther, 2018. **9**(1): p. 133.
203. Sasaki, R., et al., *A protocol for immunofluorescence staining of floating neurospheres.* Neurosci Lett, 2010. **479**(2): p. 126-7.
204. Boiani, M. and H.R. Scholer, *Regulatory networks in embryo-derived pluripotent stem cells.* Nat Rev Mol Cell Biol, 2005. **6**(11): p. 872-84.
205. Pesce, M. and H.R. Scholer, *Oct-4: gatekeeper in the beginnings of mammalian development.* Stem Cells, 2001. **19**(4): p. 271-8.
206. Xiong, F., et al., *Optimal time for passaging neurospheres based on primary neural stem cell cultures.* Cytotechnology, 2011. **63**(6): p. 621-31.
207. Avilion, A.A., et al., *Multipotent cell lineages in early mouse development depend on SOX2 function.* Genes Dev, 2003. **17**(1): p. 126-40.
208. Wiese, C., et al., *Nestin expression--a property of multi-lineage progenitor cells?* Cell Mol Life Sci, 2004. **61**(19-20): p. 2510-22.
209. du Puy, L., et al., *Analysis of co-expression of OCT4, NANOG and SOX2 in pluripotent cells of the porcine embryo, in vivo and in vitro.* Theriogenology, 2011. **75**(3): p. 513-26.
210. Zhang, J. and J. Jiao, *Molecular Biomarkers for Embryonic and Adult Neural Stem Cell and Neurogenesis.* Biomed Res Int, 2015. **2015**: p. 727542.
211. Gao, W., et al., *Development of a novel and economical agar-based non-adherent three-dimensional culture method for enrichment of cancer stem-like cells.* Stem Cell Res Ther, 2018. **9**(1): p. 243.
212. Kim, S.A., E.K. Lee, and H.J. Kuh, *Co-culture of 3D tumor spheroids with fibroblasts as a model for epithelial-mesenchymal transition in vitro.* Exp Cell Res, 2015. **335**(2): p. 187-96.
213. Hu, F., et al., *Effects of epidermal growth factor and basic fibroblast growth factor on the proliferation and osteogenic and neural differentiation of adipose-derived stem cells.* Cell Reprogram, 2013. **15**(3): p. 224-32.
214. Calabrese, E.J., *Neuroscience and hormesis: overview and general findings.* Crit Rev Toxicol, 2008. **38**(4): p. 249-52.
215. Zhang, L., H. Jiang, and Z. Hu, *Concentration-dependent effect of nerve growth factor on cell fate determination of neural progenitors.* Stem Cells Dev, 2011. **20**(10): p. 1723-31.
216. Krall, J.A., E.M. Beyer, and G. MacBeath, *High- and low-affinity epidermal growth factor receptor-ligand interactions activate distinct signaling pathways.* PLoS One, 2011. **6**(1): p. e15945.
217. Sondell, M., G. Lundborg, and M. Kanje, *Vascular endothelial growth factor has neurotrophic activity and stimulates axonal outgrowth, enhancing cell survival and Schwann cell proliferation in the peripheral nervous system.* J Neurosci, 1999. **19**(14): p. 5731-40.
218. Yamada, M., et al., *High concentrations of HGF inhibit skeletal muscle satellite cell proliferation in vitro by inducing expression of myostatin: a possible*

mechanism for reestablishing satellite cell quiescence in vivo. Am J Physiol Cell Physiol, 2010. **298**(3): p. C465-76.
219. Oka, M., et al., *Differential role for transcription factor Oct4 nucleocytoplasmic dynamics in somatic cell reprogramming and self-renewal of embryonic stem cells.* J Biol Chem, 2013. **288**(21): p. 15085-97.
220. Lobo, M.V., et al., *Cellular characterization of epidermal growth factor-expanded free-floating neurospheres.* J Histochem Cytochem, 2003. **51**(1): p. 89-103.
221. Singec, I., et al., *Defining the actual sensitivity and specificity of the neurosphere assay in stem cell biology.* Nat Methods, 2006. **3**(10): p. 801-6.
222. Brooks, A.E., et al., *Culture and Expansion of Rodent and Porcine Schwann Cells for Preclinical Animal Studies.* Schwann Cells: Methods and Protocols, 2018. **1739**: p. 111-126.
223. Wang, X., et al., *Isolation and Culture of Pig Spermatogonial Stem Cells and Their in Vitro Differentiation into Neuron-Like Cells and Adipocytes.* Int J Mol Sci, 2015. **16**(11): p. 26333-46.
224. Kwon, B.K., et al., *Large animal and primate models of spinal cord injury for the testing of novel therapies.* Exp Neurol, 2015. **269**: p. 154-68.
225. Jett, K. and J.M. Friedman, *Clinical and genetic aspects of neurofibromatosis 1.* Genet Med, 2010. **12**(1): p. 1-11.
226. Sabbagh, A., et al., *Unravelling the genetic basis of variable clinical expression in neurofibromatosis 1.* Hum Mol Genet, 2009. **18**(15): p. 2768-78.
227. Ozarslan, B., et al., *Cutaneous Findings in Neurofibromatosis Type 1.* Cancers (Basel), 2021. **13**(3).
228. Allaway, R.J., et al., *Cutaneous neurofibromas in the genomics era: current understanding and open questions.* Br J Cancer, 2018. **118**(12): p. 1539-1548.
229. Costa, A.D.A. and D.H. Gutmann, *Brain tumors in Neurofibromatosis type 1.* Neuro-Oncology Advances, 2019.
230. Quintans, B., et al., *Neurofibromatosis without Neurofibromas: Confirmation of a Genotype-Phenotype Correlation and Implications for Genetic Testing.* Case Rep Neurol, 2011. **3**: p. 86-90.
231. Pros, E., et al., *Nature and mRNA effect of 282 different NF1 point mutations: focus on splicing alterations.* Hum Mutat, 2008. **29**(9): p. E173-93.
232. Venkataramany, A.S., et al., *Alternative RNA Splicing Defects in Pediatric Cancers: New Insights in Tumorigenesis and Potential Therapeutic Vulnerabilities.* Ann Oncol, 2022.
233. Hinman, M.N., et al., *Neurofibromatosis type 1 alternative splicing is a key regulator of Ras signaling in neurons.* Mol Cell Biol, 2014. **34**(12): p. 2188-97.
234. Vandenbroucke, II, et al., *Quantification of splice variants using real-time PCR.* Nucleic Acids Res, 2001. **29**(13): p. E68-8.
235. Park, S.J., et al., *Selection of appropriate reference genes for RT-qPCR analysis in Berkshire, Duroc, Landrace, and Yorkshire pigs.* Gene, 2015. **558**(1): p. 152-8.
236. Markham, N.R. and M. Zuker, *UNAFold: software for nucleic acid folding and hybridization.* Methods Mol Biol, 2008. **453**: p. 3-31.
237. Desmet, F.O., et al., *Human Splicing Finder: an online bioinformatics tool to predict splicing signals.* Nucleic Acids Res, 2009. **37**(9): p. e67.

238. Reuter, J.S. and D.H. Mathews, *RNAstructure: software for RNA secondary structure prediction and analysis.* BMC Bioinformatics, 2010. **11**: p. 129.
239. Dasgupta, B. and D.H. Gutmann, *Neurofibromin regulates neural stem cell proliferation, survival, and astroglial differentiation in vitro and in vivo.* J Neurosci, 2005. **25**(23): p. 5584-94.
240. Liao, C.P., et al., *Contributions of inflammation and tumor microenvironment to neurofibroma tumorigenesis.* J Clin Invest, 2018. **128**(7): p. 2848-2861.
241. Assunto, A., et al., *Isoform-specific NF1 mRNA levels correlate with disease severity in Neurofibromatosis type 1.* Orphanet J Rare Dis, 2019. **14**(1): p. 261.
242. Kahen, E.J., et al., *Neurofibromin level directs RAS pathway signaling and mediates sensitivity to targeted agents in malignant peripheral nerve sheath tumors.* Oncotarget, 2018. **9**(32): p. 22571-22585.
243. Pires, V.B., et al., *Short (16-mer) locked nucleic acid splice-switching oligonucleotides restore dystrophin production in Duchenne Muscular Dystrophy myotubes.* PLoS One, 2017. **12**(7): p. e0181065.
244. Meijboom, K.E., M.J.A. Wood, and G. McClorey, *Splice-Switching Therapy for Spinal Muscular Atrophy.* Genes (Basel), 2017. **8**(6).
245. Biayna, J., et al., *Using antisense oligonucleotides for the physiological modulation of the alternative splicing of NF1 exon 23a during PC12 neuronal differentiation.* Sci Rep, 2021. **11**(1): p. 3661.
246. Miller, D.T., et al., *Health Supervision for Children With Neurofibromatosis Type 1.* Pediatrics, 2019. **143**(5).
247. Yang, X., et al., *Characteristics, treatment patterns, healthcare resource use, and costs among pediatric patients diagnosed with neurofibromatosis type 1 and plexiform neurofibromas: a retrospective database analysis of a medicaid population.* Curr Med Res Opin, 2021. **37**(9): p. 1555-1561.
248. Stewart, D.R., et al., *Care of adults with neurofibromatosis type 1: a clinical practice resource of the American College of Medical Genetics and Genomics (ACMG).* Genet Med, 2018. **20**(7): p. 671-682.
249. Robertson, K.A., et al., *Imatinib mesylate for plexiform neurofibromas in patients with neurofibromatosis type 1: a phase 2 trial.* Lancet Oncol, 2012. **13**(12): p. 1218-24.
250. Lin, A.L. and D.H. Gutmann, *Advances in the treatment of neurofibromatosis-associated tumours.* Nat Rev Clin Oncol, 2013. **10**(11): p. 616-24.
251. Williams, K.B. and D.A. Largaespada, *New Model Systems and the Development of Targeted Therapies for the Treatment of Neurofibromatosis Type 1-Associated Malignant Peripheral Nerve Sheath Tumors.* Genes (Basel), 2020. **11**(5).
252. Casey, D., et al., *FDA Approval Summary: Selumetinib for Plexiform Neurofibroma.* Clin Cancer Res, 2021. **27**(15): p. 4142-4146.
253. Hwang, J., et al., *Efficacy and Safety of Selumetinib in Pediatric Patients With Neurofibromatosis Type 1: A Systematic Review and Meta-analysis.* Neurology, 2022. **98**(9): p. e938-e946.
254. Mashour, G.A., et al., *Differential modulation of malignant peripheral nerve sheath tumor growth by omega-3 and omega-6 fatty acids.* Oncogene, 2005. **24**(14): p. 2367-74.

255. Summers, M.A., et al., *Dietary intervention rescues myopathy associated with neurofibromatosis type 1.* Hum Mol Genet, 2018. **27**(4): p. 577-588.
256. McLaughlin, M.E. and T. Jacks, *Progesterone receptor expression in neurofibromas.* Cancer Res, 2003. **63**(4): p. 752-5.
257. Isikoglu, M., et al., *Plexiform neurofibroma during and after pregnancy.* Arch Gynecol Obstet, 2002. **267**(1): p. 41-2.
258. Sheynkman, G.M., et al., *ORF Capture-Seq as a versatile method for targeted identification of full-length isoforms.* Nat Commun, 2020. **11**(1): p. 2326.
259. Gutmann, D.H., et al., *Expression of two new protein isoforms of the neurofibromatosis type 1 gene product, neurofibromin, in muscle tissues.* Dev Dyn, 1995. **202**(3): p. 302-11.
260. Ebinger, M., et al., *No aberrant methylation of neurofibromatosis 1 gene (NF1) promoter in pilocytic astrocytoma in childhood.* Pediatr Hematol Oncol, 2005. **22**(1): p. 83-7.
261. Lev Maor, G., A. Yearim, and G. Ast, *The alternative role of DNA methylation in splicing regulation.* Trends Genet, 2015. **31**(5): p. 274-80.
262. Li, Y. and T.O. Tollefsbol, *DNA methylation detection: bisulfite genomic sequencing analysis.* Methods Mol Biol, 2011. **791**: p. 11-21.
263. Lu, A., et al., *Reprogrammable CRISPR/dCas9-based recruitment of DNMT1 for site-specific DNA demethylation and gene regulation.* Cell Discov, 2019. **5**: p. 22.
264. Juliano, R.L., *The delivery of therapeutic oligonucleotides.* Nucleic Acids Res, 2016. **44**(14): p. 6518-48.